

**MULTIVARIATE CHARACTERIZATION OF NATURAL  
RADIOACTIVITY SYSTEMATICS IN LAKE MAGADI  
BASIN GEOTHERMAL SYSTEM IN RELATION TO  
QUALITY OF TRONA DEPOSITS**

By

**TAMBO, Paul Sati** B.Ed(Egerton)

**This thesis is submitted for examination in partial fulfillment of the requirements for the  
award of the degree of Master of Science in Physics of the University of Nairobi.**

**August 2014**

# DECLARATION

This thesis is my own work and has not been previously examined or presented for examination at any other University or academic institution for any award.

**TAMBO, Paul Sati**

(I56/70622/2011)

Department of Physics, University of Nairobi.

Signature..... Date.....

This thesis has been submitted for examination with our approval as University supervisors

**Prof. J.P. Patel**

Department of Physics, University of Nairobi.

Signature ..... Date .....

**Dr. Angeyo H. Kalambuka**

Department of Physics, University of Nairobi.

Signature ..... Date .....

**Mr. Michael J. Mangala**

Institute of Nuclear Science & Technology, University of Nairobi.

Signature ..... Date .....

# **DEDICATION**

Timothy Sati Tambo

1964-1996

## ACKNOWLEDGEMENTS

This thesis, like any other, owes much to the contributions and participation of many people. A very special acknowledgement is due to my thesis supervisors; Prof. J.P. Patel, Dr. Angeyo H. Kalambuka, and Mr. Michael J. Mangala, for their invaluable inputs throughout the entire period of the research. I profoundly thank Prof. J.P. Patel and Dr. Angeyo H. Kalambuka for taking time off their busy schedules to accompany me to Lake Magadi for field work and for their guidance on problem formulation and proposal writing.

Thanks are due to the Director and laboratory staff of the Institute of Nuclear Science & Technology of the University of Nairobi for allowing me access as well as giving necessary guidance to the Institute's analytical laboratory facilities, with a special mention to the Chief Technologist Mr. S.K. Bartilol for his guidance on gamma spectrometry instrumentation and spectral deconvolution.

Special thanks are also due to the Chief Chemist Mr. Steve Okiri and Senior Technologist Mr. Edward Kimeu of Magadi Chemical Laboratory for providing useful information about the extraction process as well as samples of finished products from the Magadi Soda Company for analysis in this research.

I also wish to sincerely thank the Mines and Geology Department of the Ministry of Environment and Mineral Resources of Kenya for their assistance in the preparation of solid samples for gamma-ray spectrometry.

I thank the staff of the following laboratories of the University of Nairobi: Physical Chemistry Laboratory of the Department of Chemistry for assisting with pH and TDS measurements; Soil Science Laboratory of the Department of Land Resource Management and Agricultural Technology (LARMAT) for their assistance with CEC measurements; and Public Health Laboratory of the Department of Civil and Construction Engineering for assisting with TOC measurements. I also wish to thank all laboratory staff of the Department of Physics for their assistance at various stages, with special mention to Mr. Muthoka for his cooperation and invaluable help throughout the project.

Finally, my gratitude and thanks to the Chairman and administrative staff of the Department of Physics for facilitating so much in the course of this work, and to all who gave moral and material support.

# TABLE OF CONTENTS

<b>Title</b>	<b>i</b>
<b>Declaration</b>	<b>ii</b>
<b>Dedication</b>	<b>iii</b>
<b>Acknowledgements</b>	<b>iv</b>
<b>Table of contents</b>	<b>v</b>
<b>List of Figures</b>	<b>viii</b>
<b>List of Tables</b>	<b>x</b>
<b>List of symbols and abbreviations</b>	<b>xii</b>
<b>Abstract</b>	<b>xiv</b>
<b>Chapter 1: Introduction</b>	<b>1</b>
1.1 Background to the study	1
1.2 Magadi area	3
1.2.1 Location of Magadi area	3
1.2.2 Geology and physiography	4
1.3 Statement of the research problem	6
1.4 Objectives	6
1.4.1 General objective	6
1.4.2 Specific objectives	7
1.5 Justification and significance of the study	7
<b>Chapter 2: Literature Review</b>	<b>8</b>
2.1 Chapter overview	8
2.2 Analysis of radionuclides in ground waters	8
2.3 Salinization of the Magadi geothermal springs	11
2.4 Multivariate data analysis	12
<b>Chapter 3: Theoretical Background</b>	<b>14</b>
3.1 Chapter overview	14
3.2 Theory of gamma ray emission	14
3.3 Interaction of gamma rays with matter	15
3.3.1 Photoelectric absorption	15
3.3.2 Compton scattering	16

3.3.3 Pair production	17
3.4 Detection and measurement of gamma radiation	18
3.4.1 HPGe based gamma-ray spectrometry	18
3.4.2 Secular equilibrium	21
3.4.3 Determination of radionuclide activity concentrations	22
3.5 Multivariate chemometric methods	23
3.5.1 Principal Components Analysis (PCA)	23
3.5.2 Hierarchical Cluster Analysis (HCA)	24
3.5.3 Classification Trees (CT)	25
<b>Chapter 4: Materials and Methods</b>	<b>26</b>
4.1 Chapter overview	26
4.2 Sampling sites	26
4.3 Sample collection procedures	28
4.3.1 Collection of thermal water samples	28
4.3.2 Collection of rock samples	28
4.3.3 Collection of sediment samples	28
4.3.4 Collection of trona samples	28
4.3.5 Collection of control samples	29
4.3.6 Sample coding	29
4.4 Sample preparation	29
4.4.1 Preparation of solid samples for gamma-ray spectrometry	29
4.4.2 Preparation of liquid samples for gamma-ray spectrometry	29
4.5 Gamma-ray spectrometric analysis	30
4.5.1 Identification of radionuclides	30
4.5.2 Calculation of detection limits for gamma spectroscopic analysis	31
4.5.3 Determination of activity concentrations of radionuclides	31
4.6 Multivariate analysis physico-chemical data	32
<b>Chapter 5: Results and Discussion</b>	<b>34</b>
5.1 Chapter overview	34
5.2 Field observations	34
5.3 Gamma-ray spectrometry of field samples	36
5.3.1 Gamma-ray spectra	36
5.3.2 Detection Limits (DL)	37
5.3.3 Radionuclide activity concentrations	37
5.3.4 Statistical analysis of measured activity concentrations	42
5.4 Comparison with activity levels in endorheic basins and salts from different regions	51
5.5 Trona quality parameters	51
5.6 Multivariate chemometric analysis of spectral and calculated data	53
5.6.1 Principal components analysis (PCA)	53
5.6.2 Hierarchical cluster analysis (HCA)	60

5.6.3 Classification trees (CT)	62
<b>Chapter 6: Conclusion and recommendations</b>	<b>67</b>
<b>References</b>	<b>70</b>
<b>Appendix</b>	<b>76</b>

## LIST OF FIGURES

Figure 1.1: Location map of Magadi area	3
Figure 1.2: Lakes and other features along the Kenya and northern Tanzania Rift Valley	5
Figure 1.3: Relative elevations and groundwater links between Kenya Rift Valley lakes	6
Figure 3.1: Decay scheme of Cobalt-60	14
Figure 3.2: Schematic representation of positron annihilation after pair production	15
Figure 3.3: Schematic representation of the photoelectric effect	15
Figure 3.4: Schematic representation of Compton scattering	16
Figure 3.5: Schematic representation of the pair production process	17
Figure 3.6: Relative predominance of the three gamma ray interaction processes	18
Figure 3.7: Block diagram for HPGe based gamma-ray spectrometry	19
Figure 3.8: Comparative pulse height spectra for gamma rays in HPGe and NaI(Tl) detectors	20
Figure 4.1: Sampling locations	27
Figure 4.2: Schematic of gamma-ray spectrometry instrumentation	30
Figure 5.1: Gamma-ray spectrum for sample R8	36
Figure 5.2(a): Correlation curve for $^{238}\text{U}$ and $^{40}\text{K}$ activities in rocks	45
Figure 5.2(b): Correlation curve for $^{232}\text{Th}$ and $^{238}\text{U}$ activities in rocks	45
Figure 5.3: Correlation curve for $^{238}\text{U}$ and $^{40}\text{K}$ activities in sediments	46
Figure 5.4(a): Correlation curve for $^{232}\text{Th}$ and $^{40}\text{K}$ activities in spring waters	46
Figure 5.4(b): Correlation curve for $^{232}\text{Th}$ and $^{238}\text{U}$ activities in spring waters	47
Figure 5.5: Comparison of Th-232 activity concentration at different sampling locations	48
Figure 5.6: PCA plots for rock samples based on radionuclide activity concentrations	54
Figure 5.7: PCA plots of correlation loadings for radionuclides in rocks	54
Figure 5.8: PCA plots for rock samples based on gamma-ray spectra	56

Figure 5.9: PCA plots of rotated scores for sediment samples	57
Figure 5.10: PCA plots for thermal water samples based on radionuclide concentrations	58
Figure 5.11: PCA plots for thermal water samples based on gamma-ray spectra	59
Figure 5.12: PCA scatter plots for thermal water samples based on trona quality parameters	59
Figure 5.13: Dendrogram generated by hierarchical clustering of rock samples	61
Figure 5.14: Dendrogram generated by hierarchical clustering of thermal water samples	62
Figure 5.15: CT for predicting spring TDS based on their K-40 activity	64
Figure 5.16: CTs for predicting other spring water parameters	65
Figure 5.17: Correlation between measured and predicted spring TDS values	66

## LIST OF TABLES

Table 4.1: Locations of the sampled springs	26
Table 4.2: Recommended energy lines for gamma-ray analysis of environmental samples	31
Table 4.3: Reference data from certified reference materials (CRM)	32
Table 5.1: Physico-chemical properties of the Magadi spring waters	35
Table 5.2: Detection limits of radionuclides for HPGe gamma-ray spectrometry	37
Table 5.3: Average activity concentrations of radionuclides in rock samples	38
Table 5.4: Average activity concentrations of radionuclides in sediment samples	38
Table 5.5: Average activity concentrations of radionuclides in water samples	39
Table 5.6: Average activity concentrations of radionuclides in trona samples	39
Table 5.7: Activity concentrations of radionuclides in control samples	40
Table 5.8: Average activity concentrations in processed salt products and mine tailings	40
Table 5.9: Statistical summary of activity concentrations of radionuclides in rock samples	42
Table 5.10: Statistical summary of activity concentrations of radionuclides in sediments	42
Table 5.11: Statistical summary of activity concentrations of radionuclides in thermal waters	43
Table 5.12: Summary of correlation analyses of radionuclides in samples	44
Table 5.13(a): Radionuclide activity ratios in rock samples	49
Table 5.13(b): Radionuclide activity ratios in sediment samples	49
Table 5.13(c): Radionuclide activity ratios in thermal water samples	50
Table 5.14: Correlation coefficients between ratios of radionuclide pairs	50
Table 5.15: Comparison of radionuclide activities in salts from different parts of the world	51
Table 5.16(a): Solute content of the Magadi springs	52
Table 5.16(b): Relative solute content of the Magadi springs	52
Table 5.17: PC scores and correlation loadings for K-40, U-238 and Th-232 in rock samples	55



## LIST OF SYMBOLS, ACRONYMS AND ABBREVIATIONS

ADC	Analog to Digital Converter
asl	above sea level
BDL	Below detection limit
BqKg <sup>-1</sup>	Becquerels per kilogram
Bqm <sup>-3</sup>	Becquerels per cubic meter
CT	Classification Trees
CEC	Cation Exchange Capacity
cmol <sup>+</sup> /Kg	centi-mols of hydrogen ions per kilogram
COD	Chemical Oxygen Demand
FWHM	Full Width at Half Maximum
Ge(Li)	Lithium drifted germanium (detector)
GPS	Global Positioning System
HBRA	High Background Radiation Area
HPGe	Hyper Purity Germanium (detector)
HCA	Hierarchical Cluster Analysis
IAEA	International Atomic Energy Agency
INAA	Instrumental Neutron Activation Analysis
LSC	Liquid Scintillation Counting
LDA	Linear Discriminant Analysis
MCA	Multi-Channel Analyzer
meq <sup>+</sup> /100g	milliequivalent H <sup>+</sup> per 100 grammes of sample
meq <sup>+</sup> /g	milliequivalent H <sup>+</sup> per gramme of sample
NaI(Tl)	Thallium activated sodium iodide (detector)
NORM	Naturally Occurring Radioactive Materials
%m/m	percentage mass per mass
PCR	Principal Components Regression
PCA	Principal Components Analysis
PLS	Partial Least Squares

ppm	parts per million
ppb	parts per billion
r	correlation coefficient
s.g.	specific gravity
Si(Li)	Lithium drifted silicon (detector)
TDS	Total Dissolved Solids
TIMS	Thermal Ionization Mass Spectrometry
TOC	Total Oxidizable Carbon
T <sup>0</sup>	Temperature
UNESCO	United Nations Educational, Scientific and Cultural Organization
UNSCEAR	United Nations Scientific Committee on the Effects of Atomic Radiation
REE	Rare Earth Element
Z	Nuclear charge
2D	Two Dimensional
XRF	X-ray fluorescence

## ABSTRACT

The Magadi endorheic basin of Kenya, with its high heat flows due to magmatic activity, extremely saline geothermal manifestations, and vast deposits of trona, presents a complex closed ecosystem that is challenging to characterize and model. The Magadi basin is located in the southern part of the Kenya Rift Valley; an arid volcano-active continental rift that is part of the East African Rift Valley system. The area is bound by longitudes  $36^{\circ} 00'E$  and  $36^{\circ} 30'E$  and latitudes  $1^{\circ} 40'S$  and  $2^{\circ} 10'S$ . Lake Magadi lies to the south of the basin and is recharged mainly by highly alkaline geothermal springs around it. Being endorheic, the lake depends entirely on evaporation for hydrogeological balance. This, however, could make the lake a natural sink for radiopollutants from the surrounding geological, geothermal and anthropogenic activities.

We have measured activity concentrations and performed multivariate exploratory characterization of the radionuclides in relation to the modulating physico-chemical parameters of the Magadi basin. The main goal was to detect, measure and quantify as well as classify and relate the activity levels of  $^{40}K$ ,  $^{238}U$  ( $^{226}Ra$ ),  $^{232}Th$ , and  $^{210}Pb$ , and to characterize their sources and distribution within the Magadi basin in relation to the quality of trona mined from the lake. This was realized via HPGe based gamma-ray spectrometry of trachyte rock, thermal water, sediments and raw trona from the basin as well as of processed soda ash and cattle salt from the Magadi Soda Company. The radionuclide activity concentrations and gamma spectra of the samples were analyzed using PCA, HCA and CT chemometric tools in order to classify, extract latent patterns, and model the radionuclide levels with respect to the sampling sites and spring  $T^{\circ}$ , pH, s.g., TDS, TOC,  $Na_2CO_3$ ,  $NaHCO_3$  and NaCl levels.

The mean activity concentrations of K-40, U-238 and Th-232 radionuclides in Bq/Kg were  $1614 \pm 14.0$ ,  $162.3 \pm 13.5$  and  $120.1 \pm 15.1$  respectively in rocks,  $1875.8 \pm 10.8$ ,  $131.2 \pm 9.9$  and  $188.2 \pm 5.6$  respectively in sediments and  $127.6 \pm 21.7$ ,  $41.7 \pm 22.3$  and  $55.9 \pm 17.8$  respectively in thermal water samples. K-40 and Th-232 were found to be accumulating within the Magadi basin with enrichment coefficients of 1.2 and 1.6 respectively. These levels are not as significant as would be expected for such a sink with constant contribution from the geothermal springs and weathering of surrounding volcanics in addition to both wet and dry atmospheric deposition; showing that the spring recharges have low-level radioactivity. Temperatures above  $80^{\circ}C$  were observed to enhance thorium sorption capacity in sediments. Three regimes of alkaline spring inflows were found to contribute to and affect the quality of trona deposits in the lake and were delineated based on their radionuclide activity concentrations, feature selected gamma spectral signatures and solute content. These are:  $Na_2CO_3$ - and NaCl- rich inflows from the south;  $NaHCO_3$ - rich inflows from the north; and saline fluid inflows from the host bedrock bounding the western edges of the lake.

Statistical analysis showed log normal distribution of the radionuclides within the basin, probably due to different radionuclide signatures of the spring recharges. PCA, HCA, CT and statistical analysis of the radionuclide levels and distributions in relation to thermal water temperatures, pH, TDS, TOC, and sediment CEC revealed marked diversity in the geochemical properties of the source rocks responsible for the spring solutes, and the presence of an underlying uranium-rich rock source. The Magadi basin is a sink for radiopollutants and a quasi HBRA.

## Chapter One

# INTRODUCTION

### 1.1 Background to the study

Every geothermal system has an underlying heat source which heats its reservoir. This can be ambient heat from deep in the interior of the earth or hot magmatic intrusions. The intrusions may be hot from their origin (interior of the earth) or due to decay of radioactive elements like uranium, thorium, and potassium in them (Burger *et al.*, 2006; UNESCO, 2008). About twenty percent of geothermal systems on earth draw their heat from the earth's interior while the rest draw heat from radioactive decay of elements (Burger *et al.*, 2006). Most of these geothermal fields occur in continental rifts which are characterized by high heat flows and volcanism. These geothermal fields may be associated with the volcanoes or fissure eruptions that occur on the floors of these rift systems (Riaroh and Okoth, 1994).

Volcanic lava is rich in silicate minerals but a few volcanoes produce lava which is rich in carbonatite. Several carbonatite volcanoes and extrusions are found in East Africa (Yanda and Madulu, 2005). Such areas are known to exhibit higher than normal background radiation levels which have been associated with the carbonatite rocks. This suggests high activity concentration levels of radionuclides in carbonatites. Such places include among others Homa and Ruri hills in South Nyanza (Achola *et al.*, 2012), Mrima hill at the Coast (Patel, 1990), Oldonyo Nyegi and Shompole volcanoes in Magadi area (Mustapha, 1999) -all in Kenya, and Oldonyo Lengai to the south of Lake Natron in northern Tanzania (UNESCO, 2008).

Oldonyo Lengai is the only active carbonatite volcano on earth and produces a special type of lava called natrocarbonatite which is extremely soluble in water and is easily washed away by rains or circulating ground water (UNESCO, 2008). The radionuclides in carbonatites are also believed to be carried along in the ground water flows. These ground waters ultimately flow into Lake Magadi; being the lowest point in this region, likely causing radiogenic enrichment in the lake. Volcanic rocks influence the chemical composition of spring waters since their weathering produces ground flows and run-off waters rich in dissolved minerals and elements (Yanda and Madulu, 2005; Eugster, 1986). Volcano-sedimentary accumulation due to such kind of weathering results in the presence of several minerals within rift basins including trona, gypsum and fluorspar (Yanda and Madulu, 2005). The large trona deposits in Lake Magadi are produced by such a process.

Lake Magadi, and associated geothermal features, is located at the centre of a flat depression which occurs at the lowest point in the southern Kenya Rift Valley (Riaroh and Okoth, 1994). Hydrogeological studies based on isotopic evidence and piezometric levels indicate that this is the point to which all ground water flows in the southern Kenya and northern Tanzania rift is directed (Clarke *et al.*, 1990; Munro, 2002; Becht, 2005). This makes Lake Magadi a possible sink

for radionuclides and heavy metals from the weathering of surrounding volcanics in addition to both wet and dry atmospheric deposition. The geothermal features consist of over 200 hot springs and seepages distributed along the shores of Lake Magadi, which issue from the base of fault scarps bounding the lake and flow into the lake through small channels in the shore sediments (Riaroh and Okoth, 1994). Radionuclides having two or more oxidation states like  $^{238}\text{U}$  can easily form complexes with water thereby enhancing their solubility and immobilization in ground water flows (Arogunjo, 2007). Due to their interaction with the underlying magmatic intrusions which heat them, these spring waters may have enhanced NORM levels which also impact Lake Magadi.

Lake Magadi is a major source of soda ash and other products like common salt, industrial salt and cattle salt, which are processed from its trona deposits. Soda ash and industrial salt are used for industrial purposes like glass and detergent manufacture as well as production of other industrial chemicals while the other products are mainly used for domestic purposes. These are possible radionuclide exposure avenues should the products be contaminated.

Samples of fine and coarse trachytes, sediment, and thermal fluid from 48 sites around Lake Magadi were studied in order to verify the hypothesis of radiopollutants accumulating in Magadi basin and to achieve the research objectives. Of great interest were sites adjacent to alkaline hot springs; this is because the hot springs are believed to be the entry points for the radiopollutants into the lake. Sediments were used to evaluate radionuclide accumulation levels within the basin. This is because sediments have good sorption ability for radionuclides and trace heavy metals. Trachyte rocks served as reference matrix in evaluating the possible accumulation of the radiopollutants. Thermal fluid was used to evaluate the possible enhancement and immobilization of NORM in the lake by the hot springs. Raw trona from the lake, processed soda ash and cattle salt as well as mine tailings from the Magadi Soda Company plant were also sampled for analysis. The raw trona samples were used to evaluate the possible exposure of the public to the radiopollution. The samples were analyzed for their radionuclide content using HPGe gamma-ray spectrometry. CEC for each of the sediment samples were determined. For each sampled spring, the temperature of thermal fluid was determined *in-situ* using a digital thermometer while the pH, s.g., TOC and TDS were determined in the laboratory. These were determined in order to relate their levels to the radionuclide activity concentrations.

The radionuclide activity concentrations were analyzed using multivariate chemometric techniques in order to classify, extract patterns, and model the occurrence and levels with respect to temperature, pH, s.g., TOC, TDS values and sampling sites. The chemometric techniques employed were Principal Components Analysis (PCA), Hierarchical Cluster Analysis (HCA), and Classification Trees (CT). PCA and HCA were used for classification and pattern recognition while CT was used to model radionuclide activity in relation to TDS levels in the spring waters.

## 1.2 Magadi area

### 1.2.1 Location

Magadi area is located in the southern part of the Kenya Rift Valley; an active continental rift that is part of the East African Rift Valley system. The area is bound by longitudes  $36^{\circ} 00' E$  and  $36^{\circ} 30' E$  and latitudes  $1^{\circ} 40' S$  and  $2^{\circ} 10' S$ , and covers approximately  $1600 \text{ Km}^2$ . Lake Magadi lies in the southern end of the area and covers approximately  $100 \text{ Km}^2$ . Magadi township lies on the eastern shores of the lake and is the home of Magadi Soda Company- presently owned by Tata Chemicals Limited of Mumbai, India. The lake is approximately 40 km long and 3.2 km broad along a causeway across it (Fig 1.1).

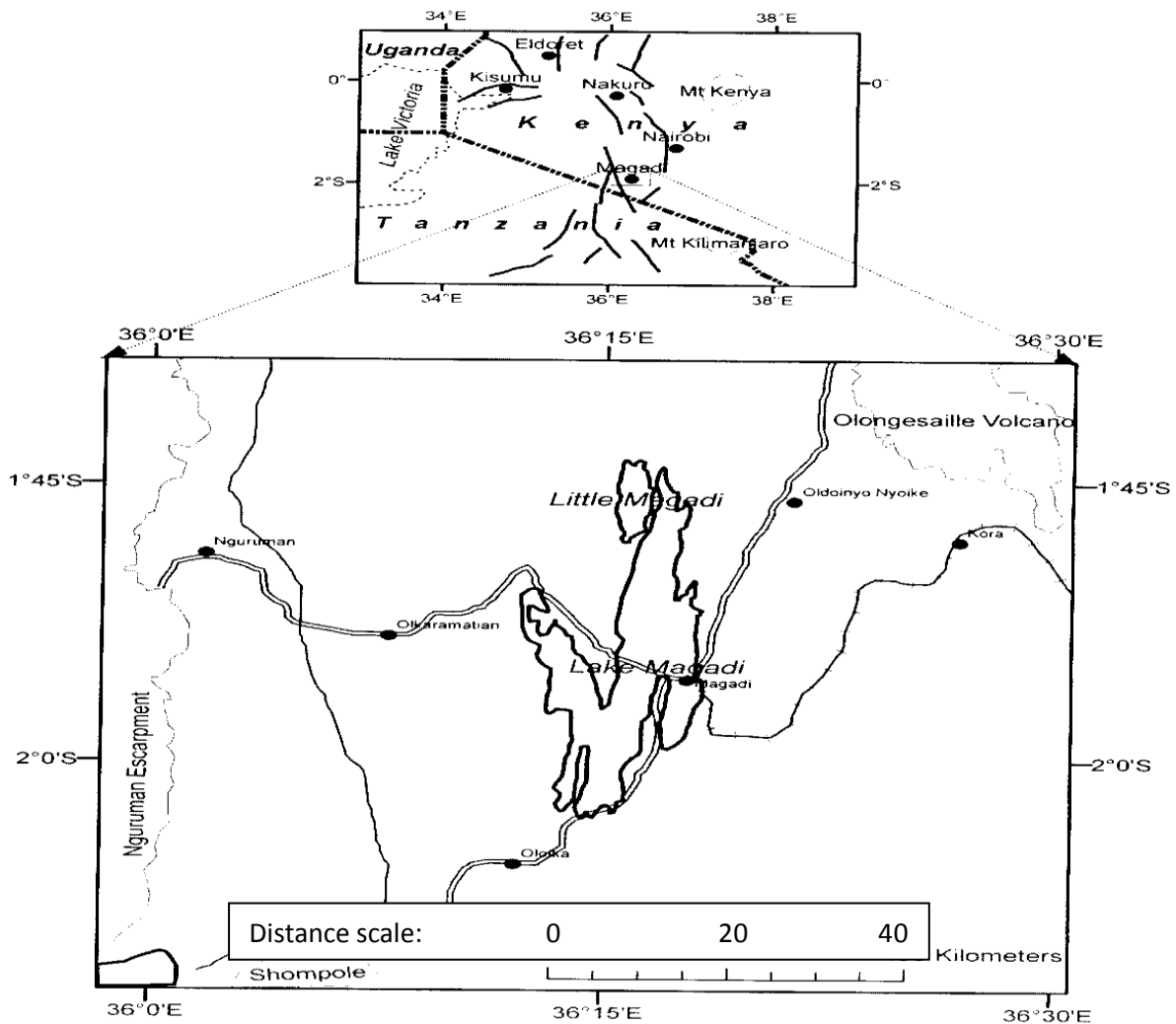


Figure 1.1: Location map of Magadi area(Ibs-Von,2001).

### 1.2.2 Geology and physiography of Magadi area

According to Baker (1958), the central part of the Magadi area is broken by numerous sub-parallel youthful escarpments characterized by quartzite and biotite gneiss. The hills on the south east have numerous kyanite and gneiss outcrops. The remainder of the area is characterized by tertiary and quaternary volcanic rocks comprising trachytes (60-65% silica and the rest  $\text{Na}_2\text{O}/\text{K}_2\text{O}$ ), nephelinites (about 95 % silica), olivine basalts (20% quartz, 10% feldspathoid and the rest silica), andesites (57-63 % silica), tephrites (about 95 % feldspathoid), and fluvial sediments. The greater part of the area is semi arid. January and February are the hottest months with temperatures at times rising to  $42^\circ\text{C}$  in the early afternoon. During the dry season, the lake is 80 % covered by trona, making it a large salt pan. During the rainy season, a thin layer of brine coats the lake but soon evaporates leaving vast amounts of salt. Thermal manifestations in the form of hot springs on the shores of the lake and high heat flows of between  $69.92^\circ\text{C}/\text{Km}$  and  $111.53^\circ\text{C}/\text{Km}$  suggest magmatic activity in the area (Githiri *et al.*, 2011) and/or, probably, natural radioactivity as the source of the heat.

The Magadi basin, in which Lake Magadi is located, is the centre and lowest point of a region of about 100 km radius in the southern Kenya and northern Tanzania Rift Valley (Riaroh and Okoth, 1994). Along the Rift Valley, this region stretches from Lake Naivasha in Kenya to the Oldonyo Lengai volcano in northern Tanzania (Fig 1.2). Lake Naivasha provides underground recharge for Lake Magadi as shown in Figure 1.3. This may also be the case with Lake Natron in northern Tanzania.

The base of Lake Magadi is just about 430 m above sea level. The lake has no outflows and all surface and ground water flows in the region are directed towards it (Clarke *et al.*, 1996; Munro, 2002; Becht, 2005). These ground water flows and rainfall that drain underground are heated geothermally. The hot water then dissolves chemical compounds of sodium and potassium that occur in underground rock strata and the solution comes to the surface in the form of hot alkaline springs along the edges of the lake. The lake was probably formed, and is maintained, by these springs. The number of individual springs near the lake is large since a group of springs often consists of a large number of small seepages rising in the sediment deposits at the lake shore. Although certain sections of the lake shore have no springs at all, there are many stretches along which there are innumerable seepages, rising usually within a meter of lake level and running down to form a strip of thick alkaline flow that separates the trona from the shore (Baker, 1958).

Surface recharge for the lake is mainly by these hot springs since there is very little surface runoff in this region. Over the years, extensive studies have been done on the springs to identify and quantify their solutes in order to determine their contribution to the salt deposits in Lake Magadi. Several theories have been advanced to explain the origin of the solutes in the hot springs. Such theories include Parkinson's theory (Parkinson, 1914), Steven's hypothesis and The Recirculation theory (Stevens, 1932) among others. The most interesting feature is that the amount of soda in the lake is increasing much faster than the Magadi Soda Company can remove it

(Stevens,1932). On this estimate, therefore, the soda deposits are almost inexhaustible. According to Baker(1958), the factors responsible for the soda accumulation at Lake Magadi are:

- i. The complete absence of outlets.
- ii. Absence of significant surface inflows of fresh water.
- iii. Large area of surrounding volcanics over which leaching takes place.
- iv. High rate of surface evaporation due to the semi arid climate.
- v. Accumulation of a body of alkaline ground water beneath the Magadi basin due to its location in the lowest part of the Rift Valley.
- vi. The activity of the springs in keeping the lake in existence as a large evaporating pan and in supplying the alkaline waters for evaporation.

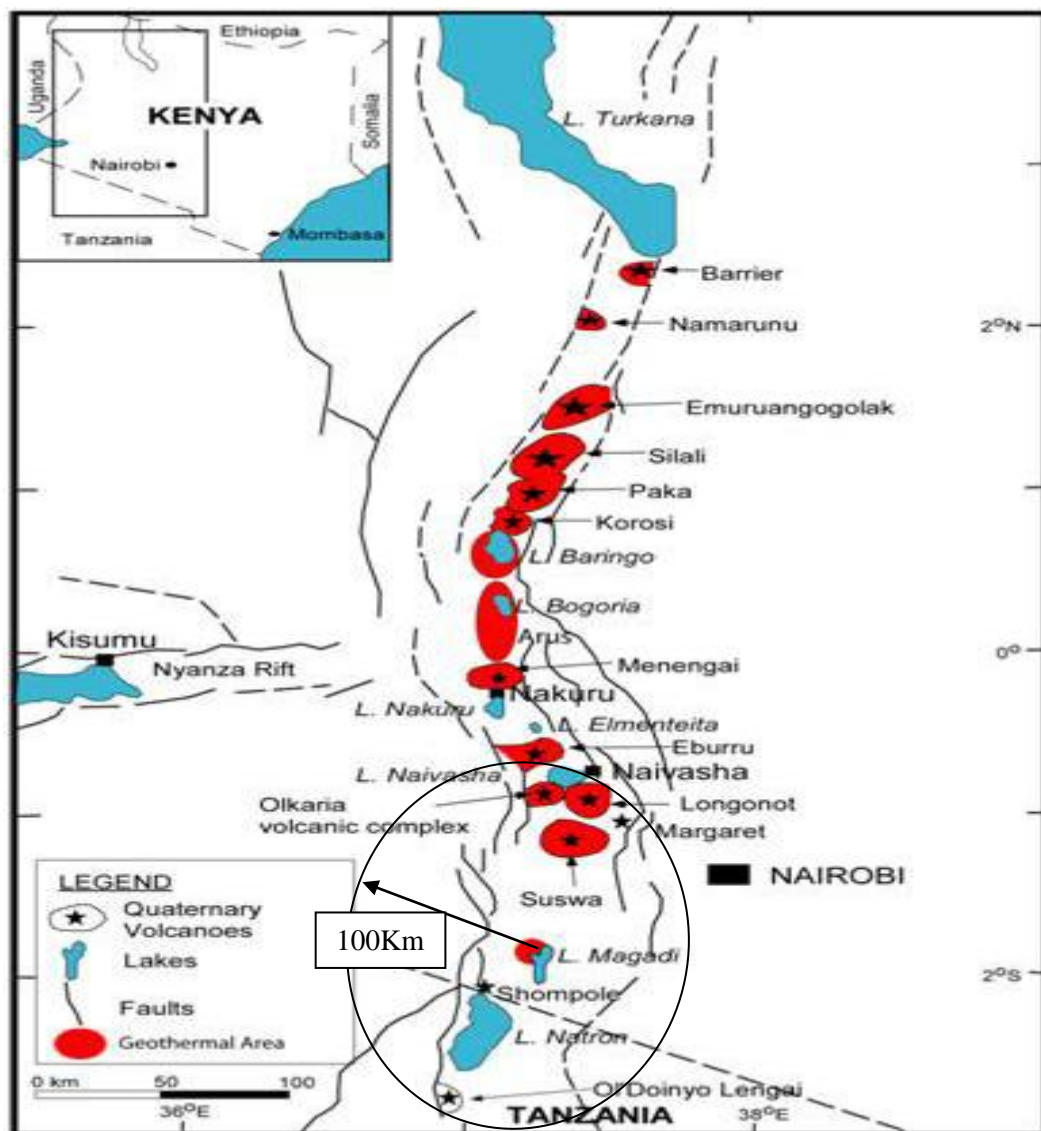


**Figure 1.2:** Lakes and other features along the Kenya and northern Tanzania Rift Valley (Modified from Riaroh and Okoth (1994)).

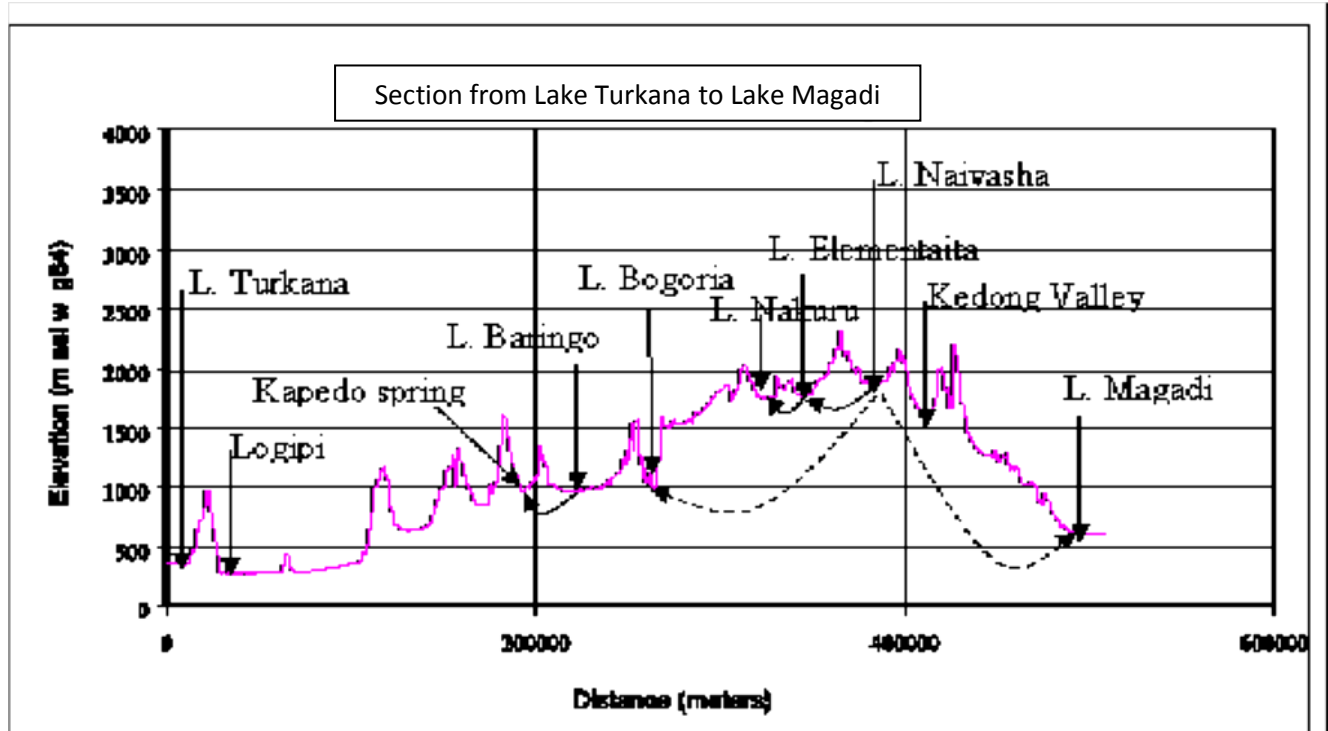


*Figure 1.3: Relative elevations and groundwater links between Kenya Rift Valley lakes (Becht, 2005).*

### 1.3 Statement of the research problem

Lake Magadi is an ‘inexhaustible’ natural source of trona. The trona accumulates in the lake because the lake has no outflows of water whatsoever and depends entirely on evaporation for hydrogeological balance. The solute content of the lake water is not lost during evaporation, making the lake a possible sink for radiopollutants from the surrounding geological, geothermal and man-made activities, particularly the frequent natrocarbonatite eruptions of the Oldonyo Lengai volcano. A comprehensive radiometric analysis of the lake’s water sources and associated matrices is necessary in order to characterize and model their radionuclide levels in relation to temperature, pH and salinity, and delineate the basin’s radiogenic systematics. So far however, most studies in the area have focused on quantifying the saline content of the waters. Combined with multivariate data analysis, such a study could provide a rapid and efficient method for ecosystem quality assessment in relation to trona quality.

### 1.4 Objectives

#### 1.4.1 General objective

The goal of this study was to measure, classify and relate the origin and activity concentrations of  $^{40}\text{K}$ ,  $^{238}\text{U}$  ( $^{226}\text{Ra}$ ),  $^{232}\text{Th}$ , and  $^{210}\text{Pb}$  in rocks, sediments, spring waters and trona, and to characterize their sources and interrelations within the Magadi basin in relation to trona quality.

### 1.4.2 Specific objectives

The specific objectives were:

- i. To identify, measure and determine activity concentrations of  $^{40}\text{K}$ ,  $^{238}\text{U}$  ( $^{226}\text{Ra}$ ),  $^{232}\text{Th}$  and  $^{210}\text{Pb}$  in trachyte rocks, sediments and thermal fluids from the Lake Magadi basin using HPGe based gamma-ray spectrometry.
- ii. To identify, measure and determine the activity concentrations of  $^{40}\text{K}$ ,  $^{238}\text{U}$  ( $^{226}\text{Ra}$ ),  $^{232}\text{Th}$  and  $^{210}\text{Pb}$  in raw trona from Lake Magadi and processed soda ash and cattle salt as well as settler tailings from the Magadi Soda Company using HPGe based gamma-ray spectrometry.
- iii. To characterize the alkaline hot springs around Lake Magadi based on their radionuclide activity concentrations in relation to their locations and levels of  $\text{Na}_2\text{CO}_3$ ,  $\text{NaHCO}_3$  and  $\text{NaCl}$ .
- iv. To perform a multivariate exploratory analysis of the data in (i), (ii) and (iii) above using PCA, HCA and CT chemometric tools in order to classify, discern latent patterns, and relate the radionuclide identity and activity concentrations of the hot springs to variations in their pH,  $T_0$ , s.g., TOC and TDS, sediment CEC, and their location within the Magadi basin.

### 1.5 Justification and significance of the study

Radionuclides, which have serious long term effects on flora and fauna, could be accumulating with the trona deposits in Lake Magadi based on the foregoing analysis. The trona comes from various springs characterized by different temperatures and which are also thought to have different types and activity concentrations of the radionuclides as well as pH, TDS, TOC and s.g. The univariate statistical methods normally used for analysis of data from Lake Magadi are insufficient for purposes of classification, pattern recognition and correlation between variables since these relationships are multivariate and complex. Multivariate chemometric analysis techniques are better suited for such kind of analysis.

Besides industrial uses, salt products processed from the trona at Lake Magadi also have some domestic uses including seasoning of food, softening of hard water for home use, as mineral supplement for cattle, manufacture of soaps and baking powder, among others. Many ethnic groups in East and Central Africa have for a long time been, and still continue, using magadi soda as a condiment in cooking traditional dishes. These are possible exposure pathways to radionuclides should the products be contaminated. It is therefore important to characterize the alkaline springs around Lake Magadi in terms of their radionuclide signatures as well as to monitor the radionuclide content of trona products from the lake. It should also be interrogated whether the Magadi Soda Company further contributes to the possible build up of contaminants in the lake by disposing of settler tailings, and probably other effluent from its plant, into the Lake.

## Chapter Two

# LITERATURE REVIEW

### 2.1 Chapter overview

This chapter explains the basis of this study. Section 2.2 presents an overview of radionuclide analyses of ground waters and minerals in continental rifts and geothermal fields around the world. Section 2.3 explores the geophysical and geological factors possibly responsible for the salinization of the springs at Lake Magadi and attempts to explain the origin of the spring solutes. Section 2.4 enumerates the range and complexity of environmental and geochemical problems that can be solved by analytical spectroscopy coupled with multivariate chemometrics.

### 2.2 Analysis of radionuclides in ground waters

Radionuclide analyses have been done in several regions around the world for various purposes including; geothermal reservoir exploration (Jennejohn, 2009), ecological impact assessment (Kansaana *et al.*, 2012), geochemical characterization (Agora, 2012), and tracing ground water evolution (Ammar *et al.*, 2011) among others. In such studies, normally activity concentrations and spectra are analyzed multivariately to achieve these objectives.

Yadav and Sarin (2009) analyzed waters of Lake Sambhar in India for salt and NORM content in order to geochemically characterize the water sources of the lake. Based on differences in the distribution of Ra-226 and Ra-228, the authors identified two distinct regimes of waters in the lake: saline lake waters associated with evaporating pan and subsurface brines, and ground waters. Within the Jordan valley of Middle East, which has same physiographical characteristics as the Magadi basin of Kenya, chemical and isotope composition has been used to delineate three major sources of solutes that differentially affect the quality of ground water and salt deposits within the valley: hypersaline brines, highly soluble salts in the host sediments, and recharge of anthropogenic effluents (Faber *et al.*, 2012).

Tagma *et al.* (2011) investigated the geochemistry and abundances of naturally occurring radionuclides in shallow ground water from the western part of Al Bahira aquifer in Youssofia area of Morocco and used this information to characterize these ground waters. They discovered wide ranging TDS in the waters (275 mg/L – 5000 mg/L), which showed the activity concentration of Radium-226 in the ground water did not directly correlate to TDS but seemed to be affected by other factors such as water temperature. They interpreted the ratios of the short-lived Ra-224 to Ra-223 to indicate that the radium was derived from a uranium-rich source with a low Th/U ratio in the rock source and the water was unsafe for drinking.

In another study by Warner *et al.* (2011), geothermal waters from southern and central Morocco were analyzed for naturally occurring radionuclides (Ra and U) and isotopes of strontium, boron and radium. The waters were characterized by a wide range of salinity (400 – 2200 mg/L) with the ratio of the short lived Ra-224 to Ra-223 ranging from 2 to 40 while that of Sr-87 to Sr-86 ranged from 0.7076 to 0.7122. Both results indicated that the Ra was derived from a uranium rich rock source with low Th/U ratio.

In an attempt to determine the influence of geological characteristics on ground water and the vulnerability of aquifers to the influences of anthropogenic activities in Slovenia, Korun *et al.*(2011) measured the concentrations of U-238, Ra-226, Pb-210, Ra-228, and Th-228 in the waters. These ranged from 1.2 Bq/m<sup>3</sup> to 16.9 Bq/m<sup>3</sup>, 0.2 Bq/m<sup>3</sup> to 16.2 Bq/m<sup>3</sup>, 0.5 Bq/m<sup>3</sup> to 32.8 Bq/m<sup>3</sup>, 0.1 Bq/m<sup>3</sup> to 5.1 Bq/m<sup>3</sup> and 0.1 Bq/m<sup>3</sup> to 1.0 Bq/m<sup>3</sup> respectively. The authors employed data mining to achieve their main goal by correlating the results with the properties of the sampling points and concluded that aquifers were quite vulnerable to pollution by anthropogenic activities.

Ammar *et al.*(2011) used uranium isotopes to trace the evolution of ground waters in Complexe terminal aquifer in Tunisia. They used Thermal Ionization Mass Spectrometry (TIMS) to analyze ground water samples for uranium isotopes and reported a range in U-238 concentration and U-234/ U-238 activity ratios of 1.75 - 8.12 ppb, and 1.14 to 3.18 respectively. Because the mobility of uranium in ground water is controlled by many factors including pH and Eh, and also because high U-234/ U-238 ratios reflect preferential dissolution of U-234 relative to U-238 due to the alpha recoil, the authors concluded that there was a mixing between recharging and aquifer waters with distinct U-234/U-238 activity ratios as well as U-238 concentrations. An investigation has also been carried out using radionuclide levels, salinity and temperature to characterize expected sources of ground water in the United Arab Emirates (UAE). Two water modes were relatively easily separated by their TDS content and temperature as well as Cl<sup>-</sup>, CO<sub>3</sub><sup>2-</sup> and SO<sub>4</sub><sup>2-</sup> (Murad *et al.*, 2011).

The Dead sea basin of Israel has very similar physiographical and geological characteristics with the Magadi basin of Kenya. Both occur in large depressions at very low altitudes within continental rifts. The Dead sea occurs below sea level. Both also have very high TDS levels in their waters due to lack of outflows from them. Characterization of the carbon system in the saline ground water of the Dead sea has been done using analysis of stable and radiogenic carbon isotopes in order to estimate the flow rates of both fresh and saline ground water (Avrahmov *et al.*, 2011). The study concluded that the dominant process was not just a mixing between fresh ground water and Dead sea water but that there were additional processes involved. The relatively high levels of <sup>14</sup>C in some ground waters (86 against 80 pmc in Dead sea) were interpreted to imply that despite the general trend of decreasing sea levels, sea brine still penetrates into the aquifer.

The mean annual effective dose due to intake of salt from the Kherwa salt mines of Pakistan has been determined and found to be lower than the average annual effective dose rate received from the ingestion of natural radionuclides in water and foods (Balochi *et al.*, 2012). Amid concern that people are consuming inadequate amounts of iodine, scientists have found that 53% of iodized table salt samples in the US, and perhaps rest of the world, contain less than the recommended level of this key radionuclide nutrient (Science Daily, 2008). Kansaana *et al.*(2012) have investigated radioactivity levels in saline waters and salts from the Panbros salt industry of Accra, Ghana in order to assess human exposure to NORMs due to the intake of the salts. The results indicate insignificant radiological health hazard to the public due to consumption of the salts since, according to their results, the annual effective dose to an individual due to intake of natural radionuclides in the salts was below  $0.29 \text{ mSvyr}^{-1}$ - the average radiation dose received per person worldwide due to ingestion of natural radionuclides (UNSCEAR,1998).

Kerich *et al.*(2010) analyzed trace elemental composition of cherts and magadite from Magadi, Bogoria, Eburu, and Olkaria East fields within the Kenya Rift Valley in order to relate these sites and reported that cherts from some of these sites shared distinctive elemental and radiogenic compositional characteristics (like high U to Th ratios and high absolute concentrations of U, Nb and Zr relative to REEs); implying ground water links between some of these sites. Agora (2012) has analyzed the levels and distribution of natural radionuclides in different rock types within Kerio valley and reported elevated natural radionuclide activity in rocks from the fluorspar mines to the south compared to the rest of the valley; probably due to volcano-sedimentary accumulation of radionuclides with the fluorspar. This, probably, is also the case with the accumulation of trona in Lake Magadi.

Hardly have any studies been done to characterize sources and levels of radionuclides in an endorheic basin. Over the years, extensive chemical studies have been done on the spring and lake waters at Lake Magadi for purposes of identifying their saline solutes. It has been discovered that the various springs that dot the shores of the lake have varying saline content (Stevens,1932). However, information on radionuclide occurrence and levels within the Magadi basin is almost non-existent. Lake Magadi is endorheic and depends on evaporation for water balance. However, evaporation does not carry away the solute content of the lake hence the accumulation of trona. Radionuclides are also thought to accumulate this way in the lake. Fine shore sediment is also known to have good sorption ability for trace elements (Minervini,1998) and probably radioisotopes. The aim of this study was to identify, measure and characterize the radionuclides and their activity concentrations within the Magadi basin in relation to the saline content and other physico-chemical parameters of the spring waters and the geophysical characteristics of the area.

### 2.3 Salinization of the Magadi geothermal springs

Lake Magadi is a semi solid soda lake completely surrounded by vast natural salt deposits. It is the second largest source of Soda Ash in the world; producing in excess of 150,000 metric tonnes annually. The lake has in the past been described by some researchers as a natural wonder of the world (Parkinson, 1914 and Stevens, 1932). These researchers wondered the process that gave rise to large accumulations of salts in the lake, since, they argued, there are several other rift valley lakes in East Africa with no outlets, whose waters also come from volcanic rocks and geothermal springs, yet have no deposits of salts. These other rift valley lakes have underground outflows of water. Lake Magadi has none.

Even though underneath water sources are suspected based on water balance studies, the springs around Lake Magadi are so far thought to be solely responsible for the vast salt deposits there. The sources of the springs could be varied. Based on water balance, relative elevations, and analysis of isotopes, it has been shown that ground water flows from Lake Naivasha to Lake Magadi (Becht, 2005). Muno (2002) suggested that basins in the southern rift valley of Kenya are hydrologically connected by a regional flow system perhaps through a yet little understood basal aquifer. The area is highly characterized by shallow magmatics and grid faults, which allow escape of underground water as hot springs (Githiri *et al.*, 2011). The Lake Magadi geothermal field is characterized by fissural eruptions which are essentially trachytic in composition (Riaroh and Okoth, 1994). The chemical compositions of the spring inflows into Lake Magadi are influenced by the weathering of these trachyte volcanic (Eugster, 1998). Weathering of volcanic rocks produces waters rich in  $\text{Na}^+$  and  $\text{HCO}_3^-$  - the major ions in trona (Yanda and Madulu, 2005). The bicarbonates of the base elements sodium, potassium, calcium and magnesium are formed by the action of carbonated meteoric water and can convert to normal carbonates by the loss of carbon dioxide.

Due to the frequent eruptions of the Oldonyo Lengai volcano near the south end of Lake Natron in northern Tanzania, a thin white crust of soda has been observed on the ash beds laid down as a result of the eruptions. These soda crusts are left after various eruptions have been leached by rain water (Yanda and Madulu, 2005). The solutions resulting from such leaching have contributed to the accumulation of sodium carbonate in Lake Natron. There is a likelihood that Lake Natron provides underground recharge for Lake Magadi hence transferring some of its salt content there, and probably radionuclides, because trona from the two lakes have been found to have very similar chemical composition; consisting mainly of trona ( $\text{CO}_3^{2-}$  and  $\text{HCO}_3^- > 10.4$  meq/g) mixed with halite and either kogarkoite or villiaumite respectively (Nielsen and Dahi, 2011).

These possible explanations are not exhaustive and a lot still needs to be explained about the origin of the Lake Magadi spring solutes. The springs and trona deposits at Lake Magadi therefore come from different sources with different geological characteristics hence could probably have different radioactivity levels and physical-chemical parameters. This research

sought to measure and characterize radionuclide types and levels in relation to TDS, temperature, pH, TOC and s.g. in the spring waters, rock and trona quality.

## **2.4 Multivariate chemometric analysis of environmental and geochemical data**

Multivariate exploratory analysis of data has been used in various studies to derive useful information from large data sets and variables supplied by analytical techniques. Voncina *et al.* (2007) applied multivariate analysis (HCA, PCA and LDA) to radionuclide levels in relation to pH, temperature, time, and 9 other physical chemical parameters of ground waters from 214 wells around Slovenia in order to monitor their general pollution, identify pollution sources and plan pollution prevention measures. The study enabled the opportunity to follow the quality of ground waters from different wells at different times of the year. Farmaki *et al.* (2012) have proposed a new optimization for sampling and monitoring the quality of water for domestic and industrial supply to the city of Athens, Greece based on multivariate exploratory analysis. They achieved this by applying supervised (LDA and CT) and unsupervised (PCA and HCA) multivariate pattern recognition techniques to physical chemical data sets of water reservoir sources.

Chemical compositional information of Instrumental Neutron Activation Analysis (INAA) has been combined with multivariate techniques to create a geographical classification of pottery sherds from the South East of USA by Pizarro *et al.* (2008). The application of multivariate exploratory analysis combined with variables selection and data pre-treatments is therefore useful in recognizing compositionally homogeneous groups of samples that may be associated with different geographical sites.

A study of major and trace elements, O-18, H-2, H-3, C-13, C-14 and strontium isotopes combined with multivariate analysis and remote sensing data have been used to better understand the complex groundwater flow pattern and water-rock interactions in the tectonically active Ethiopian Rift Valley (Osenbrueck *et al.*, 2013). The study indicates that groundwater flows from the escarpments into the rift valley, complying with the general hydro-chemical evolution towards NaHCO<sub>3</sub> type ground water. Additional information on contributing groundwater components and processes were obtained from a PCA of the hydro-chemical and isotopic data.

The applicability of multivariate data analysis to extract latent relationships in EDXRF spectral data, and the feasibility of forming a chemical compound classification based on characteristic fluorescence and scattered X-ray radiation has been demonstrated (Kesller *et al.*, 2002). PCA was exploited to distinguish between spectra from different chemical compounds and also played an important role in the estimation of influences of different physical and technical parameters on spectra of different chemical compounds without packing. Goraieb *et al.* (2006) used X-ray fluorescence (XRF) spectroscopy and multivariate data analysis to distinguish types of Portland cements as well as quantify some of their constituent elements. The cement samples were classified by their distinct calcium concentrations and their origins defined by means of PLS.

Direct differentiation of ionic species in different matrices has been achieved through application of multivariate data analysis on spectral data (Oliveira *et al.*, 2010). The study achieved direct speciation of chromium (Cr-III and Cr-VI) using conventional X-ray spectrometry with calculated limits of detection and quantification being lower than 17 and 50 ppm for the two ionic species respectively.

It can be seen from these studies that the range and complexity of problems that can be solved by analytical spectroscopy may be increased by application of multivariate data analysis e.g. chemometrics. Chemometrics is a chemical discipline that uses mathematical and statistical procedures to provide maximum information by analyzing data obtained from analytical techniques (Kurt and Peter, 2008). Chemometrics is most popular in the application of multivariate data analysis of complex sample matrices. Chemometrics enables extraction of relevant physical and chemical information from extensive and complex multivariate data such as spectroscopic measurements. In this study, multivariate chemometrics has been used to analyze gamma-ray spectrometric and physical-chemical data of geothermal field matrices from Lake Magadi for purposes of classification, pattern recognition and exploratory modeling.

## Chapter Three

# THEORETICAL BACKGROUND

### 3.1 Chapter overview

In this chapter, the basic principles of HPGe based gamma-ray spectroscopy and the quantification approaches in gamma-ray spectral data analysis are presented. The principles of chemometrics techniques (PCA, HCA and CT) as well as their utility in multivariate data analysis are also discussed.

### 3.2 Theory of gamma-ray emission

Gamma rays are high energy electromagnetic waves produced by the disintegration of nuclei and also decay of certain sub-atomic particles. Gamma radiation is often produced alongside other forms of radiation such as alpha and beta particles. When an unstable atomic nucleus decays to a stable state, the daughter nucleus is sometimes produced in an excited state. The subsequent decay of excited daughter results in the emission of gamma rays (Fig 3.1). One or more gamma photons can be emitted from the excited state of the daughter nucleus following decay.

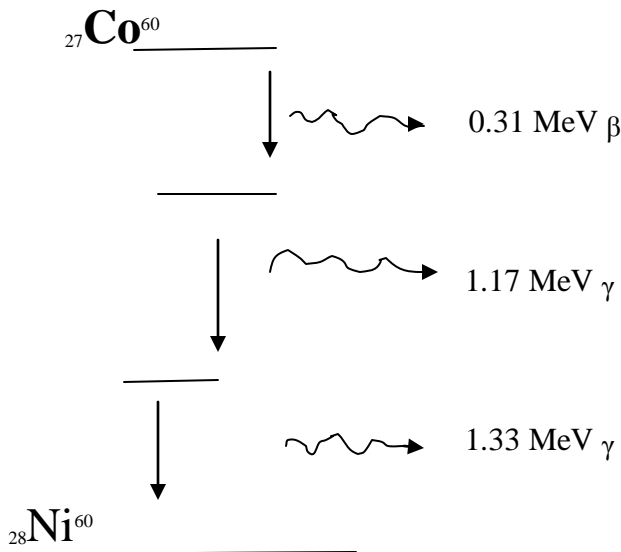


**Figure 3.1:** Decay scheme of Cobalt-60.

Gamma rays can also be produced through the process of positron annihilation. As a positron ( $e^+$ ) comes to rest, it combines with one of the many free electrons in the surroundings to produce two annihilation gamma photons. Since momentum is conserved during this process, the photons are of the same energy (511 KeV) and recoil in opposite directions. The energies of the two gamma ray photons add up to an energy equivalent of  $2m_0c^2$ - the energy sum of the disappearing electron-positron pair.

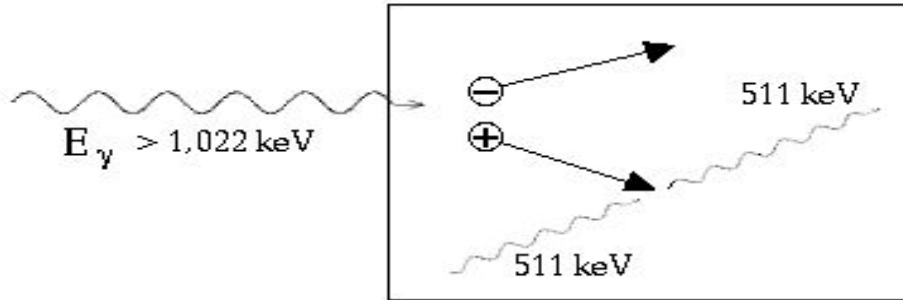


**Figure 3.2:** Diagrammatic depiction of positron annihilation preceded by pair production. (Knoll, 1997)

### 3.3 Interaction of gamma rays with matter

Gamma photons interact with matter in various ways as they move through it. The three predominant interaction processes are photoelectric absorption, Compton scattering, and pair production. In all the three processes, electrons are generated which deposit their energy as they move through matter (Knoll,1997).

#### 3.3.1 Photoelectric absorption

In photoelectric absorption, a gamma photon is absorbed by an atomic electron with the subsequent ejection of an electron from the atom. The energy of the ejected electron ( $E_e$ ) is given by the relation (Debertin and Helmer,1988):

$$E_e = h\nu - E_b \quad (3.1)$$

where  $h\nu$  is the incident gamma photon energy and  $E_b$  is the binding energy of the photoelectron (ejected electron) in the atom.

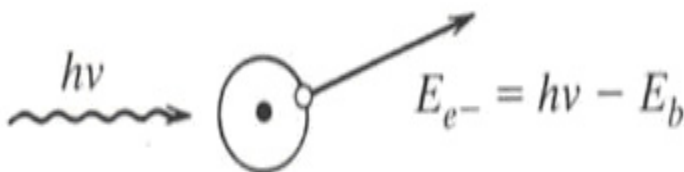


**Figure 3.3:** Diagrammatic representation of photoelectric effect.(IAEA,2003)

The nucleus absorbs the recoil momentum resulting from the ejection of the photoelectron since a free electron cannot absorb a photon and also conserve momentum at the same time (Nicholas,1995). An electron from an outer atomic shell falls into the empty inner state left by the ejected photoelectron. This transition results in the emission of an X-ray photon with energy

in the range of 100 KeV. This X-ray photon may generate another photoelectron, with the net result of successive interactions and the net energy deposited in matter being proportional to the incident photon energy. The initial photoelectron carries off the greater percentage of the original gamma photon energy.

The probability of photoelectric absorption per atom ( $\tau$ ) over all ranges of E and Z is given by (Knoll,1997):

$$\tau = \text{constant } (Z^n/E^{3.5}) \quad (3.2)$$

where n varies between 4 and 5 over the gamma ray region of interest. The dependence of  $\tau$  on Z of absorber material is the principal reason for the use of high Z materials in gamma ray shields e.g. lead. The photoelectric process is the predominant mode of interaction for gamma rays of relatively low energy but negligible for high energy gamma rays. This is because of the strong dependence of  $\tau$  on E as seen in equation (3.2). The photoelectric attenuation coefficient ( $\mu_{pe}$ ) can be given by (Gordon, 2008):

$$\mu_{pe} = \tau\rho N_A/A \quad (3.3)$$

where  $\rho$  is the density of the absorber material, A is its average atomic mass and  $N_A$  is the Avogadro's number.

### 3.3.2 Compton scattering

In Compton scattering, only a portion of the incident gamma photon is transferred to a free (recoil) electron while the remainder appears as a secondary (scattered) photon. The scattered photon is deflected through an angle  $\Theta$  with respect to the direction of the incident gamma photon. The recoil electron exits at an angle  $\phi$  with respect to the direction of the incident gamma photon.

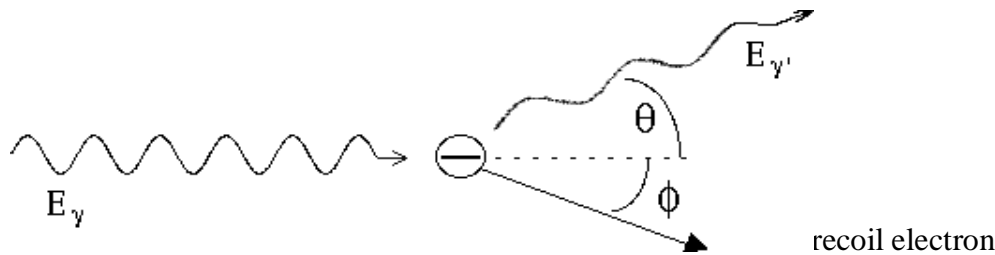


**Figure 3.4:** Diagrammatic representation of Compton scattering.(Johnson,2011)

Because all angles of scattering are possible, the energy transferred to the electron varies from zero to a maximum of the incident gamma photon energy. The scattered gamma photon has a longer wavelength and therefore less energy than the incident photon. The change in wavelength of the scattered photon ( $\Delta\lambda$ ) depends on the angle of scattering ( $\Theta$ ) according to the equation below:

$$\Delta\lambda = [h/m_0C] (1-\cos \Theta) \quad (3.4)$$

where  $m_0$  is the electron rest mass,  $C$  is the speed of electromagnetic radiation in vacuo and  $h$  is Planck's constant. The probability of the scattered photon interacting a second time depends on several factors including its energy, size and type of the medium of interaction, and the position of the first interaction. Depending on the size of the interacting medium, there is always a chance that the scattered photon may escape without a second interaction.

### 3.3.3 Pair production

Pair production involves the conversion of a gamma photon into a positron-electron pair within the nuclear Coulomb field. For this process to occur, the incident photon energy must be at least twice the rest mass energy of an electron (1.022 MeV). Because of this, pair production is predominant with high energy gamma photons. Any excess energy is shared by the resulting particle pair as kinetic energy. Thus, the total kinetic energy ( $T$ ) of the electron-positron pair is given by the relation:

$$T = (E - 1.022) \text{ MeV} \quad (3.5)$$

where  $E$  is the energy of the incident gamma photon in MeV. The kinetic energy of the pair is deposited in the interacting matter. While in motion, the positron can combine with an atomic electron resulting in the production of two annihilation gamma photons each of energy 511 KeV.

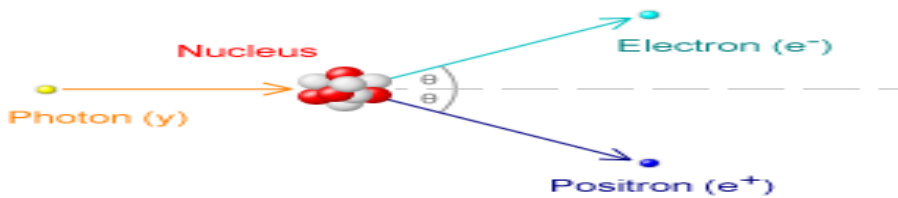


**Figure 3.5:** Diagrammatic representation of pair production process. (Johnson, 2011)

The probability of each of the three interaction mechanisms occurring varies with the gamma ray energy and  $Z$  of the absorber material (Fig 3.6). Photoelectric absorption predominates at low energies and is greatly enhanced in materials with high atomic number. For this reason, elements of high atomic number are preferred for use as detectors for gamma ray energy measurements. Compton scattering is the most common interaction mechanism for moderate energies (few hundred KeV to several MeV). Pair production predominates for higher energies and it is also enhanced in materials with high atomic numbers. Figure 3.6 shows the relative predominance of the three gamma ray interaction mechanisms.

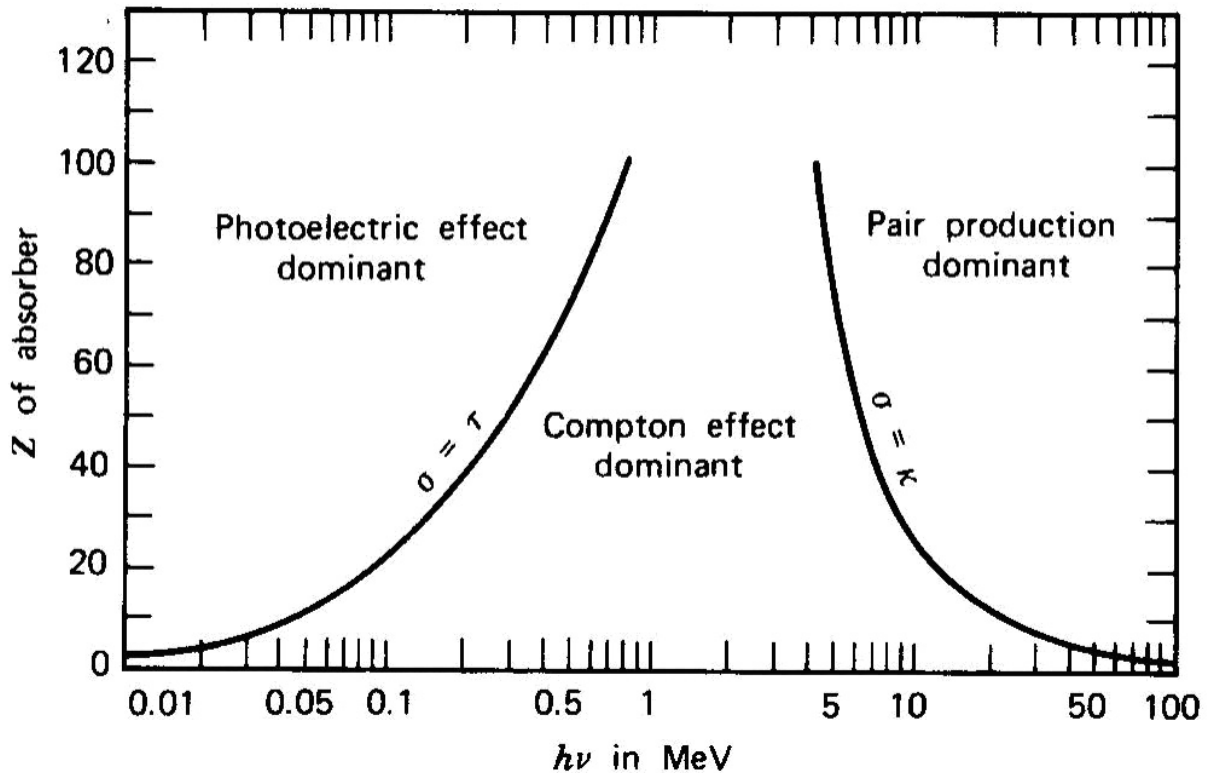


*Figure 3.6: Relative predominance of gamma ray interaction processes (Knoll,1997).*

### 3.4 Detection and measurement of gamma radiation

Gamma radiation can be measured by detecting atomic disintegrations that occur in a sample and counting the number of these events that occur during a specific time period. Scientific instruments employ one of several technologies including HPGe crystal detection, LSC, proportional counting, among others. HPGe crystal counting was used in this work.

#### 3.4.1 HPGe based gamma-ray spectrometry

HPGe based gamma-ray spectrometry is a technique that can be used to detect and measure gamma ray photons from radionuclide sources. The HPGe detector system consists of a lead shielded HPGe detector, a multi-channel analyzer (MCA) and analysis software on a desktop computer (Fig 3.7). The HPGe detector has a much greater thickness and narrower band gap compared to other detectors because it is constructed from ultrapure germanium so as to improve depletion depth. These characteristics give it better counting efficiency and high energy resolution, making it very convenient for use in gamma-ray spectroscopy. Because of its small band gap (0.7 eV), room-temperature operation of germanium detectors of any type is impossible due to the large thermally induced leakage current that would result (Knoll,1997). The HPGe detector must be cooled to reduce the leakage current to the point that the associated noise does not compromise its good energy resolution. Normally, the temperature is reduced to 77 K

through the use of an insulated dewar in which a reservoir of liquid nitrogen is kept in thermal contact with the detector, or other cooling alternatives. However, the HPGe detector can be allowed to warm up to room temperature between measurements without any problem unlike the Ge(Li) which must be continuously maintained at low temperatures to prevent a catastrophic redistribution of the drifted lithium that will rapidly take place at room temperature. This operational advantage is the major reason that the HPGe detectors have supplanted Ge(Li) configurations. Fabrication techniques have been developed to the point that modern HPGe detectors will withstand indefinite cycling of the temperature. Modern HPGe systems incorporate a preamplifier as part of the cryostat package. This is important in order to locate the preamplifier as close as possible to the detector so as to minimize capacitance. The input stages of the preamplifier normally are also cooled along with the detector to reduce electronic noise. Figure 3.7 shows the arrangement of the components of HPGe based spectrometry. Germanium detectors have excellent energy resolution for gamma-ray spectroscopy compared to other detector types for this range of energies (Knoll,1997). This allows for the separation of many closely spaced gamma-ray energies which remain unresolved in other detectors like NaI(Tl); HPGe can resolve up to two gamma rays that are within 0.8 KeV of each other (Randolph,1996). Figure 3.8 compares pulse height spectra for HPGe and NaI(Tl).

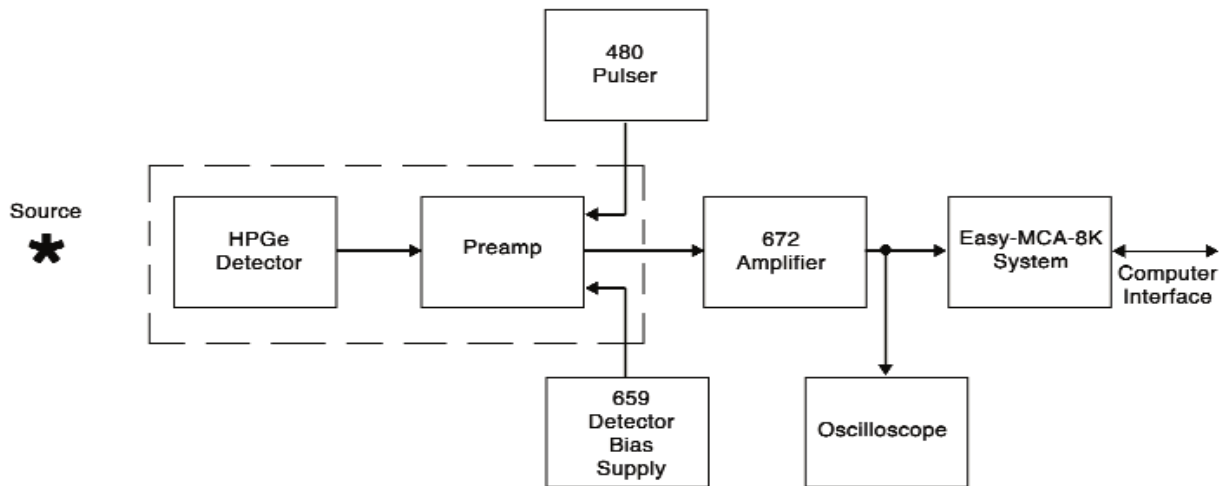


**Figure 3.7:** Block diagram for HPGe based gamma-ray spectrometry.(Knoll,1997)

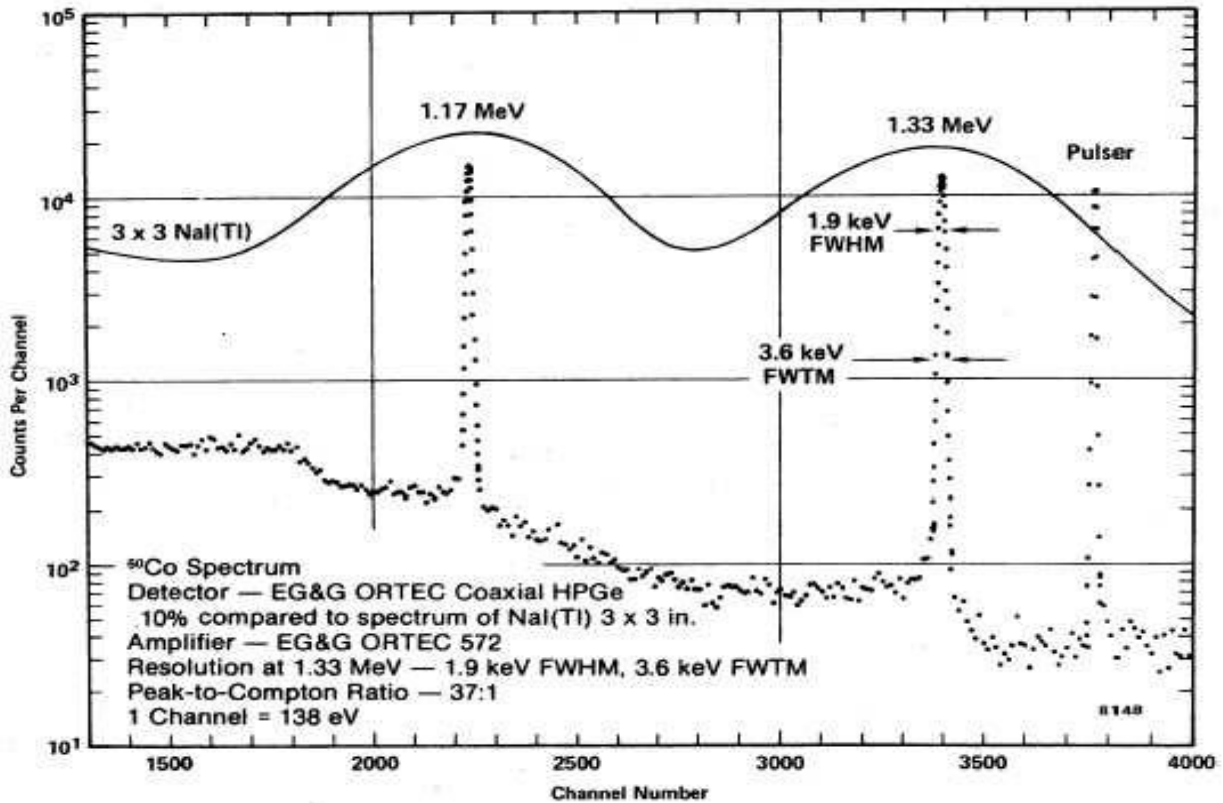


*Figure 3.8: Comparative pulse height spectra for HPGe and NaI(Tl) detectors. (Knoll,1997)*

The MCA, which may be considered as a series of single channel analyzers (SCA) with incrementing narrow windows, consists of an ADC, control logic, memory and display. The MCA achieves pulse height analysis by sorting successive signal pulses into parallel amplitude channels. The ADC converts analog signals (pulse amplitudes from detector) to equivalent digital signals (numbers). An input gate controls movement of pulses from the detector into the ADC by blocking pulses from reaching the ADC during the time period when it is busy digitizing a previous pulse. The control logic picks memory locations for storage of the digitized signals, holds the input gate open when the ADC is not busy, and closes it when the ADC is busy. The memory stores the digitized pulses and has addressable locations corresponding to the maximum number of channels into which the recorded spectrum can be divided. The number of channels to be used for measurements depends on the degree of resolution required and the total number of counts that can be obtained. Having very few number of channels results in distortions and loss of resolution in the spectrum, while having too many channels leads to a low number of counts per channel resulting in large statistical fluctuations (noise) which could obscure small additional peaks. Depending on the resolution of a detector, the optimum number of channels should be 4 per FWHM of peak (Knoll,1997). The MCA used for this work had 8192 channels. The display presents the digitized information as pulse height spectra.

The resolution (R) of the detector can be worked as below (Knoll,1997):

$$R = \frac{\text{FWHM}}{H_0} \quad (3.6)$$

where FWHM is the width of the response function at half its height while  $H_0$  is the energy of the centroid channel. The resolution of a detector improves as the response function gets narrower. R is dimensionless and conveniently expressed as a % or simply as the FWHM.

The time during which a MCA cannot take in an analog pulse is called its dead time ( $\tau$ ).  $\tau$  comprises of the processing time of the ADC and the memory storage time, and can be worked out as below (Knoll,1997)

$$\tau = N (1/\nu) + B \quad (3.7)$$

where N is the channel number in which the pulse is stored,  $\nu$  is the frequency of the clock oscillator and B is the pulse storage time.

### 3.4.2 Secular equilibrium

Total activity of a radionuclide undergoing a radioactive process is calculated by considering a long-lived parent decaying into a short-lived daughter which in turn decays into a stable nuclide. In this case the half life of the two radionuclides - the parent and the daughter, are such that the half life of the parent ( $T_1$ ) is far much greater than that of the daughter ( $T_2$ );  $T_1 \gg T_2$ . The total activity at any time is the sum of the parent radionuclide and daughter radionuclides. The rate of decay of daughter atoms -  $dN_2/dt$  is equal to the rate at which they are produced.

The relationship between the activity of the parent radionuclide ( $A_1$ ) and that of the daughter radionuclide ( $A_2$ ) at any time t is given by the equation

$$A_2 = A_1 [1 - \exp(-\lambda_2 t)] + A_{20} \exp(-\lambda_2 t) \quad (3.8)$$

where  $\lambda_2$  is the decay constant of the daughter radionuclide, t is the time lapse, and  $A_{20}$  is the initial activity of the daughter radionuclide.

The activity  $A_2$  then builds up after several daughter half-lives to the point when  $A_2 = A_1$  at which time the daughter activity is equal to that of the parent (Gordon, 2008). This condition is termed secular equilibrium between the parent radionuclide and its decay products. This means that a chain of short lived daughter radionuclides can be in secular equilibrium with a long lived parent. The activity of each member of the chain is equal to that of the parent. Hence, any member of the chain can be used to present the activity concentration of the parent radionuclide.

### 3.4.3 Determination of activity concentrations of radionuclides from gamma-ray spectra

Because of the different types of gamma interactions that take place inside the detector, energy from the photons is not always completely absorbed by the detector, which results in variations in detector efficiency. There occur peaks representing total absorption of gamma rays from the source and other peaks that represent partial absorption. Based on the measured count rates under the photopeaks corresponding to the gamma rays of  $^{40}\text{K}$  and other radionuclides in the  $^{232}\text{Th}$  and  $^{235}\text{U}$  decay series, the activity concentrations of relevant radionuclides in the samples can be determined. The procedure for quantification relies on the establishment of secular equilibrium between  $^{226}\text{Ra}$  and the short-lived decay products of radon in the samples (Mohanty *et al.*, 2004). The activity concentration of  $^{232}\text{Th}$  is determined from the average concentrations of  $^{212}\text{Pb}$  and  $^{228}\text{Ac}$  in the samples while that of  $^{226}\text{Ra}$  ( $^{238}\text{U}$  equivalent) is determined from the average concentrations of  $^{214}\text{Pb}$  and  $^{214}\text{Bi}$ . The well known spectral interference between the gamma lines of  $^{226}\text{Ra}$  (186.20 KeV) and  $^{235}\text{U}$  (185.70 KeV) is inevitable, especially in the presence of a relatively high uranium concentration, and therefore the 186.20 KeV line is normally not used for the determination of activity concentration of  $^{238}\text{U}$  equivalent.

The activity concentrations of natural radionuclides in the samples ( $A_s$ ) are computed after spectral deconvolution by custom software on a computer linked to the spectrometer. Several quantification methods are available for use. The comparative method uses the following relation (Mustapha, 1999):

$$\frac{A_s M_s}{I_s} = \frac{A_r M_r}{I_r} \quad (3.9)$$

where  $A_s$ ,  $M_s$  and  $I_s$  are radionuclide activity concentration, mass and radionuclide intensity of sample while the right hand side are the same quantities for the reference standard. The second method involves efficiency calibration of the detector and uses the following relation (Arogunjo, 2007):

$$A_s = \frac{A}{\epsilon P_r M} \quad (3.10)$$

where  $A$  is radionuclide intensity in counts per second,  $\epsilon$  is the detector efficiency for a particular gamma-ray energy,  $P_r$  is the transition probability of gamma decay and  $M$  is mass of the sample. Another method also involves efficiency calibration of the detector system and uses the relation (Otwoma *et al.*, 2013)

$$A_s = \frac{C}{\epsilon t f} \quad (3.11)$$

where  $C$  is radionuclide intensity in counts per second,  $\epsilon$  is detector efficiency,  $t$  is counting time in seconds and  $f$  is the branching ratio i.e. number of photons per hundred disintegrations of the radionuclide of interest.

The gamma-ray detector is normally calibrated for energy and detection efficiency using certified reference materials and standard reference sources. The comparative method was used in this study because it was not possible to determine the efficiency of the detector system as at the time of counting; a requirement for the two other methods.

### **3.5 Multivariate chemometrics methods**

Chemometrics is the science of relating analytical measurements and physical-chemical data obtained from samples via application of mathematical or statistical methods (Hibbert *et al.*, 2009). Chemometrics is most popular in application of multivariate data analysis. Chemometric methods have the ability to extract important features from complex spectral data and hence can be developed for a specific use. Chemometrics can handle several problems such as determination of the concentration of a chemical specie in a complex mixture (Angeyo *et al.*, 1999), classification of the origins of samples (Voncina *et al.*, 2007; Pizarro *et al.*, 2008), prediction of a property or activity of a chemical compound (Jing *et al.*, 2011), recognition of the presence or absence of substructures in the chemical structure of an unknown compound (Oliveira *et al.*, 2010), and industrial and environmental process monitoring (Peters *et al.*, 2011; Goraieb *et al.*, 2006). Multivariate chemometrics considers the correlation, both linear and non-linear, of many variables simultaneously. The typical chemometrics strategy is data driven and consists of the following steps: (i) collection of data, (ii) generation of a mathematical model, (iii) interpretation of model parameters in terms of underlying relationships, and (iv) application of the model to new cases (Hibbert *et al.*, 2009).

A set of multivariate data describes objects (gamma-ray spectra in this case) and features (radionuclide activity concentration in the sample matrix). Multivariate chemometric tools are used in an attempt to overcome the limitations of classical analytical techniques. Environmental measurements are generally multivariate in nature (Richard, 1998) with some information hidden in the complex data. Multivariate analysis makes it possible to structure the data sets in a way that makes more sense from them. Multivariate techniques can be classified into two broad categories: Supervised and unsupervised methods. Supervised methods are used to construct prediction models based on current measurements to classify future samples (Kenneth and Randy, 1998) while unsupervised methods are used for pattern recognition in data sets (clustering). Examples of supervised methods are Partial Least Squares Regression (PLSR), Linear Discriminant Analysis (LDA), Classification Trees (CT) and Soft Independent Modeling of Class Analogies (SIMCA) while examples of unsupervised methods are Principal Component Analysis (PCA), Principal Components Regression (PCR) and Hierarchical Cluster Analysis (HCA). PCA, HCA and CT were employed in this study as explained below:

#### **3.5.1 Principal Components Analysis (PCA)**

PCA is a bilinear modeling technique which gives an interpretable overview of spectral data in a reduced multidimensional space. It performs dimension reduction of the original data set,

modeling of data, detection of outliers, selection of main variables, pattern recognition, and validation and prediction of samples (Brereton, 2003). PCA eliminates redundant information by obtaining a small data set that makes the data treatment and interpretation easier. The original data matrix is mean centered by subtracting the mean spectrum  $\bar{x}$  from each sample spectrum. The centered data matrix  $\mathbf{x}_c$  is decomposed to a score matrix  $\mathbf{T}$  and loading matrix  $\mathbf{P}$  by consecutive orthogonal subtraction of the target variation in data until the variation left is unsystematic.

$$\mathbf{X}_c = \mathbf{TP}^T + \mathbf{E} \quad (3.12)$$

where  $\mathbf{T}$  = scores matrix ( $\mathbf{T} = n \times A$ ),  $\mathbf{P}^T$  = loading matrix ( $\mathbf{P}^T = A \times \mathbf{P}$ ),  $\mathbf{E}$  = matrix of residuals, and  $A$  = intrinsic dimension (no. of principal components [PCs] necessary to describe all the information in the data set).  $\mathbf{P}$  describes the new axis which is built on the original.  $\mathbf{T}$  describes the position of the samples in the new co-ordinate system. The loading vectors can be considered as hidden profiles in the data that are common to all data. The scores are the amount of hidden profile in the individual spectra: the scores contain quantitative information such as activity levels. The PCs are plotted as orthogonal axes giving 2D scatter plots of the score vectors. These depict covariance between samples hence providing a data overview. In this study, PCA was used to classify the samples based on their gamma-ray spectra and activity levels, and to probe for any patterns in their distribution in relation to thermal water temperature, pH, TOC and trona quality.

### 3.5.2 Hierarchical Cluster Analysis (HCA)

HCA is a distance based pattern recognition technique that employs the interpoint distances between data sets to draw a relationship between samples. Several distance types can be used for such classification: (i) Euclidian distance; which uses straight line distances between points, (ii) Squared Euclidian; which uses squared Euclidian distances, (iii) Manhattan; which uses vector component distances between points, (iv) Pearson correlation; uses Pearson correlation coefficient, and (v) Squared Pearson; which uses squared Pearson correlation coefficient. Manhattan, Pearson and squared Pearson are not preferred for use in HCA because they are more likely to change the output due to the several steps involved in computing them. Squared Euclidian uses the same method as Euclidian but does not take the square root of the value obtained. As a result, clustering with squared Euclidian is faster than clustering with Euclidian. However this is also likely to change the output of HCA. These methods are preferred for use in K-Means clustering. Euclidian distance was used in this study. The Euclidian distance  $\mathbf{d}$  between any two samples is defined by

$$\mathbf{d} = \sum_{i=1}^i \sqrt{(x_i - j)^2} \quad (3.13)$$

where  $i$  is the number of measurements, and  $x$  and  $j$  are distance measurements from a reference point to any two successive samples in a set. Results of HCA are often presented in a graphical form called a dendrogram. Samples are organized in a row on the horizontal axis according to their similarities. The vertical axis represents the similarity measure at which successive objects join a group. The dendrogram is thus presented using the nearest neighbor or average linkage and correlation coefficient for similarities. For this work, dendrograms were used to examine the relationships between the sampling sites, based on their radionuclide species and activity levels in relation to spring pH, temperature, TDS, s.g. and TOC. This related sites with near similar parameters by linking them to each other in clusters. It was important to examine the dendrograms in conjunction with PCA because they both perform classification and pattern recognition but in different forms.

### **3.5.3 Classification Trees (CT)**

A CT is a rule for predicting the class (e.g. sampling site) of an object (sample) from the values of its predictor variables (e.g. radionuclide activity level). Spectral pattern CTs are used for classification and model construction, based on similarities/dissimilarities of classes. The method involves a recursive subdivision of data to produce a classification tree (also called decision tree). This procedure provides validation tools for exploratory and confirmatory classification analysis and applies any one of three methods to produce the CT: segmentation; to identify samples that are likely to be members of a particular group, stratification; assign samples into one of several categories such as high, medium and low, and prediction; create rules and use them to predict future events

The trees can be constructed based on any one of the criteria CHAID, CRT or QUEST. The CHAID criterion allows for identification of homogenous samples with low uncertainties and makes it easy to construct rules for making predictions about other measurements.

CTs based on CHAID criterion were used to discover features and extract patterns from the data sets that were important for discrimination and predictive modeling of the sampling sites based on their radionuclide type and activity levels in relation to other physico-chemical parameters.

These multivariate chemometric techniques, and more, have been developed into application software packages that are available for use from different software development houses e.g. The Unscrambler from Camo Inc., Statistica from Umetrics, Matlab from MathWorks and SPSS from IBM.

## Chapter Four

# MATERIALS AND METHODS

### 4.1 Chapter overview

This chapter explains the field experimental and laboratory (analytical) procedures employed in this study. The multivariate chemometric procedures used in the analysis of the spectral and measured physico-chemical data are also explained.

### 4.2 Sampling sites

Forty eight (48) sites in the Magadi basin were sampled for trachyte rock, bottom sediment, thermal water, and trona. Trachyte was chosen because the Magadi basin is characterized by fissural eruptions which are trachytic in nature (Riaroh and Okoth,1994). The sampling sites were adjacent to 12 springs having clear points of issue and significant thermal water flows along the shores of Lake Magadi. Table 4.1 describes the locations of the 12 sampled springs while Figure 4.1 shows their positions in the Magadi basin.

**Table 4.1:** Locations of the sampled springs

Spring no. code	Geographical location	Position of spring
1	North of the North-West lagoon	36 <sup>0</sup> 11.20°E, 1 <sup>0</sup> 54.10°S
2	North of the western end of the Magadi causeway	36 <sup>0</sup> 12.50°E, 1 <sup>0</sup> 55.30°S
3	South-Western lagoon	36 <sup>0</sup> 11.50°E, 1 <sup>0</sup> 58.30°S
4	West of Bird Rock lagoon	36 <sup>0</sup> 11.50°E, 1 <sup>0</sup> 59.60°S
5	East of Bird Rock lagoon	36 <sup>0</sup> 13.00°E, 1 <sup>0</sup> 59.40°S
6	Graham's lagoon	36 <sup>0</sup> 13.50°E, 1 <sup>0</sup> 58.60°S
7	North-Eastern lagoon	36 <sup>0</sup> 15.00°E, 1 <sup>0</sup> 50.90°S
8	North-East of "Little Magadi"	36 <sup>0</sup> 15.00°E, 1 <sup>0</sup> 50.60°S
9	North of "Little Magadi"	36 <sup>0</sup> 14.60°E, 1 <sup>0</sup> 50.50°S
10	North-West of "Little Magadi"	36 <sup>0</sup> 14.40°E, 1 <sup>0</sup> 50.20°S
11	West of "Little Magadi"	36 <sup>0</sup> 13.80°E, 1 <sup>0</sup> 50.50°S
12	Western shores, opposite Northern lagoon	36 <sup>0</sup> 13.60°E, 1 <sup>0</sup> 53.70°S

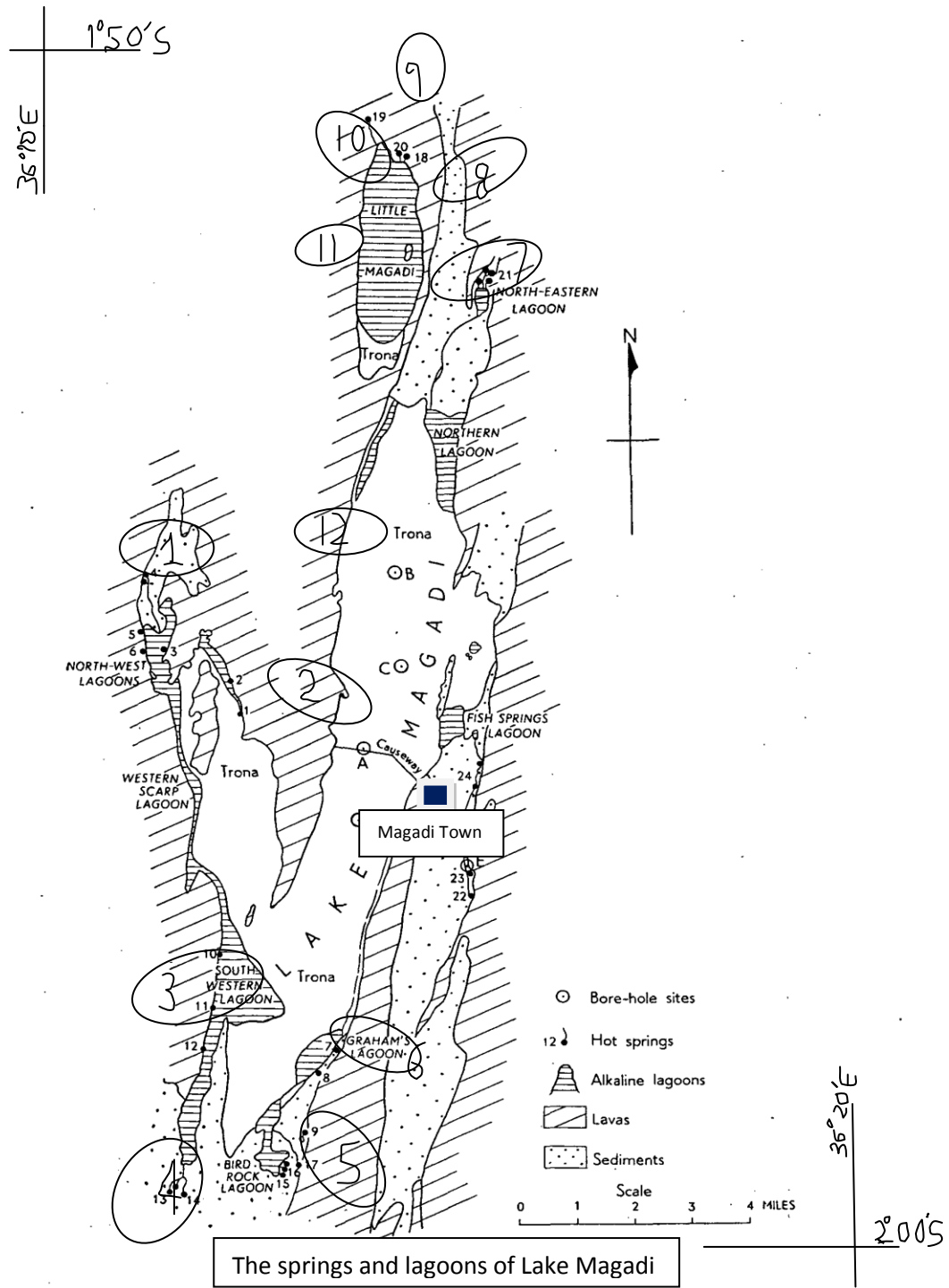


Figure 4.1: Sampling locations (Modified from Baker (1958)).

### **4.3 Sample collection procedures**

The sampling locations were accessed using an off-road vehicle where possible and by foot where the local terrain did not permit use of the off-road. The locations of the sampling sites were recorded using a mobile phone based GPS. Trachyte rock, bottom sediment, thermal water and trona were collected from each of the twelve sampling location and packed in labeled containers ready for transportation to the laboratory. Processed soda ash and cattle salt, as well as settler tailings from the Magadi Soda Company, were also collected for analysis.

#### **4.3.1 Collection of thermal water samples**

The temperatures of the springs were determined *in-situ* using an electronic thermometer before sample collection. Twelve thermal water samples were collected in 500 cc plastic bottles. The bottles were rinsed thrice in the spring waters before the samples were collected. The samples were collected at surface since these were shallow bubbling pools with very little possibility for atmospheric contamination. The bottles were allowed to cool then tightly sealed and appropriately labeled. The labeling included date, time, temperature, location, and sample code.

#### **4.3.2 Collection of rock samples**

Pieces of local fine and coarse trachyte rock were chipped using a geologist's sledge hammer and broken into even smaller pieces. About 500 g of these pieces were packed in plastic bags and appropriately labeled.

#### **4.3.3 Collection of sediment samples**

Bottom shore sediment was dug up using a hand trowel from sites around the sampled hot springs. About 500 g of the dug up sediment was scooped into sample collection bags and appropriately labeled.

#### **4.3.4 Collection of trona samples**

Crystallized trona deposits were collected from sites at least 15 m into the lake from each of the sampled springs. About 500 g of the trona was scooped into sample collection bags and appropriately labeled.

500 g each of processed soda ash, industrial salt and cattle salt were collected from the Magadi Soda Company's chemical laboratory. 500 cc of mine tailing from the Magadi Soda Company plant was also collected in a sealed plastic bottle.

### **4.3.5 Collection of control samples**

Six control samples were collected from random sites outside the sampling locations. Three samples each were collected for rocks and sediment as described above.

### **4.3.6 Sample coding**

An alphanumeric coding scheme was used to identify the samples. Alphabets indicated sample type while numbers gave sampling locations/spring number. The following alphabetic code was used: W for thermal waters, R for rock, S for sediment and Tr for trona. Therefore W8 denotes thermal water from spring number 8, R3 denotes rock sample from around spring number 3, S10 denotes sediment sample from around spring number 10, Tr2 denotes trona sample from around spring number 2, etc. Also used were CR for rock control samples, CSD for sediment control samples and CW for thermal water control samples.

## **4.4 Sample preparation**

### **4.4.1 Preparation of solid samples for gamma-ray spectrometry**

The rock, sediment, raw trona, and processed salt samples were unsealed and air dried over a period of three weeks before being crushed and pulverized into fine powder. The pulverizing machine was set for 150 microns particle size. Pulverizing was done to ensure homogeneity in the samples. The samples were then placed into labeled 300 cc plastic jars, weighed and sealed using airtight lids to prevent escape of gaseous  $^{220}\text{Rn}$  and  $^{222}\text{Rn}$ . Two sets of jars were prepared for each of the rock, sediment and trona samples while three each were prepared for the processed products. The masses of the samples ranged from 194.00 g to 358.20 g. The samples were then stored for at least 28 days before gamma-ray analysis was done. This was to allow for the in-growth of gaseous  $^{222}\text{Rn}$  (half life of 3.8 days) and achievement of secular equilibrium between  $^{226}\text{Ra}$  and the decay products of  $^{222}\text{Rn}$  ( $^{214}\text{Bi}$  and  $^{214}\text{Pb}$ ). A background sample was also prepared by sealing distilled water in a similar jar. Distilled water was chosen because it is considered a blank reference standard hence appropriate for background correction.

### **4.4.2 Preparation of liquid samples for gamma-ray spectrometry**

The thermal waters and settler tailings were placed into labeled 300 cc plastic jars, weighed and sealed using airtight lids to prevent atmospheric contamination. Two sets of jars were prepared for each of the thermal water samples while three sets were prepared for settler tailings. The masses of the jars ranged from 278.20 g to 320.00 g. The samples were then stored for at least 28 days to allow for the achievement of secular equilibrium before gamma-ray analysis. A background sample was also prepared by sealing distilled water in a similar jar.

## 4.5 Gamma-ray spectrometric analysis

Gamma ray spectroscopy using HPGe detector was chosen for the determination of activity concentrations of gamma emitting radionuclides because the HPGe has better counting efficiency and energy resolution for measurement of gamma ray energies above several hundred KeV compared to the only other detector category of major importance available for such measurements - NaI(Tl). The gamma-ray spectrometer used in this work consisted of an HPGe detector in a lead shield and cooled by liquid nitrogen in a dewar, voltage bias, amplifier, MCA, and Oxford PCA3 v.1 software on a desk top computer(Fig 4.2). The voltage bias was set at 5 KV. Gamma-ray photons from radionuclides in the sample interact with the detector and are converted into voltage pulses which are amplified and then processed by the MCA into digital pulse height spectra for analysis. By analyzing the energy of the centroid channel and the height of a particular pulse (intensity in counts per second), the identity and activity concentration of the nuclei that emitted the radiation are determined.

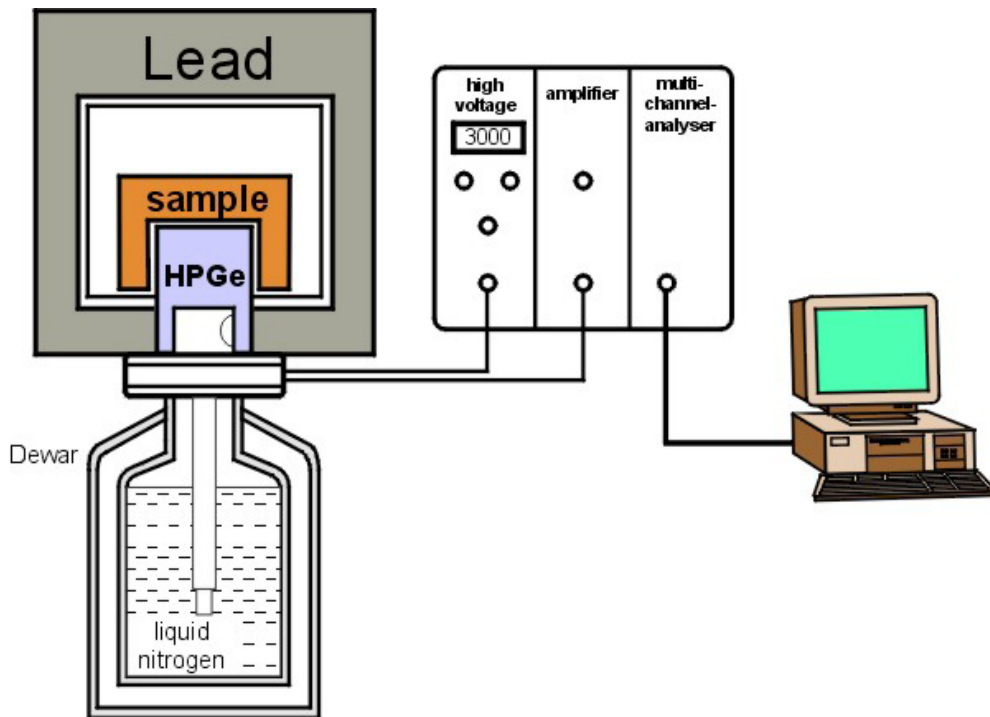


*Figure 4.2: Schematic of gamma-ray spectrometry instrumentation.(Randolph,1996)*

### 4.5.1 Identification of radionuclides

Table 4.2 gives the centroid channel energies used to identify and quantify the radionuclides of interest in the samples.

**Table 4.2:** Recommended energy lines for gamma-ray analysis of environmental samples (IAEA, 2003)

Radionuclide	Isotope(s)	Spectral line (KeV)
K-40	<sup>40</sup> K	1460.81
Th-232	<sup>212</sup> Pb	238.63
	<sup>228</sup> Ac	911.21
U-238 ( <sup>226</sup> Ra)	<sup>214</sup> Pb	351.92
	<sup>214</sup> Bi	609.31
		1764.7
	<sup>210</sup> Pb	46.5
	<sup>131</sup> I	364.50

#### 4.5.2 Calculation of detection limits

The detection limits (DL) of the various radionuclides were calculated using the equation below (Philips,1981):

$$DL = \frac{3C\sqrt{Bg}}{PA} \quad (4.1)$$

where Bg is the background counts obtained from a gamma peak, PA is the net area under respective gamma photo peaks and C is the activity concentration of the specific radionuclide of interest (in Bq/Kg). Gamma-ray spectral data from the IAEA reference standards RGU, RGK and RGTh were used.

#### 4.5.3 Determination of radioactivity concentrations

The HPGe detector used had 144 ml active volume and 76 mm outside diameter. Its average resolution over the period of measurements was 2.83 KeV FWHM at the 1332.50 KeV peak of <sup>60</sup>Co while the average efficiency was 30.60 %. Each sample and background was counted for between 30,000 to 60,000 seconds for significant peaks (with high signal to background ratio) to form, depending on their activities. The detector was calibrated for energy using a calibration source SRM1 containing <sup>137</sup>Cs, <sup>54</sup>Mn and <sup>60</sup>Co. A performance test was done using IAEA standard reference materials RGU, RGK, RGTh and Soil-375(IAEA,1987) to check the efficiency of the energy calibration. To assure quality in the measurements, energy calibration checks (to correct peak shifts) were done every morning and evening by running SRM1 for 500 seconds and also by repeating several sample measurements. The 661.66 KeV line of <sup>137</sup>Cs and the 1173.24 KeV and 1332.50 KeV lines of <sup>60</sup>Co were used for the peak shift corrections. The background measurements were later subtracted from the measured gamma-ray spectra of each sample to correct the net peak areas for counts. These results, and those from the reference

standards (as given in table 4.3), were then used in equation 3.9 to compute the activity concentrations of the radionuclides of interest in the samples. The gamma-ray spectra were deconvoluted using the Oxford PCA3 v.1 software on a computer interfaced to the spectrometer. The software performed simultaneous fitting and identification to all the significant photopeaks in the spectra and displayed menu driven reports that included centroid channel energy, FWHM of identified peak, net peak area, background counts, intensity and percentage margin of uncertainty.

**Table 4.3:** Reference data from certified reference materials (CRM).

CRM	Mass ( $M_r$ ) (g)	Radionuclide intensity ( $I_r$ ) (cps)	Radionuclide activity ( $A_r$ ) (Bq/Kg)
RGTh-1	260.7	Th-232: 2.218	3250±90
RGK-1	306.3	K-40: 1.245	14000±400
RGU-1	263.4	U-238: 1.427	4940±30
IAEA 375	347.96	Ra-226: 0.722	20±5

$A_r$  values are from IAEA CRM data sheets

#### 4.6 Multivariate chemometric analysis

Multivariate exploratory data analysis involved the application of both supervised and unsupervised pattern recognition techniques to detect and explore the distribution of radionuclide types and activity levels in relation to the other physico-chemical parameters of the samples. Unsupervised techniques were used for site clustering with respect to radionuclide activity concentrations and spring temperature, TDS, s.g., pH and TOC; while the supervised ones were used for classification and data modeling of the samples. Mean centered data sets were used in the analyses. The samples were characterized by their gamma-ray spectral data or activity concentrations,  $T_o$ , pH, s.g., TDS, TOC and CEC. The data were arranged in form of matrices with the samples as rows and variables as columns.

Thermal water, rock and sediment data were subjected to PCA analysis. The data matrices were column centered by subtracting the mean value of each column from each of the 12 individual elements followed by column standardization (autoscaling) of individual variables. This was done by subtracting the mean of column elements from individual elements and then dividing by individual column standard deviation. These were then subjected to PCA to give a visualization of the data structure in the form of 2D plots of residual variances, variances against PCs, rotated scores for PCs, and rotated loadings for PCs.

Only data from thermal waters and rock samples were analyzed by HCA. Column standardized data sets for thermal waters were used. The Euclidian distance between any pair of the 12

samples were computed based on the variables used to characterize them and compared. Those with shorter distances between them were then clustered together. These were then subjected to HCA to give 2D relations between sampling sites and cluster distances - dendrograms. These show similarity relationships between any sample and the entire set. The more similar samples are those with shorter distances between them while the most dissimilar are those with the greatest distances between them.

CTs were constructed for thermal waters and sediment data in a top-down fashion, starting from a root node. For each CT, a splitting rule was selected for the nodes by determining the variables and threshold values to be used to split the data. Terminal nodes were then determined and values assigned to them.

Thermal waters were characterized by 12 variables:  $\text{Na}_2\text{CO}_3$ ,  $\text{NaHCO}_3$  and  $\text{NaCl}$  contents (as determined by Baker (1958)), mean activity levels [ $^{40}\text{K}$ ,  $^{232}\text{Th}$ ,  $^{238}\text{U}$ ( $^{226}\text{Ra}$ ) and  $^{210}\text{Pb}$ ],  $T_0$ , pH, s.g., TOC and TDS; in a 12 x 12 data matrix. Rock samples were characterized by their gamma-ray spectra; giving a 12 x 8192 data matrix since the MCA used had 8192 channels. Sediment samples were characterized by 6 variables: mean activity levels of  $^{40}\text{K}$ ,  $^{232}\text{Th}$ ,  $^{238}\text{U}$  ( $^{226}\text{Ra}$ ) and  $^{210}\text{Pb}$ , and CEC; giving a 12 x 5 data matrix. Data from raw trona and processed product samples were not subjected to chemometric analyses but were only compared to the same for thermal waters, rock and sediment samples.

Mean, maxima, minima, standard deviation, skewness, kurtosis and correlation analyses were done using SigmaPlot v11.0 and Statistica v.10 software packages while the multivariate chemometric analyses were done using Unscrambler Camo v.9.7 and SPSS v.20 software packages.

## Chapter Five

# RESULTS AND DISCUSSION

### 5.1 Chapter overview

Field observations and measurements, gamma-ray spectrometry, data analyses and results of the thesis research are presented and discussed in this Chapter. Radiogenic diversity within the Magadi basin, its origin, classification, and relationships with spring temperatures, pH, TOC and TDS, as well as  $\text{Na}_2\text{CO}_3$ ,  $\text{NaHCO}_3$  and  $\text{NaCl}$  content in the trona, are presented and discussed with the aid of multivariate statistical data analysis.

### 5.2 Field observations

Lake Magadi has numerous springs and lagoons around it and is covered by vast deposits of trona. The springs flow into the lagoons which then drain into the Lake through the trona deposits. The largest of the lagoons is actually a small lake to the north of Lake Magadi referred to as 'Little Lake Magadi'. It is separated from the main Lake Magadi by a strip of larva horst and sediments (Fig 4.1). The twelve springs studied in this work are gently bubbling pools of hot water issuing from distinct point sources. The temperatures of the springs vary from  $39.0\text{ }^\circ\text{C}$  to  $85.9\text{ }^\circ\text{C}$  with those to the north of Little Lake Magadi having the highest temperatures. The spring waters are clear and colourless at their points of issue; but in the small pools into which they flow, dark green and dark brown algae of the *Nitzschia* and *Spirulina* species (Mutie, 2012) and some tiny fish of the dwarf tilapia *Oreochromis alcalicus grahami* specie (Frankline *et al.*, 1995) were observed. The algae and fish are able to tolerate temperatures upto  $66\text{ }^\circ\text{C}$  and alkalinity levels upto pH 9.82. None of the springs could throw a fountain into the air, and no gas was observed to bubble with the spring waters.

In between the sampled springs are numerous seepages and steaming ground; probably smaller springs buried under shingle and silt deposits. The northern and southern springs had greater flows than those on the eastern and western edges of the Lake, most which were just seepages. Springs to the north had the heaviest flows. This shows that most ground water flow in this region is along the Rift Valley; either northwards into Lake Magadi or southwards into Little Lake Magadi. This plausibly explains the hypothesis of underground recharges from Lakes Naivasha (Becht, 2005) and Natron. Springs on the eastern shores of the lake have been disturbed by the construction of large salt pans as well as connecting roads and rail lines by the Magadi Soda Company. The northern shore lines of the main and Little Lake Magadi, and the southern shore line of the main Lake Magadi are receding due to heavy siltation brought by sporadic surface inflows.

Little Lake Magadi, at an elevation that is 15 m higher than that of the main Lake Magadi, has no significant deposits of trona. This could be due to several reasons: (i) low TDS levels of the springs recharging it, (ii) heavy inflows from the springs resulting in insignificant evaporation

rates, (iii) high water temperatures due to its very hot springs thus enhancing the solubility of the solute content, and (iv) underground water flow from Little Lake Magadi into main Lake Magadi, leaving Little Lake Magadi relatively fresh.

Results of temperature ( $T^{\circ}$ ), total dissolved solids(TDS), specific gravity(s.g.), pH and total oxidizable carbon(TOC) measurements on the sampled spring waters are given in Table 5.1.

**Table 5.1:** Physico-chemical properties of the Magadi spring waters

Spring No.	$T^{\circ}$ ( $^{\circ}$ c) $\pm 0.1$	TDS (% m/m) $\pm 0.034$	s.g. $\pm 0.005$	pH $\pm 0.01$	TOC (mg/L) $\pm 0.20$
1	43.30	2.092	1.019	9.82	7.40
2	41.80	2.349	1.019	9.05	10.10
3	44.60	2.160	1.019	9.19	12.70
4	44.20	3.068	1.028	9.22	17.55
5	40.20	3.035	1.027	9.20	18.40
6	39.00	3.093	1.023	9.26	13.26
7	85.90	2.495	1.017	8.55	2.20
8	85.00	2.564	1.024	8.56	2.95
9	84.70	2.913	1.026	8.60	2.20
10	83.10	2.569	1.024	8.81	2.20
11	82.00	2.567	1.024	8.73	2.20
12	42.60	2.564	1.024	8.74	15.80

As can be seen in Table 5.1, the concentrations of the springs vary significantly with the hottest springs being the least alkaline/most dilute (lowest TDS values). Because the alkalinity of most groundwater is primarily a function of dissolved carbonates and hydrogencarbonates (Keith,1988), pH is taken as an indication of the concentrations of these constituents. This is consistent with the measurements as given in Table 5.16(a).

The springs to the north are more dilute than those to the south. This indicates heavier fresh ground water inflows from the north; probably underground recharge from the ‘fresh’ Lake Naivasha (Becht, 2005) in addition to other sources. Those to the south are the most concentrated (higher TDS); probably due to highly alkaline inflows from Lake Natron resulting from the leaching of natrocarbonatite larva from the frequent eruptions of the Oldonyo Lengai volcano, in addition to weathering of rocks along the paths of the ground flows. This is very probable because natrocarbonatite ash yields Na-HCO<sub>3</sub> waters upon leaching (just like the trachytes in this area) and is extremely soluble in water (UNESCO, 2008). Eugster (1986) and Baker (1987) both concluded that the single most important source of the substantial salt accumulations at Lakes Magadi and Natron is the natrocarbonatite ash from the still active Oldonyo Lengai volcano.

A comparison of the TDS and T<sup>0</sup> values as measured in this study with previous measurements on the same springs by Stevens (1932) shows that the concentrations and temperatures of the sampled springs have not changed significantly in the last 80 years (Appendix A). Variations may be attributed to different times and conditions of sampling; sampling for this study was done during the dry season of January 2013 while sampling for Stevens (1932) was done in 1930, an unusually wet year according to Baker (1958). It would be interesting to monitor these properties at different times in the course of an average year.

### 5.3 Gamma-ray spectrometry of the field samples

#### 5.3.1 Gamma-ray spectra

A gamma-ray spectral plot for a sample is presented below.

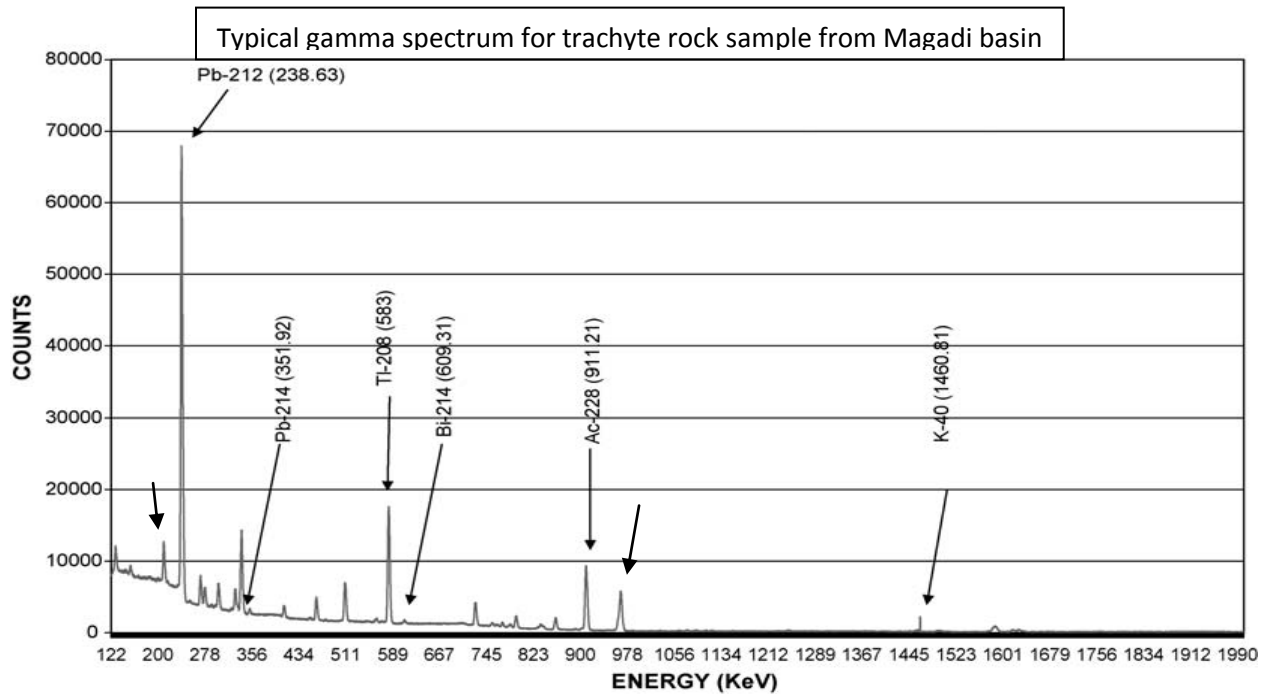


Figure 5.1: Gamma-ray spectrum for sample R8.

### 5.3.2 Detection limits (DL)

In order to determine the detection limits for the radionuclides of interest in the samples, background spectral data of the IAEA calibration standards RGU, RGTh and RGK were used in equation 4.1. The detection limits are different for different progeny of the same parent radionuclide because of different half lives and rates of production. For example, the rate of production of  $^{214}\text{Pb}$  is faster than that of  $^{214}\text{Bi}$  by a factor of 9 even though their half lives are in the same range. The values are summarized in Table 5.2.

**Table 5.2:** Detection limits of radionuclides

Radionuclide	Progeny	Energy Line (KeV)	Detection limit ( $\text{BqKg}^{-1}$ )
$^{238}\text{U}$	$(^{214}\text{Pb})$	351.92	$127.30 \pm 5.2$
	$(^{214}\text{Bi})$	609.31 $\sqrt{\quad}$	$27.57 \pm 3.1$
$^{232}\text{Th}$	$(^{212}\text{Pb})$	238.63	$86.68 \pm 4.5$
	$(^{228}\text{Ac})$	911.21 $\sqrt{\quad}$	$39.86 \pm 3.5$
	$(^{208}\text{Tl})$	583.00	$84.05 \pm 4.5$
$^{40}\text{K}$		1460.81 $\sqrt{\quad}$	$53.40 \pm 2.5$

$\sqrt{\quad}$ -line used for analysis

### 5.3.3 Radionuclide activity concentrations

The average activity concentrations of the radionuclides of interest in all the samples are summarized in tables 5.3 through 5.8. For purposes of working the mean concentrations of the radionuclides, all activities below detectable limits were substituted with half the value of the detection limit for that particular radionuclide (IAEA ,2003). In all the tables, BDL denotes 'below detection limit'.

**Table 5.3:** Average activity concentrations in rock samples

Sample	Average activity concentration (BqKg <sup>-1</sup> )		
	<sup>40</sup> K	<sup>238</sup> U ( <sup>226</sup> Ra)	<sup>232</sup> Th
R1	953.44±31.20	92.46±16.40	103.00±12.00
R2	1158.72±19.40	69.75±18.20	137.25±13.40
R3	1761.50±14.11	74.31±18.50	83.26±12.50
R4	1840.72±6.70	210.47±12.10	83.47±17.60
R5	1811.68±7.80	232.8±3.50	98.21±20.60
R6	1750.80±11.30	203.51±16.20	106.70±22
R7	1852.30±4.20	197.43±17.10	111.23±12.60
R8	1818.17±7.50	223.56±3.24	120.80±15.00
R9	1824.60±6.21	172.67±23.10	160.30±16.68
R10	1829.59±9.30	260.4±4.20	125.13±10.50
R11	1845.10±5.62	105.14±15.85	184.29±14.64
R12	922.71±43.70	104.6±14.00	127.8±14.20
<b>Mean</b>	<b>1613.98±13.96</b>	<b>162.26±13.53</b>	<b>120.12±15.09</b>
<b>Maximum</b>	<b>1852.30±4.20</b>	<b>260.4±4.20</b>	<b>184.29±14.64</b>
<b>Minimum</b>	<b>922.71±43.70</b>	<b>69.75±18.20</b>	<b>83.26±12.50</b>
<b>Std Dev</b>	<b>352.98</b>	<b>65.47</b>	<b>28.64</b>

R: rock

**Table 5.4:** Average activity concentrations in sediment samples

Sample	Average activity concentration (BqKg <sup>-1</sup> )		
	<sup>40</sup> K	<sup>238</sup> U ( <sup>226</sup> Ra)	<sup>232</sup> Th
S1	230.12±47.10	63.24±18.60	86.70±14.80
S2	1815.3±6.20	66.77±18.10	152.69±3.20
S3	2091.2±3.50	98.70±12.60	102.80±11.10
S4	2246.22±2.70	146.00±7.30	73.80±15.20
S5	2482.10±3.80	207.4±5.40	130.4±4.36
S6	2511.23±2.70	217.80±3.20	117.30±6.20
S7	2209.00±5.90	180.20±6.70	132.40±4.03
S8	2191.11±4.60	145.71±8.16	326.63±1.44
S9	1392.90±8.80	109.5±12.20	346.21±2.40
S10	2240.80±7.10	180.7±7.00	317.90±2.20
S11	2229.70±6.80	75.91±24.50	391.25±2.11
S12	870.17±19.80	82.70±14.20	80.47±15.16
<b>Mean</b>	<b>1875.80±10.75</b>	<b>131.21±9.94</b>	<b>188.21±5.58</b>
<b>Maximum</b>	<b>2511.23±2.70</b>	<b>217.80±3.20</b>	<b>391.25±2.11</b>
<b>Minimum</b>	<b>230.12±57.10</b>	<b>63.24±18.60</b>	<b>73.80±15.20</b>
<b>Std Dev</b>	<b>669.60</b>	<b>55.83</b>	<b>119.54</b>

S: sediment

**Table 5.5:** Average activity concentrations in thermal water samples

Sample	Average activity concentration (BqKg <sup>-1</sup> )		
	<sup>40</sup> K	<sup>238</sup> U ( <sup>226</sup> Ra)	<sup>232</sup> Th
W1	80.60±51.80	34.21±18.60	47.25±24.12
W2	85.21±48.60	30.73±17.00	52.82±21.70
W3	98.17±47.70	66.0±34.17	44.80±25.60
W4	98.18±52.10	72.18±30.38	49.26±22.70
W5	91.27±50.60	70.48±29.10	42.34±25.30
W6	96.14±45.20	61.24±26.78	43.90±24.80
W7	279.20±12.20	31.86±17.00	51.8±22.40
W8	112.60±18.00	27.80±20.10	55.6±19.50
W9	186.08±13.20	28.43±19.70	54.8±19.80
W10	159.18±12.70	27.63±19.80	62.7±19.10
W11	183.75±14.80	29.80±17.30	120.13±43.79
W12	73.40±44.67	30.20±18.50	44.6±24.10
<b>Mean</b>	<b>127.55±21.71</b>	<b>41.73±22.30</b>	<b>55.85±17.80</b>
<b>Maximum</b>	<b>279.20±12.20</b>	<b>72.18±30.38</b>	<b>120.13±13.79</b>
<b>Minimum</b>	<b>73.20±44.67</b>	<b>27.63±19.80</b>	<b>42.34±25.30</b>
<b>Std Dev</b>	<b>62.34</b>	<b>16.97</b>	<b>20.19</b>

W: water

**Table 5.6:** Average activity concentration in trona samples

Sample	Average activity concentration (BqKg <sup>-1</sup> )		
	<sup>40</sup> K	<sup>238</sup> U ( <sup>226</sup> Ra)	<sup>232</sup> Th
Tr1	93.10±13.70	BDL	BDL
Tr2	89.67±15.40	BDL	BDL
Tr3	93.70±21.50	BDL	BDL
Tr4	86.78±27.60	BDL	BDL
Tr5	82.47±25.30	BDL	BDL
Tr6	87.51±23.40	BDL	BDL
Tr7	118.76±16.20	28.70±17.20	56.80±19.70
Tr8	96.86±17.20	32.70±16.60	51.40±20.70
Tr9	94.80±16.72	31.60±16.90	BDL
Tr10	276.38±6.17	33.40±16.20	53.40±20.30
Tr11	101.73±12.40	27.90±17.80	61.13±23.79
Tr12	96.82±18.90	BDL	BDL
<b>Mean</b>	<b>109.63±17.87</b>	<b>20.88±8.80</b>	<b>31.88±9.71</b>
<b>Maximum</b>	<b>276.38±6.17</b>	<b>33.40±16.20</b>	<b>61.13±23.79</b>
<b>Minimum</b>	<b>82.47±25.30</b>	<b>&lt; 27.57</b>	<b>&lt; 39.86</b>
<b>Std Dev</b>	<b>53.32</b>	<b>8.93</b>	<b>17.74</b>

Tr: trona

**Table 5.7:** Activity concentrations in control samples

Sample	Activity concentration(Bq/Kg)		
	<sup>40</sup> K	<sup>238</sup> U	<sup>232</sup> Th
CR1	972.71±24.20	72.36±18.80	130.65±10.40
CR2	1230.16±18.90	192.36±17.20	101.12±12.80
CR3	1620.12±14.20	78.67±18.60	88.90±17.10
CSD1	927.13±19.10	64.34±18.20	120.36±5.80
CSD2	2221.32±5.20	93.46±13.10	157.81±3.90
CSD3	2044.36±3.50	132.56±7.82	246.76±2.70
CW1	76.40±43.12	33.80±17.20	42.28±24.00
CW2	110.52±17.40	25.30±16.20	50.62±19.00
CW3	86.21±47.10	31.73±17.38	47.21±22.40

CR: rock control sample, CSD: sediment control sample, CW: water control sample

**Table 5.8:** Average activity concentrations in processed salt products and settler tailings

Sample	Average activity concentration (BqKg <sup>-1</sup> )		
	<sup>40</sup> K	<sup>238</sup> U ( <sup>226</sup> Ra)	<sup>232</sup> Th
Soda Ash	568.37±88.20	122.76±24.70	44.3±21.20
Cattle Salt	133.54±26.81	87.6±14.20	BDL
Settler Tailing	93.28±23	39.16±21.70	41.71±22.30

As seen in Table 5.3, activity concentrations of the radionuclides in rock samples from all the sampling locations are generally comparable; ranging from 922.71 to 1852.30, 69.75 to 260.40 and 83.26 to 184.29 BqKg<sup>-1</sup> for <sup>40</sup>K, <sup>238</sup>U and <sup>232</sup>Th respectively. The mean concentrations of <sup>40</sup>K, <sup>238</sup>U and <sup>232</sup>Th in the rocks from around Lake Magadi are 1613.98±13.96, 162.26±13.53 and 120.12±15.09 BqKg<sup>-1</sup> respectively, with corresponding standard deviations of 352.98, 65.47 and 28.64 respectively. The standard deviations indicate remarkable spatial variability of the activity concentrations of the radionuclides in the rock samples from this basin. <sup>210</sup>Pb was not detectable in any of the rock samples. The mean activities of <sup>40</sup>K, <sup>238</sup>U and <sup>232</sup>Th in the trachyte rocks from Magadi are all about 4 times higher than the world average values of 400, 35 and 30 BqKg<sup>-1</sup> respectively(UNSCEAR,2000). The values are however much lower compared to those for known HBRA whose activities are as high as 13 times the world averages (Patel, 1991; Achola *et al.*, 2012; Otwoma *et al.*, 2013). On this scale, the Magadi basin may be regarded as a quasi high background radiation area (HBRA). Rocks from the northern side of Little Lake Magadi have higher activity concentrations compared to those from the rest of the sampling locations; showing that the underlying geothermal reservoir has elevated radionuclide levels compared to the rest of the basin. These locations also have higher spring water temperatures (Table 5.1).

The activity concentrations of  $^{40}\text{K}$  and  $^{232}\text{Th}$  in sediments are higher than in rocks for 9 out of 12 and 8 out of 12 sampling locations respectively while this is true in only 2 out of 12 sampling locations for  $^{238}\text{U}$  as seen in Tables 5.3 and 5.4. This is expected but also shows that  $^{40}\text{K}$  and  $^{232}\text{Th}$  are accumulating within the Magadi basin as is confirmed by their higher mean activity concentrations in sediments than in rocks. The enrichment coefficients for the accumulation of the two radionuclides are 1.2 and 1.6 respectively, showing that the accumulation is not significant. Samples S7 through S11 recorded much higher  $^{232}\text{Th}$  levels compared to the rest. These samples correspond to the springs with the highest temperatures; heat seems to improve sorption capacity of  $^{232}\text{Th}$  in sediments.  $^{210}\text{Pb}$  activity was below detectable levels in all the sediment samples.

Uranium is easily oxidized in such environments and readily forms complexes with water (Tagma *et al.*, 2012). It would therefore be easily washed away from the sediments by the water. One would therefore expect higher  $^{238}\text{U}$  activity in water samples but this is not clearly the case. The mean activity concentration of  $^{232}\text{Th}$  in water samples is higher than for  $^{238}\text{U}$ . However, spring water samples from the south of Lake Magadi had higher  $^{238}\text{U}$  than  $^{232}\text{Th}$  activity, which is consistent with expectation. The source of the  $^{238}\text{U}$  could be far off since it has two oxidation states hence easily forms complexes with water thereby enhancing its solubility and immobilization in ground water flows; implying that it can be carried in groundwater for long distances. The uranium could probably be coming from Lake Natron, and by extension, the extremely soluble natrocarbonatite lava from the active Oldonyo Lengai volcano. Thermal water samples from springs to the north of Little Lake Magadi had higher  $^{40}\text{K}$  activity concentrations than the rest. This is probably due to additions by potassium fertilizers from horticultural farms in Naivasha being carried in groundwater flows to Lake Magadi (Fig 1.2, Fig 1.3). None of the water samples had detectable levels of  $^{210}\text{Pb}$  activity.

Trona samples from the northern sites had higher  $^{40}\text{K}$  and  $^{232}\text{Th}$  activity levels than those from the other sites as seen in Table 5.6. This is consistent with the same for thermal waters (Table 5.5). However, the opposite is the case for  $^{238}\text{U}$  activity; whereas water samples from the south had higher activity concentrations of the radionuclide than the rest, trona samples from the north had higher activity concentrations of the radionuclide compared to the rest. This might be due to the heavier inflows from the northern springs but insignificant trona deposits around the sites as observed in the field.

According to Table 5.8, Soda ash and Cattle salt had mean radionuclide activity concentrations higher than even the average activities for the same radionuclides in trona. This should be investigated with reference to the processing procedures for the products. Settler mine tailings had lower activity concentrations than thermal waters. On this account, therefore, the Magadi Soda Company does not possibly contribute to further radiogenic pollution of the lake by disposing of settler tailings from its plant back into the lake.

All the control samples registered activity concentrations within the ranges of the same for the test samples as seen in Table 5.7. This shows that the sampling locations selected for this research were representative of the Magadi basin.

### 5.3.4 Statistical analysis of measured activity concentrations

Summaries of statistical analyses for the measured activity concentrations in rock, sediment and thermal water samples are presented in Tables 5.9, 5.10 and 5.11 below. Skewness is a measure of symmetry, or lack of it, in a distribution while Kurtosis is a measure of whether the data are peaked or flat relative to a normal distribution. Skewness is zero or near zero for symmetric data (normal distribution). A normal distribution with a distinct peak near the mean has high kurtosis while one with a flat top has low or negative kurtosis. Standard deviation gives the degree of uniformity; a data set whose standard deviation is greater than the mean has a high degree of uniformity and vice versa.

**Table 5.9:** Statistical summary of the activity concentrations ( $\text{BqKg}^{-1}$ ) of radionuclides in rock samples

Statistical parameter	K-40	U-238	Th-232
No. of samples	12	12	12
Minimum value	922.71	69.75	83.26
Maximum value	1852.30	260.40	184.29
Mean	1613.98	162.26	120.12
Skewness	-1.29686	-0.14862	0.86635
Kurtosis	-0.08002	-1.73188	0.60568
Std. Dev.	352.98	65.47	28.64
Distribution	Log Normal	Log Normal	Log Normal

**Table 5.10:** Statistical summary of the activity concentrations ( $\text{BqKg}^{-1}$ ) of radionuclides in sediment samples

Statistical parameter	K-40	U-238	Th-232
No. of samples	12	12	12
Minimum value	230.12	63.24	78.80
Maximum value	2511.23	217.80	391.25
Mean	1875.80	131.21	188.20
Skewness	-1.55811	0.26709	0.76370
Kurtosis	1.75464	-1.49493	-1.34422
Std. Dev.	669.60	55.83	119.54
Distribution	Log Normal	Log Normal	Log Normal

**Table 5.11:** Statistical summary of the activity concentrations ( $\text{BqKg}^{-1}$ ) of radionuclides in thermal water samples

Statistical parameter	K-40	U-238	Th-232
No. of samples	12	12	12
Minimum value	73.20	27.63	42.34
Maximum value	279.20	72.18	120.13
Mean	127.55	41.73	55.85
Skewness	1.53327	0.84629	2.99880
Kurtosis	2.06556	-1.40459	9.63005
Std. Dev.	62.34	16.97	20.19
Distribution	Log Normal	Log Normal	Log Normal

The standard deviations are lower than the mean activity concentrations for each of the three radionuclides in all the samples; showing non-uniformity in the distribution of the radionuclides in the samples. As seen in Table 5.9,  $^{232}\text{Th}$  activity concentration in rock samples has positive skewness; indicating asymmetrical distribution of the radionuclide in the samples with the tail extending towards high concentrations.  $^{40}\text{K}$  and  $^{238}\text{U}$  concentrations in rock samples are skewed left showing they have longer tails towards low values.  $^{238}\text{U}$  and  $^{232}\text{Th}$  activity concentrations in sediments are skewed right; indicating asymmetrical distribution with the tails extending towards high concentrations (positive skewness) while  $^{40}\text{K}$  is negatively skewed. All the radionuclides of interest in thermal water samples are positively skewed, indicating asymmetrical distributions with tails extending towards high activity concentrations.

However, save for  $^{40}\text{K}$  and  $^{232}\text{Th}$  activities in rock samples whose values for kurtosis indicate near normal distributions, the other activity concentrations in all sample sets show a strong evidence of non-normal distribution since their values for kurtosis and skewness are outside the ranges for normal distribution (Appendix J and K). This shows that the characteristics of their sources and origin have very little in common. The high values of standard deviation for the radionuclides in all the three sample sets indicate a strong diversity of their sources and origin. This diversity may be due to different geochemical properties of the source rocks and geophysical features.

Natural radionuclides were formed at the time of formation of the earth. Only those whose half lives are in the range of the age of the earth, and perhaps their decay products, can still be found at present. Examples are  $^{40}\text{K}$  and those in the decay series of  $^{238}\text{U}$  and  $^{232}\text{Th}$ . Some correlation analyses between  $^{40}\text{K}$ ,  $^{238}\text{U}$  and  $^{232}\text{Th}$  in rock, sediment and thermal water samples are given in Figures 5.2 through 5.6 below while Table 5.12 summarizes the correlation analyses. Since  $^{238}\text{U}$  and  $^{232}\text{Th}$  activities are worked out from those of members of their natural decay series while  $^{40}\text{K}$  (although a naturally occurring radionuclide) is not part of any decay series, a high correlation

between  $^{238}\text{U}$  and  $^{232}\text{Th}$  and low or negative correlations between either of  $^{238}\text{U}$  or  $^{232}\text{Th}$  and  $^{40}\text{K}$  would be expected (Mohanty *et al.*, 2004).

All sample sets show low or negative correlation between  $^{232}\text{Th}$  and  $^{238}\text{U}$  activities, which is against expectation. This can be attributed to the property of the rock of easily losing  $^{238}\text{U}$  during leaching as concluded by Lima *et al.* (2005) and Rajesh *et al.* (2013). Rocks and sediments show high correlations between  $^{238}\text{U}$  and  $^{40}\text{K}$  activities. This is consistent since the sediments arise from weathering of the rocks, but against expectation. This points to an underlying uranium rich rock source (Tagma *et al.* 2012). The other correlations between the activities of natural radionuclides in the samples as presented above are consistent with expectation.

**Table 5.12:** Summary of correlation analyses of radionuclide concentrations in samples

Sample type	Correlated radionuclides	Correlation coefficient
Rock	Th-232/K-40	-0.44262
	U-238/K-40	0.83804
	Th-232/U-238	-0.37340
Sediment	Th-232/K-40	0.22241
	U-238/K-40	0.93401
	Th-232/U-238	-0.05464
Thermal waters	Th-232/K-40	0.70821
	U-238/K-40	-0.10309
	Th-232/U-238	-0.65085

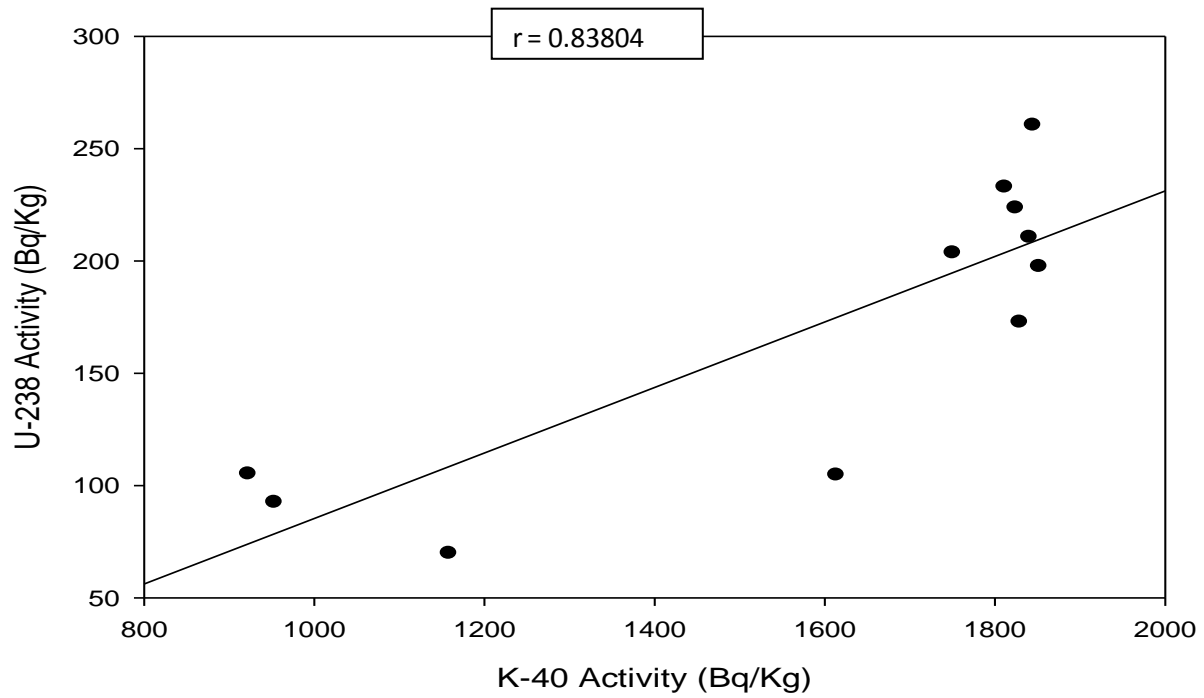


**Figure 5.2(a):** Correlation curve for  $^{238}\text{U}$  and  $^{40}\text{K}$  activities in the rocks.

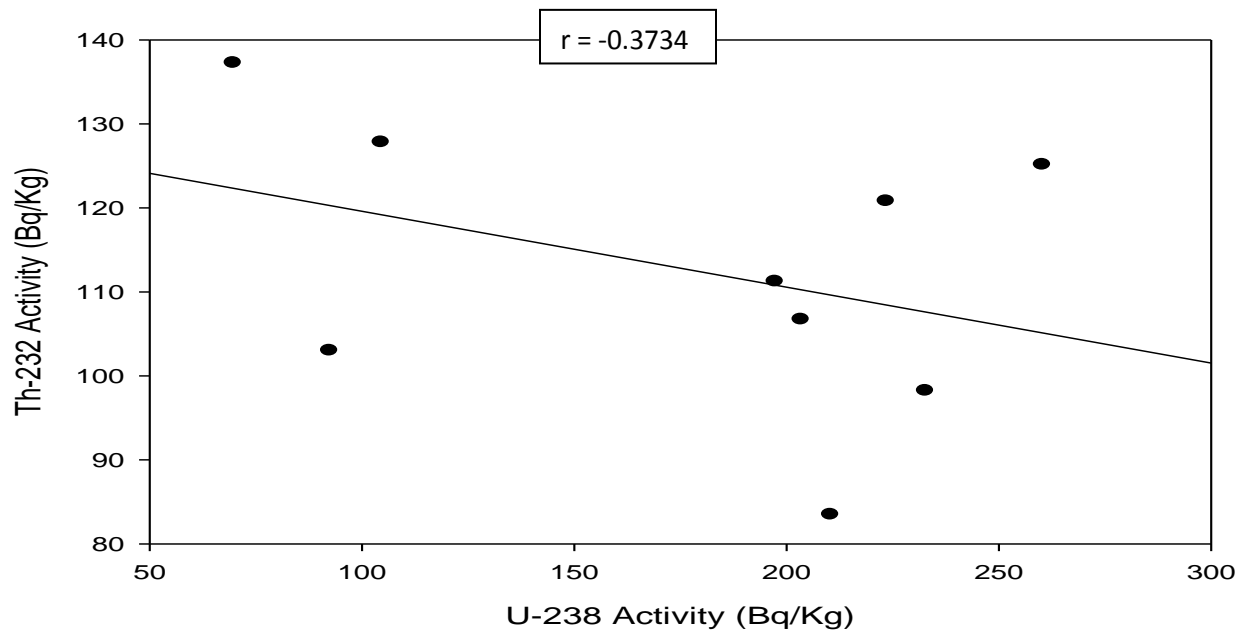


**Figure 5.2(b):** Correlation curve for  $^{232}\text{Th}$  and  $^{238}\text{U}$  activities in the rocks.

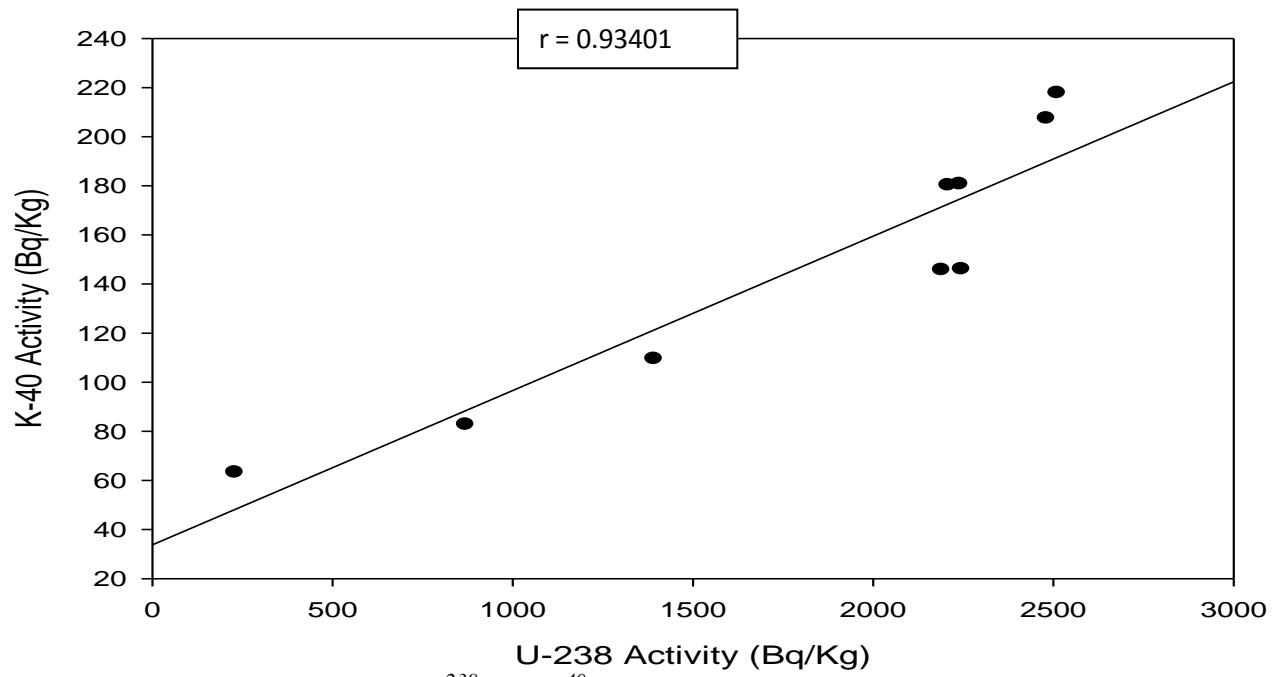


Figure 5.3: Correlation curve for  $^{238}\text{U}$  and  $^{40}\text{K}$  activities in sediments.

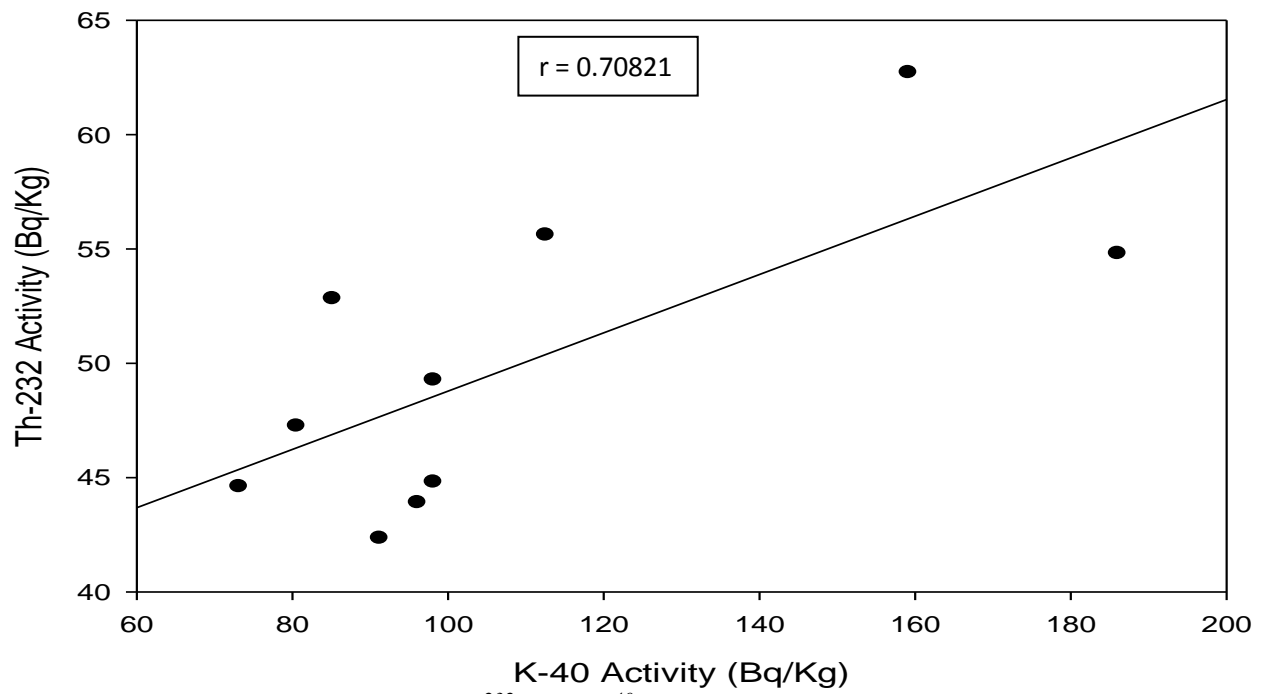
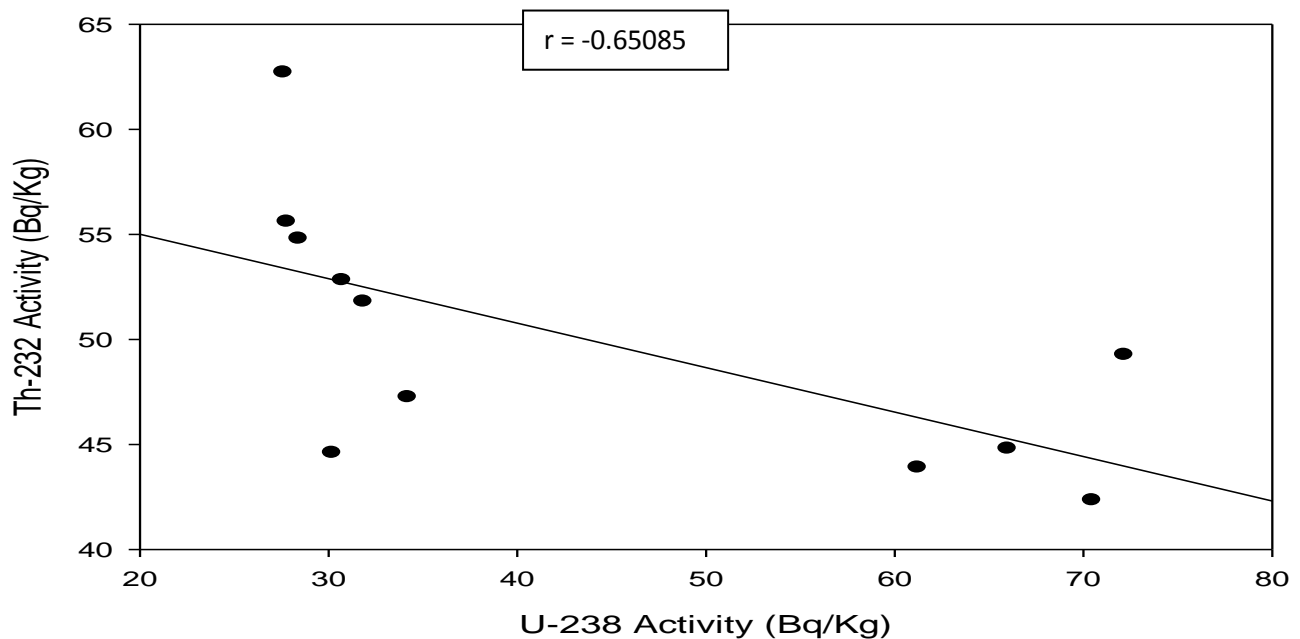


Figure 5.4(a): Correlation curve for  $^{232}\text{Th}$  and  $^{40}\text{K}$  activities in spring waters.



**Figure 5.4(b):** Correlation curve for  $^{232}\text{Th}$  and  $^{238}\text{U}$  activities in spring waters.

The activity ratios ( $^{238}\text{U}/^{232}\text{Th}$ ,  $^{238}\text{U}/^{40}\text{K}$ ,  $^{232}\text{Th}/^{238}\text{U}$ ,  $^{232}\text{Th}/^{40}\text{K}$ ,  $^{40}\text{K}/^{238}\text{U}$  and  $^{40}\text{K}/^{232}\text{Th}$ ) in rock, sediment and thermal water samples are calculated and tabulated below.  $^{238}\text{U}/^{232}\text{Th}$  ratio in rocks varied from 0.058 (R2) to 2.522 (R4) with an average of 1.401 (Table 5.13(a)). This average is higher than the upper crust value of 0.800 (Mohanty *et al.*, 2004). This shows that the concentration of uranium in the trachyte rock samples from the Magadi basin is higher than the concentration of uranium in the upper crust by a factor of about 2. Thermal water samples have the lowest mean  $^{238}\text{U}/^{232}\text{Th}$  ratio at 0.858 (Table 5.13(c)) showing relatively high levels of uranium in relation to the other radionuclides in water. Thermal water samples from the south of Lake Magadi had the highest  $^{238}\text{U}/^{232}\text{Th}$  ratios. The source of this uranium is probably the extremely soluble natrocarbonatite lava from the Oldonyo Lengai volcano since its uranium concentration is high compared to basalts and trachytes of the rift floor and has low thorium but high uranium content (Dawson and Gale, 1990). The geology of Tanzania, from where the southern springs originate, is also known to be rich in uranium (Yanda and Madulu, 2005) with several potential uranium mines including Lake Jipe near the border with Kenya, Bahi near Dodoma, Manyoni in central Tanzania, and River Mkuju to the south.

$^{232}\text{Th}/^{238}\text{U}$  ratios in thermal water samples are lower than 1 in 7 of the 12 springs. This shows low geochemical mobility of thorium compared to uranium (Rajesh *et al.*, 2013). It can also be seen in Table 5.13(c) that there is a remarkable constancy in  $^{232}\text{Th}/^{40}\text{K}$  ratio; varying minimally from 0.394 to 0.619 with two outliers W7 and W9. This shows that the geochemical

immobilizations of the two radionuclides in groundwater flows are the same in the entire Magadi basin.

The mean  $^{232}\text{Th}/^{238}\text{U}$  ratio in sediments (1.699) is higher than in rocks and thermal waters, showing a preferential accumulation of thorium by sediments as was also concluded by Ramasamy *et al.* 2009. The highest values were found in sediments from the northern sites (Table 5.13(b)). These sites correspond to springs with the highest thermal water temperatures; showing that high temperatures enhance thorium sorption capacity of the sediments. Figure 5.5 compares  $^{232}\text{Th}$  activity level of different samples and sampling locations. The figure shows that sediments have higher activities than rock and thermal water samples in 9 of the 12 sampling locations and that sediment samples from sampling locations adjacent to springs with higher temperatures (7,8,9,10,11) had higher  $^{232}\text{Th}$  activities than the rest.

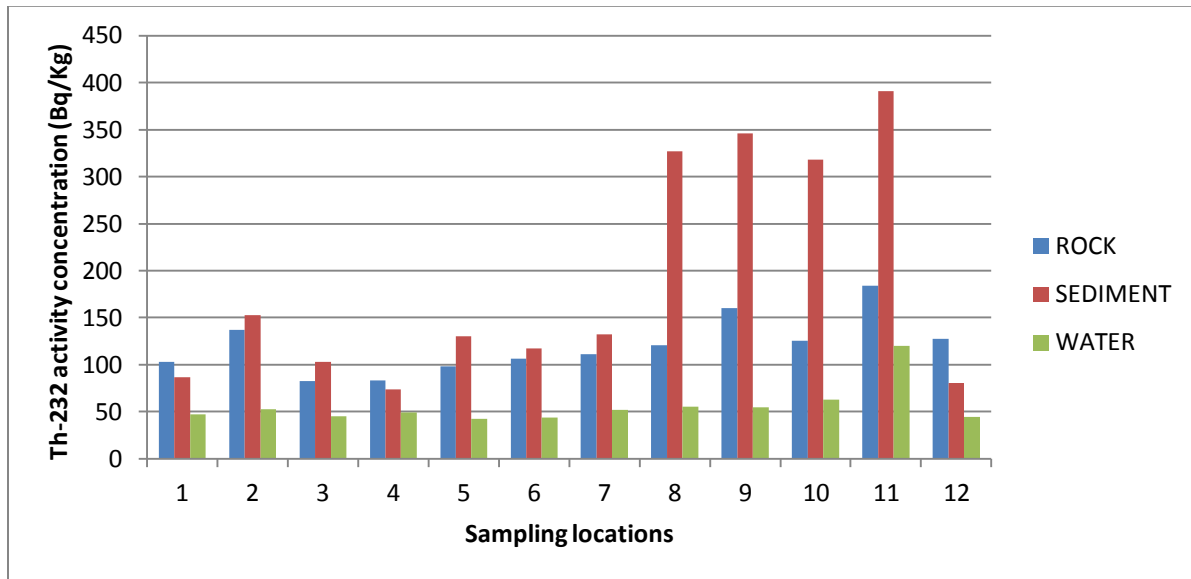


**Figure 5.5:** Comparison of Th-232 activity concentrations in different sampling locations.

**Table 5.13(a):** Radionuclide activity concentration ratios in rock samples

Sample ID	$^{238}\text{U}/^{40}\text{K}$	$^{238}\text{U}/^{232}\text{Th}$	$^{232}\text{Th}/^{238}\text{U}$	$^{232}\text{Th}/^{40}\text{K}$	$^{40}\text{K}/^{238}\text{U}$	$^{40}\text{K}/^{232}\text{Th}$
R1	0.097	0.898	1.114	0.108	10.309	9.257
R2	0.060	0.508	1.969	0.118	16.667	8.442
R3	0.042	0.892	1.121	0.047	23.809	21.157
R4	0.114	2.522	0.396	0.045	8.772	22.052
R5	0.128	2.370	0.423	0.054	7.813	18.447
R6	0.116	1.907	0.524	0.060	8.621	16.408
R7	0.107	1.775	0.563	0.060	9.345	16.653
R8	0.123	1.851	0.540	0.066	8.130	15.051
R9	0.095	1.077	0.928	0.087	10.526	11.382
R10	0.142	2.081	0.481	0.068	7.042	14.622
R11	0.056	0.570	1.754	0.099	17.636	10.012
R12	0.113	0.818	1.222	0.138	8.850	7.221
<b>Mean</b>	<b>0.099</b>	<b>1.401</b>	<b>0.919</b>	<b>0.079</b>	<b>11.460</b>	<b>14.225</b>
<b>Maximum</b>	<b>0.142</b>	<b>2.522</b>	<b>1.969</b>	<b>0.138</b>	<b>23.809</b>	<b>22.052</b>
<b>Minimum</b>	<b>0.042</b>	<b>0.058</b>	<b>0.396</b>	<b>0.045</b>	<b>7.042</b>	<b>7.221</b>

**Table 5.13(b):** Radionuclide activity concentration ratios in sediment samples

Sample ID	$^{238}\text{U}/^{40}\text{K}$	$^{238}\text{U}/^{232}\text{Th}$	$^{232}\text{Th}/^{238}\text{U}$	$^{232}\text{Th}/^{40}\text{K}$	$^{40}\text{K}/^{238}\text{U}$	$^{40}\text{K}/^{232}\text{Th}$
S1	0.275	0.729	1.371	0.376	3.638	2.654
S2	0.037	0.437	2.288	0.084	27.187	11.888
S3	0.047	0.960	1.041	0.049	21.187	20.342
S4	0.064	1.978	0.505	0.033	15.385	30.436
S5	0.083	1.590	0.629	0.052	11.967	19.034
S6	0.087	1.856	0.538	0.046	11.529	21.408
S7	0.082	1.361	0.734	0.059	12.258	16.684
S8	0.066	0.446	2.242	0.149	15.037	6.708
S9	0.078	0.316	3.164	0.248	12.720	4.023
S10	0.081	0.568	1.760	0.142	12.400	7.048
S11	0.034	0.194	5.154	0.175	29.372	5.698
S12	0.095	1.027	0.973	0.092	10.522	10.813
<b>Mean</b>	<b>0.085</b>	<b>0.955</b>	<b>1.699</b>	<b>0.125</b>	<b>15.267</b>	<b>13.061</b>
<b>Maximum</b>	<b>0.275</b>	<b>1.978</b>	<b>5.514</b>	<b>0.376</b>	<b>29.372</b>	<b>30.436</b>
<b>Minimum</b>	<b>0.034</b>	<b>0.194</b>	<b>0.505</b>	<b>0.033</b>	<b>3.638</b>	<b>2.654</b>

**Table 5.13(c):** Radionuclide activity concentration ratios in thermal water samples

Sample ID	$^{238}\text{U}/^{40}\text{K}$	$^{238}\text{U}/^{232}\text{Th}$	$^{232}\text{Th}/^{238}\text{U}$	$^{232}\text{Th}/^{40}\text{K}$	$^{40}\text{K}/^{238}\text{U}$	$^{40}\text{K}/^{232}\text{Th}$
W1	0.402	0.724	1.381	0.586	2.356	1.705
W2	0.360	0.581	1.721	0.619	2.772	1.613
W3	0.672	1.473	0.679	0.456	1.487	2.191
W4	0.735	1.465	0.682	0.501	1.360	1.993
W5	0.772	1.664	0.601	0.464	1.295	2.157
W6	0.637	1.395	0.716	0.457	1.569	2.189
W7	0.114	0.615	1.626	0.185	8.763	5.389
W8	0.247	0.500	2.000	0.494	4.050	2.025
W9	0.152	0.519	1.926	0.294	6.545	3.395
W10	0.176	0.441	2.267	0.394	5.761	2.538
W11	0.162	0.248	4.032	0.564	6.166	1.529
W12	0.416	0.677	1.477	0.604	2.430	1.645
<b>Mean</b>	<b>0.405</b>	<b>0.858</b>	<b>1.592</b>	<b>0.476</b>	<b>3.712</b>	<b>2.364</b>
<b>Maximum</b>	<b>0.772</b>	<b>1.664</b>	<b>4.032</b>	<b>0.654</b>	<b>8.763</b>	<b>5.389</b>
<b>Minimum</b>	<b>0.114</b>	<b>0.248</b>	<b>0.601</b>	<b>0.185</b>	<b>1.295</b>	<b>1.529</b>

Correlation coefficients between ratios of radionuclide pairs in rock, sediment and thermal water samples are compared in Table 5.14 below. The correlations between  $^{238}\text{U}/^{40}\text{K}$  and  $^{238}\text{U}/^{232}\text{Th}$  ratios and  $^{40}\text{K}/^{238}\text{U}$  and  $^{40}\text{K}/^{232}\text{Th}$  ratios in sediments are very low showing relatively high or low activities of one of the radionuclides in sediments compared to crustal values (Mohanty *et al.*, 2004). This is due to the high levels of thorium in the sediments (Fig 5.5) due to its preferential sorption. The very weak correlation between  $^{40}\text{K}/^{238}\text{U}$  and  $^{40}\text{K}/^{232}\text{Th}$  ratios in rocks is due to the high levels of  $^{40}\text{K}$  in the rocks from the Magadi basin. This shows that trachytes have higher  $^{40}\text{K}$  activity concentration than the upper crust. Since trachytes result from fissural eruptions on the floor of the rift valley (Riaroh and Okoth, 1994), lava from such eruptions is therefore rich in potassium and originates from below the crust.

**Table 5.14:** Correlation coefficients between ratios of radionuclide pairs

Sample type	Correlation coefficients		
	$^{238}\text{U}/^{40}\text{K}$ and $^{238}\text{U}/^{232}\text{Th}$	$^{232}\text{Th}/^{238}\text{U}$ and $^{232}\text{Th}/^{40}\text{K}$	$^{40}\text{K}/^{238}\text{U}$ and $^{40}\text{K}/^{232}\text{Th}$
Rock	0.776	0.727	0.013
Sediment	0.035	0.441	0.056
Thermal water	0.446	0.221	0.707

#### 5.4 Comparison of these results with recent findings on natural radioactivity in endorheic basins and salts from different regions

A comparison of the mean activity concentrations of natural radionuclides from Magadi basin with the same for salts and endorheic basins in other regions of the world is presented in Table 5.15. The only other endorheic lake along the East African Rift Valley with saline springs and vast salt deposits is Lake Natron, even though it is suspected to provide underground recharge to Lake Magadi. Such radionuclide analyses on its springs and salt deposits have not been done yet. It would be important for the same to be done and the results compared with those from Lake Magadi. Several other basins and lakes exist along the Great Rift Valley but past studies on them have only focused on their saline-fresh water interplays and saline contents. Table 5.15 below however compares radionuclide levels in the spring waters and trona from Lake Magadi to levels in saline waters and salts from some salt mines around the world. Activity concentrations in the spring waters and trona from Magadi basin are upto 4 times higher compared to the other places.

**Table 5.15:** Comparison of mean activity concentrations (Bq/Kg) in salts from different salt mines around the world

Sample ID	<sup>40</sup> K	<sup>238</sup> U	<sup>232</sup> Th	Reference
Saline waters (Ghana)	0.5013	0.0197	0.0648	Kansaana <i>et al.</i> (2012)
Spring waters (Kenya)	127.55±27.21	41.73±22.3	55.85±17.8	This study
Processed salt (Ghana)	37.88	1.39	2.91	Kansaana <i>et al.</i> (2012)
Salt lake[non rift valley] (Egypt)	34±2	16.6±5	4.6±1.2	El-bahi (2002)
Sea salt (Pakistan)	23±6	0.9	0.5	Tahir and Alaamer (2008)
Open salt mine (Pakistan)	36±20	3.2	1.8	Balochi <i>et al.</i> (2012)
Trona (Kenya)	109.63±17.87	20.88±8.80	31.88±9.71	This study

#### 5.5 Trona quality parameters

Trona is a double salt of Na<sub>2</sub>CO<sub>3</sub> and NaHCO<sub>3</sub>. The trona at Lake Magadi however contains many other salts in it including NaCl, Na<sub>2</sub>SO<sub>4</sub> and NaF. The major chemical components of the products from the lake are Na<sub>2</sub>CO<sub>3</sub> (Soda ash and cattle salt) and NaCl (Industrial salt). NaHCO<sub>3</sub> is converted into Na<sub>2</sub>CO<sub>3</sub> by heat during processing. The other salts occur in tiny quantities and are removed as impurities by fractional crystallization during processing. The springs around Lake Magadi are so far believed to be the only source of the trona in the lake. Na<sub>2</sub>CO<sub>3</sub>, NaHCO<sub>3</sub> and NaCl are therefore the most important of the spring solutes and their levels in the spring

waters are regarded as trona quality parameters. Table 5.16(a) gives the quantities of these salts in the sampled springs as determined by Stevens (1932) while Table 5.18(b) compares these trona quality parameters, given as percentages of TDS as determined in this study, to temperatures of the springs. The mean concentration of NaHCO<sub>3</sub> is twice that of Na<sub>2</sub>CO<sub>3</sub> and about 3 times that of NaCl. The northern springs, with higher temperatures, have higher NaHCO<sub>3</sub> content than the others while those with lower temperatures have higher Na<sub>2</sub>CO<sub>3</sub> and NaCl content than those with higher temperatures.

**Table 5.16(a):** Solute content of the springs (Stevens,1932)

Spring no.	Solute content (g/100g of spring water)			Total (g/100g of spring water)
	Na <sub>2</sub> CO <sub>3</sub>	NaHCO <sub>3</sub>	NaCl	
1	0.265	0.973	0.518	1.756
2	0.476	0.862	0.513	1.851
3	0.817	0.890	0.314	3.607
4	1.173	1.250	0.605	3.028
5	1.548	0.630	0.740	2.918
6	1.181	1.272	0.516	2.969
7	0.287	1.865	0.127	2.279
8	0.245	1.876	0.165	2.286
9	0.595	1.695	0.331	2.621
10	0.590	1.655	0.09	2.335
11	0.487	1.865	0.011	2.363
12	0.255	1.062	0.699	2.016
<b>Mean</b>	<b>0.660</b>	<b>1.325</b>	<b>0.386</b>	<b>2.502</b>
<b>Maximum</b>	<b>1.548</b>	<b>1.876</b>	<b>0.740</b>	<b>3.607</b>
<b>Minimum</b>	<b>0.245</b>	<b>0.630</b>	<b>0.011</b>	<b>1.756</b>

**Table 5.16(b):** Relative solute contents of the springs

Spring no.	T <sub>0</sub> (°C)	Solute content (% of TDS)			Total (% of TDS)
		Na <sub>2</sub> CO <sub>3</sub>	NaHCO <sub>3</sub>	NaCl	
1	43.30	12.66	46.51	24.76	83.98
2	41.80	20.26	36.69	21.83	78.78
3	44.60	37.82	41.20	14.53	93.55
4	44.20	38.23	40.74	19.71	98.66
5	40.20	51.00	20.75	24.38	96.13
6	39.00	38.18	41.12	16.68	95.98
7	85.90	11.50	74.74	5.09	91.93
8	85.00	9.55	73.16	6.43	89.14
9	84.70	20.42	58.18	11.36	89.96
10	83.10	22.96	64.42	3.50	90.88
11	82.00	18.97	72.65	0.43	92.05
12	42.60	9.94	42.59	27.26	79.79

## 5.6 Multivariate chemometric analysis of spectral and derived data

### 5.6.1 Principal components analysis (PCA) for classification and pattern recognition

PCA analyses on the data matrices for rock, thermal water and sediment samples are presented in figures 5.6 to 5.12. The analyses were done in order to classify and determine any patterns in the distribution of variables in the samples. The scores describe the salient properties of the samples e.g. sub groups within the main group; the loadings describe relationships between the variables used to characterize the sample groups e.g. correlation while the variances are error measures - showing how much information is taken into account by the successive principal components (PC's). Explained variance gives the percentage of the total variance in the data matrix that is accounted for by the current PC while residual variance gives how much variation is not explained; the two variances are complimentary.

Figure 5.6 is a 2D scatter plot of rotated scores of PC's for the data matrix for rock samples characterized by their radionuclide activity concentrations. The samples group in two clusters representing (i) the edges and (ii) floor of the Rift Valley. Samples in cluster A have K-40 activity below 1200 Bq/Kg and are from the host bedrock bounding the western edges of the lake. The eastern edges were not sampled due to disturbance of the natural set-up by activities of the Magadi Soda Company. Though in this cluster, sample R2 does not seem to have very close properties as R1 and R12. R2 was sampled close to the causeway which has a lot of human activity and vehicles crossing the lake towards Nguruman escarpment. This, probably, partly influences the radiogenic properties of the local rock material e.g. by induced wet or dry atmospheric deposition. Those in cluster B have K-40 activities above 1700 Bq/Kg and are samples from the northern edges of Little Lake Magadi and southern edges of main Lake Magadi. These are sites on the floor of the Rift Valley probably having trachytes from the most recent fissural eruptions. R3 and R11 could be said to belong to a third cluster representing trachytes from the lagoons or may just be outliers.

The two PC's are able to explain 97% of the variance in the rock sample while 2 % is residual and only 1 % unaccounted for. Most of the explained variance is taken care of by PC1 with PC2 accounting for only a small percentage. This is shown by the two clusters forming near PC1 than PC2 as seen in Figure 5.6. Of the three primordial radionuclides in the rock samples, U-238 and K-40 both lie on the 100 % explained variance circle as seen in the PCA plots of correlation loadings for radionuclides (Fig 5.7). This shows that the two radionuclides correlate positively and, probably, together form PC1 (which explains 97 % of the variance) as seen in figure 5.5. This positive correlation between U-238 and K-40 activities in rocks is confirmed by their correlation curve (Fig 5.2b). U-238 and Th-232 have opposite correlation loadings on PC2 of +0.971 and -0.271 (Table 5.17) which is confirmed by their negative correlation (Fig 5.2c). K-40 has almost zero correlation loading hence badly accounted for by PC2. Sample R7 has the greatest value of PC1 in the scatter plots of rotated scores for rock samples (Fig 5.6) while K-40 activity has the greatest value on PC1 in the plots of correlation loadings for radionuclides (Fig

5.7). This is in order since R7 has the highest K-40 activity among the rock samples as seen in table 5.3.

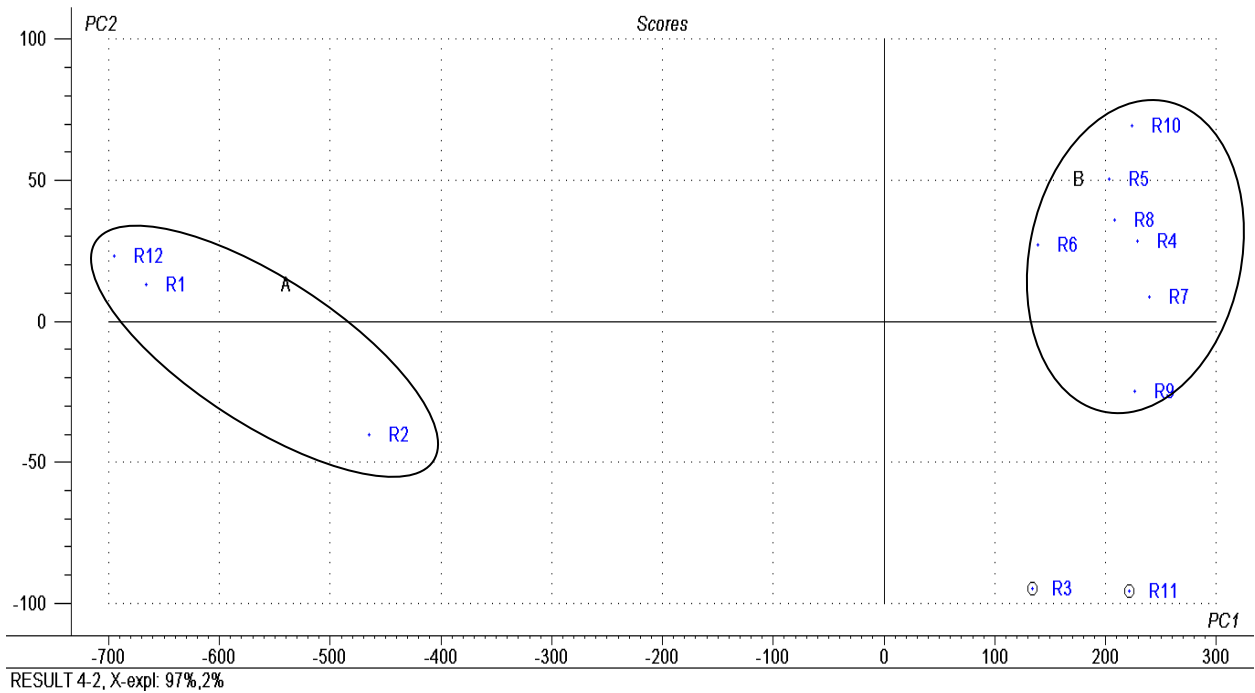


**Figure 5.6:** PCA scatter plots of rotated scores for rock samples based on radionuclide activity concentrations.

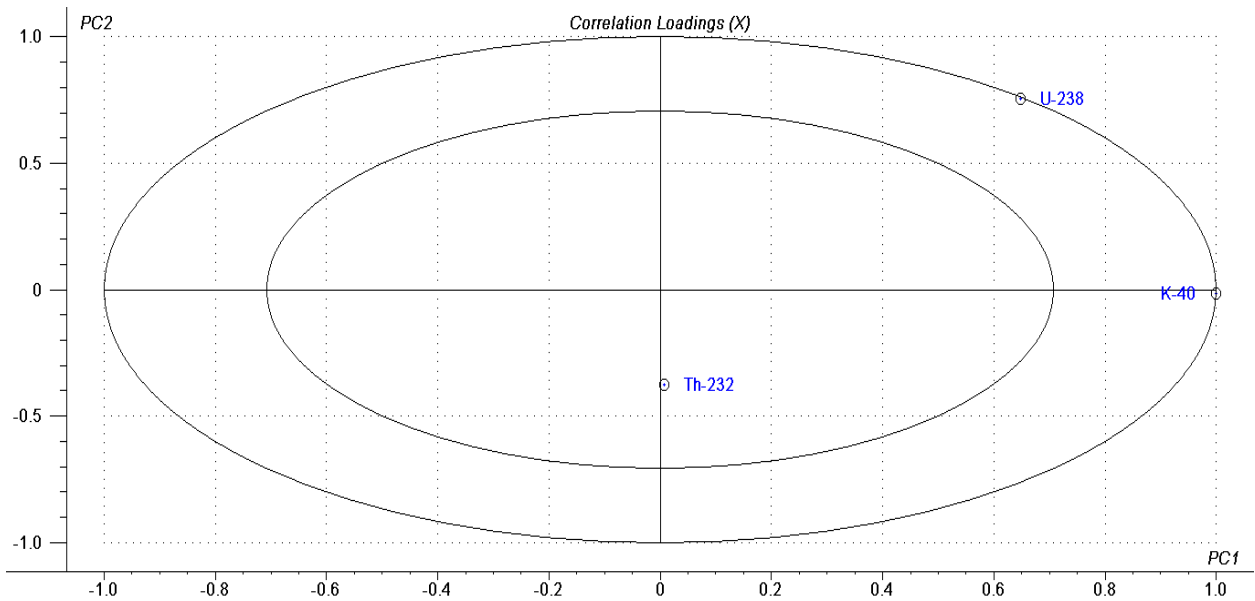
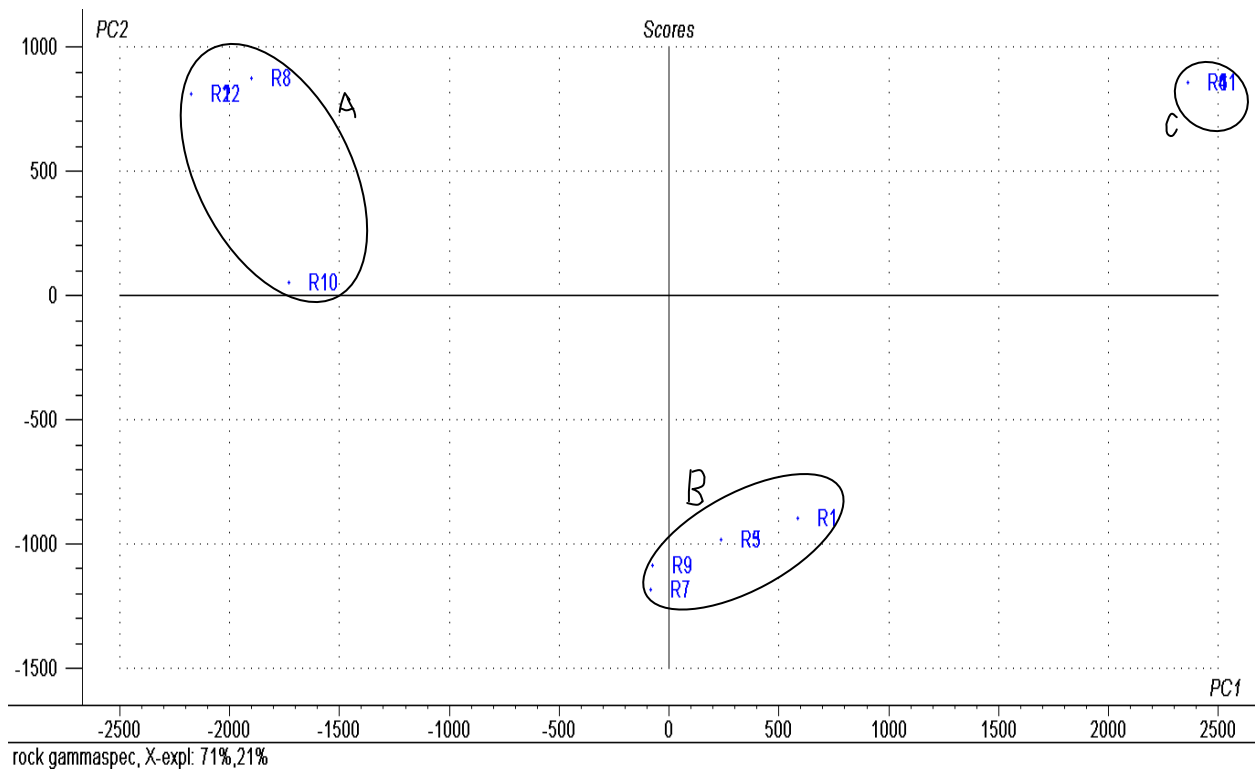


**Figure 5.7:** PCA plots of correlation loadings for radionuclides in rocks.

**Table 5.17:** PC scores and correlation loadings for radionuclides in rock samples

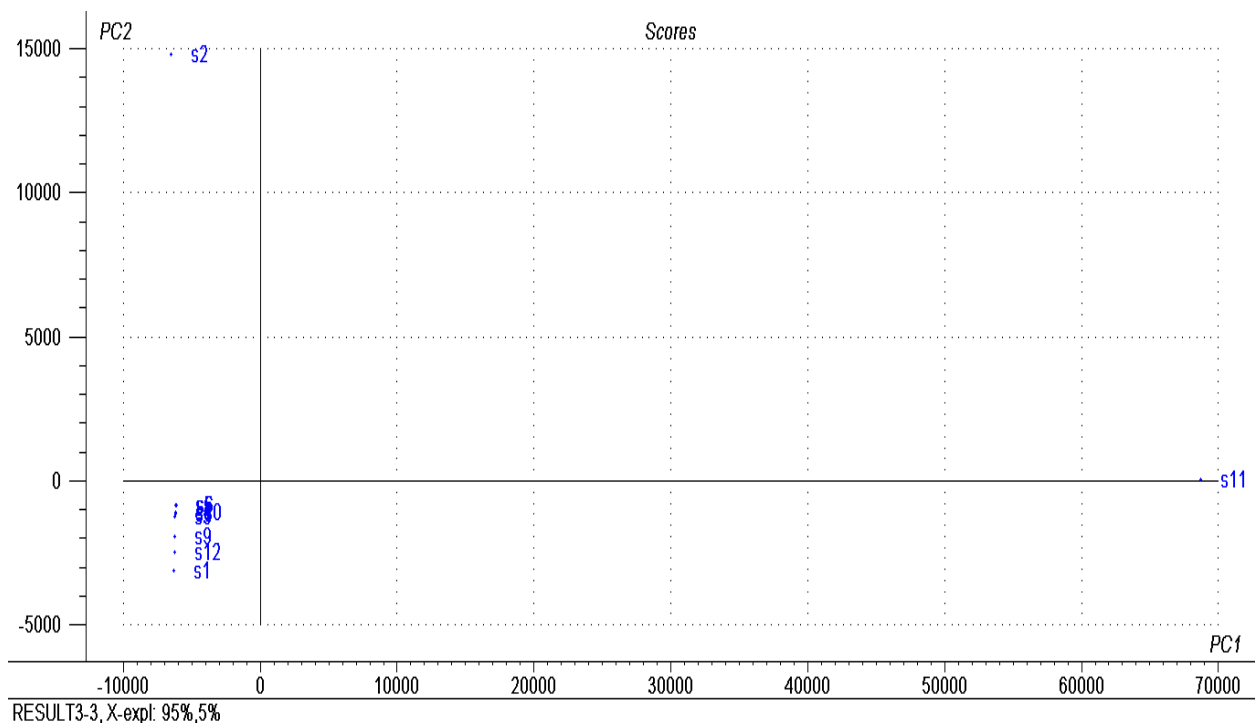
PC scores for rock samples			Correlation loadings for radionuclides in rocks		
Sample	PC1	PC2	Radionuclide	PC1	PC2
R1	-665.779	12.964	K-40	0.99300	-0.11600
R2	-464.652	-40.202	U-238	0.11900	0.97100
R3	134.342	-94.568	Th-232	0.00056	-0.211 00
R4	229.231	28.313			
R5	203.069	50.257			
R6	139.136	27.127			
R7	239.189	8.454			
R8	208.424	35.769			
R9	226.634	-24.798			
R10	224.157	69.281			
R11	221.078	-95.690			
R12	-694.828	23.093			

Figure 5.8 is a 2D scatter plot of rotated scores of PC's for the data matrix for rock samples now characterized by their feature selected gamma-ray spectra. The samples now group in three clusters: A(R2, R8, R10, R12), B(R1, R4, R5, R7, R9) and C(R3, R6, R11). Only samples in cluster A seem to have a common feature among them: Th-232 activities between 120 and 137 Bq/Kg. The three clusters do not show clear common geographical positions or activity patterns. The common feature in their gamma-ray spectra that results in such clustering is probably due to Th-232.



**Figure 5.8:** PCA scatter plots of rotated scores for rock samples based on gamma-ray spectral data.

PCA plots for sediments characterized by their K-40, U-236 and Th-232 activity concentrations do not reveal much information. This is partly because sediments do not have their own unique radionuclide signatures but are influenced by rock and thermal water signatures. It was expected that sediments would have similar patterns as thermal waters because of water sorption in sediments. The 2D plot of rotated scores shows all the sediment samples clustered together save for S11 and S2 which stick out as outliers (Fig 5.9). The single cluster is generally close to both PC's but is closer to PC1 than PC2. The two PC's explain up to 95% of the variance in the sediment samples with 5% residual variance.



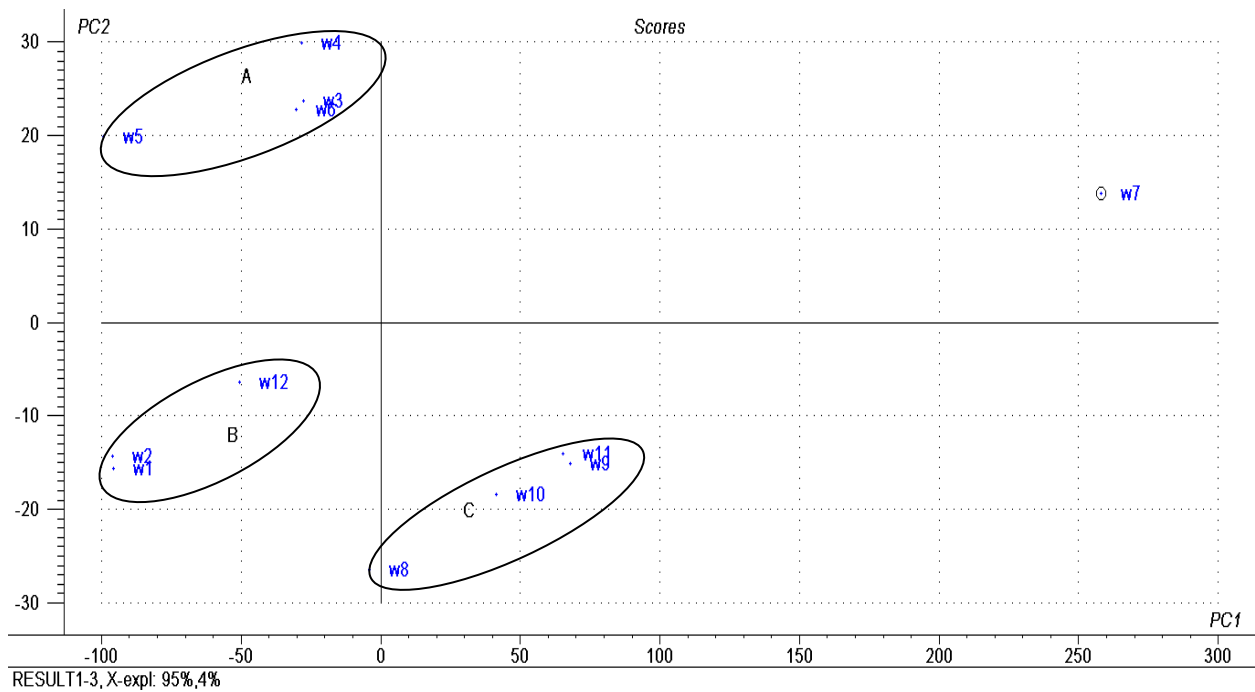
**Figure 5.9:** PCA scatter plots of rotated scores for sediment samples.

Figure 5.10 is a 2D PCA scatter plot of rotated scores for thermal water samples as characterized by their U-238, K-40 and Th-232 activity concentrations. The samples group out in 3 clusters with only W7 marked out as an outlier. Cluster A are samples from springs to the south end of Lake Magadi. The samples have relatively lower K-40 but higher U-238 activity levels compared to the rest. These springs have higher TDS/pH levels and U-238/Th-232 ratios compared to the rest. Cluster B are samples from springs on the western edges of the lake and which have the lowest K-40 levels. Cluster C are samples from springs to the northern end of little Lake Magadi. The springs have higher K-40 levels but lower U-238/Th-232 ratios compared to the other springs around the lake. These springs have higher temperatures but lower TDS/pH levels compared to the rest; springs in clusters A and B have much lower temperatures compared to those in cluster C. The three clusters therefore represent the major sources of spring solutes that contribute to and affect the quality of trona deposits in the lake: highly concentrated inflows from the south (cluster A), relatively fresh spring inflows from the north (cluster C), and saline inflows from the host bedrock on the western edges bounding the lake (cluster B).

Figure 5.11 is PCA scatter plot of rotated scores for thermal water samples as characterized by their gamma-ray spectra (counts against channel numbers). The plot produces the same three clusters observed in Figure 5.10 with the only difference being that of sample W11 being an outlier and not in cluster C. These three clusters again represent the three sources of spring solutes delineated in figure 5.10.

The same three clusters are produced when the thermal water samples are characterized by their trona quality parameters ( $\text{NaHCO}_3$ ,  $\text{Na}_2\text{CO}_3$  and  $\text{NaCl}$  levels) as seen in Figure 5.12. Cluster A are samples from the south of lake Magadi and have higher  $\text{Na}_2\text{CO}_3$  and  $\text{NaCl}$  content than the others as seen in Table 5.18(b). Cluster B are saline spring waters from the western edges of the lake with average salt content. Cluster C are spring waters from the northern end of Little Magadi with higher  $\text{NaHCO}_3$  compared to the others. This now clearly delineates the three regimes of spring inflows into the lake based on their solute contents:  $\text{Na}_2\text{CO}_3$ - and  $\text{NaCl}$ - rich inflows from the south;  $\text{NaHCO}_3$ - rich inflows from the north; and saline fluid inflows from the host bedrock bounding the western edges of the lake.

It can be seen from Table 5.16(b) that springs with higher temperatures also have higher  $\text{NaHCO}_3$  solute content but lower TDS/pH (cluster C) while springs with lower temperatures have higher  $\text{Na}_2\text{CO}_3$  and  $\text{NaCl}$  contents and higher TDS/pH levels (cluster A). Springs in cluster B have parameters that are intermediate between levels in A and B.



**Figure 5.10:** PCA scatter plots of rotated scores for thermal water samples based on radionuclide activity concentrations.

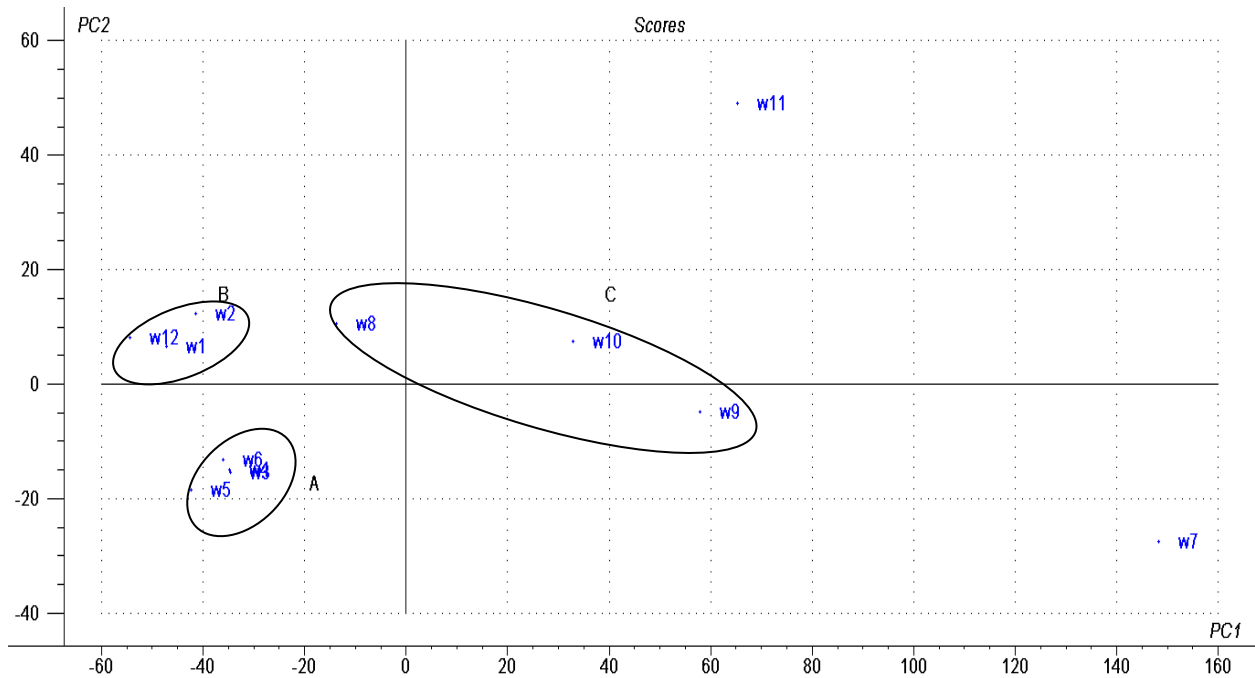


**Figure 5.11:** PCA scatter plots of rotated scores for thermal water samples based on gamma-ray spectra.

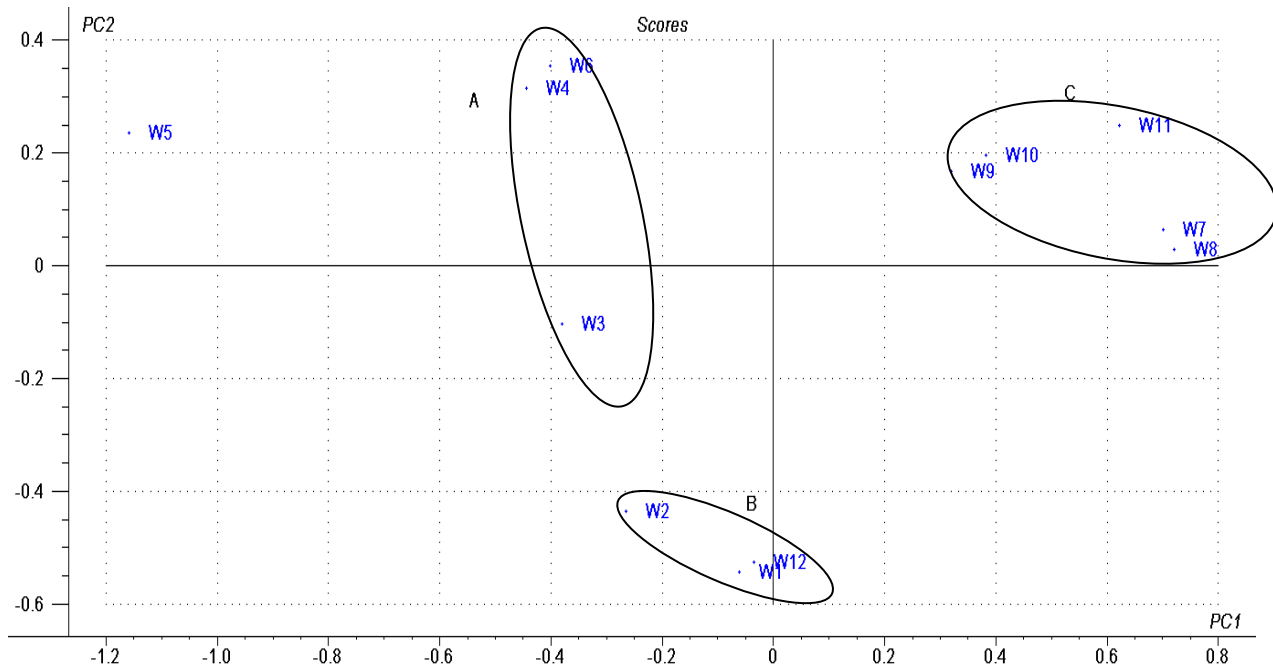


**Figure 5.12:** PCA scatter plots of rotated scores for thermal water samples based on their trona quality parameters.

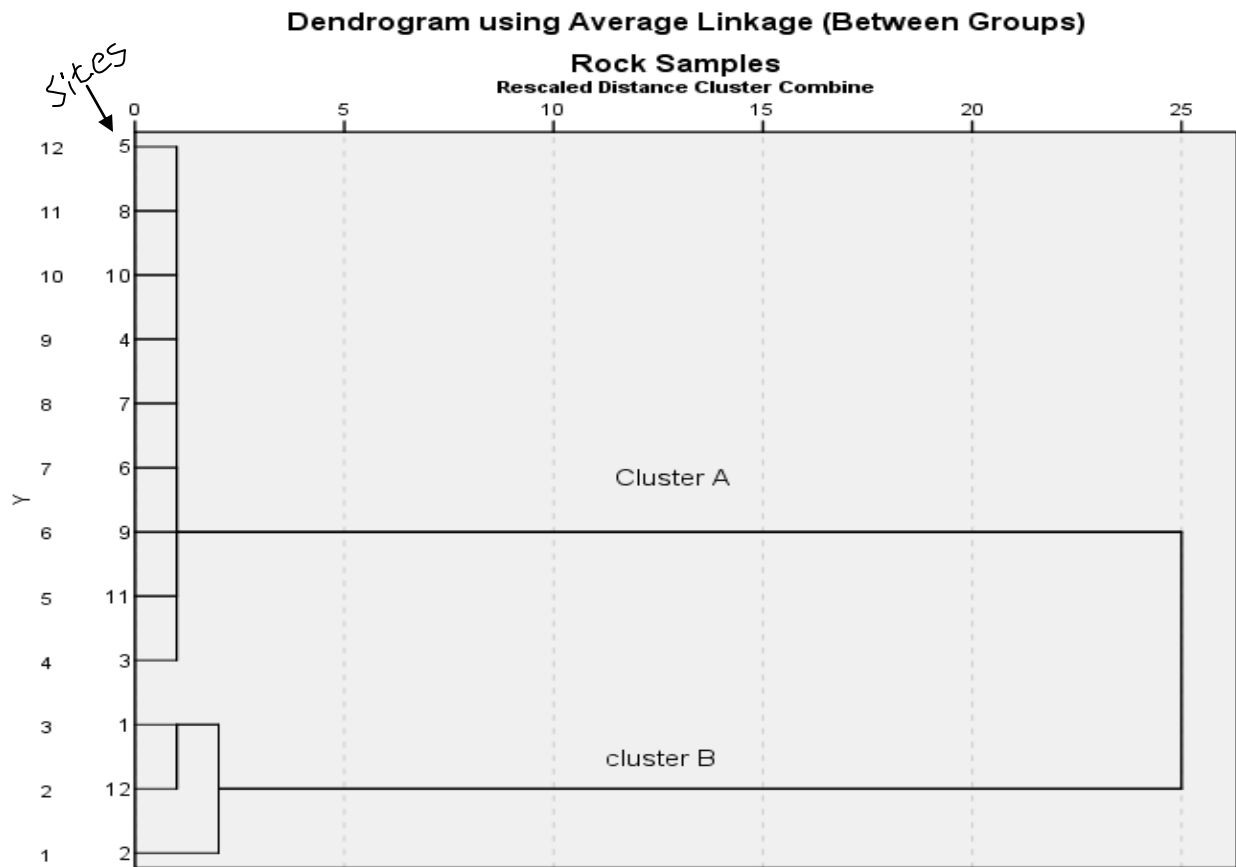
### 5.6.2 Hierarchical cluster analysis (HCA)

HCA analysis on the data from rock and thermal water samples are presented figures 5.13 and 5.14. HCA was done in order to classify and discern salient patterns in the data matrices; just like PCA. HCA classification is based on inter-point distances between sample plots in a multi dimensional space depending on the number of variables used to characterize them. The results are presented in form of dendrograms; which help visualize linkage results and provide 2D plots that indicate clustering, similarities and linkages between samples. The raw data matrices were subjected to HCA and dendrograms produced using average linkage between clusters based on Euclidian distances between sample plots. The vertical axis of the dendrogram gives the sample clusters while the horizontal axis gives level of linkage (similarity value). The lower the linkage level between any group of samples the higher the similarity between them (Peters *et al.*, 2011). The converse is also true.

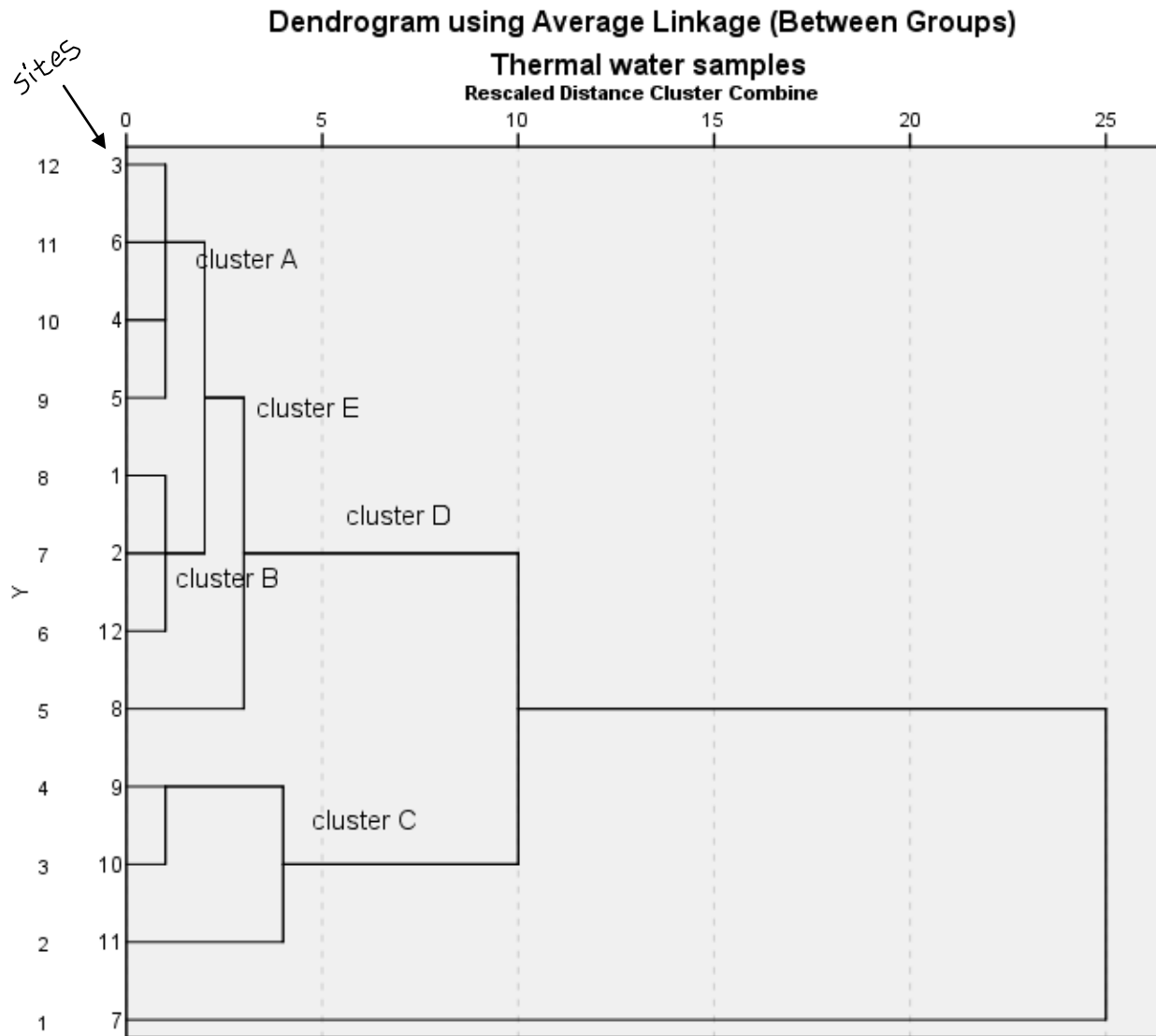
HCA on the data matrix for rocks resulted in the dendrogram shown in Figure 5.13 with the samples grouped into two clusters. The dendrogram indicates that there are two distinct groups of the rock samples which can only be linked at high level (low similarity). Cluster A, comprising of rock samples from sites 3 through 11, are samples with high K-40 concentrations (>1700 Bq/Kg). It is also evident that these are rock samples from the northern and southern edges of the Magadi basin i.e. from the floor of the rift valley. Cluster B are samples from the western edges of the rift bounding the lake. These have low K-40 concentrations (<1200 Bq/Kg). All samples in cluster A are highly similar since they are all linked at the lowest linkage level. Samples R1 and R12 are linked at the lowest level to form a sub cluster before linking with sample R2 at the next higher similarity level to form cluster B. This shows that despite being in cluster B, sample R2 is not as similar to R1 and/or R12 as the two are to each other. R2 was sampled close to the causeway and it is possible that the heavy human activity along the causeway may have altered the gamma-ray spectral signature of the local rock e.g. by induced wet and/or dry atmospheric deposition among other factors.

Figure 5.14 is a dendrogram from the application of HCA to the data matrix for thermal water samples. The spring numbers are shown by the arrow. Clusters A and B are sub clusters of cluster E which is itself a sub cluster of cluster D. The dendrogram shows that there are three groups of samples which have a lot of similarities (low linkage level). Three groups can be distinguished: cluster A (samples 3, 6, 4, 5), cluster B (samples 1, 2, 12) and cluster C (samples 9, 10). Sample 8 links to clusters A and B at the same linkage level but does not fall into either cluster. Sample 11 is linked to cluster C at a level higher than where sample 8 is linked to clusters A and B. Sample 7 is linked to the rest of the samples at a very high linkage level. This shows that it has very little in common with the rest of the water samples hence is an outlier. It is evident from Tables 5.1, 5.5 and 5.16(b) that cluster A are springs to the south of Lake Magadi and are characterized by lower temperatures but higher levels of  $\text{Na}_2\text{CO}_3$ , NaCl and U-238 activity concentration compared to the others. Cluster B are springs on the western edges of the lake and are characterized by lower U-238 and K-40 activities, while cluster C are the northern

springs characterized by high temperatures,  $\text{NaHCO}_3$  content and Th-232 activity. It is important to note from the dendrograms that the two clusters for rocks (Fig 5.6) and the three clusters for thermal waters (Figures 5.10, 5.11 and 5.12) are exactly the same as the ones in HCA as seen in Figures 5.13 and 5.14 respectively. This is consistent since both PCA and HCA are classification/clustering tools; they give similar information but in different forms.



**Figure 5.13:** Dendrogram generated by hierarchical clustering of rock samples.



*Figure 5.14: Dendrogram generated by hierarchical clustering of thermal water samples.*

### 5.6.3 Classification trees (CT)

A decision tree procedure was used to create a classification model for predicting thermal water TDS based on K-40 activity. The method classifies samples into groups and predicts values of a dependent variable (TDS in this case) based on values of an independent (predictor) variable (K-40 activity). This allows for exploratory and confirmatory classification analysis. Because of the small data sets and non normal distribution of the measurements, the stratification technique was used to construct the trees. This technique assigns samples into one of several categories such as high, medium or low depending on the variation in the independent variable (Kurt and Peter, 2008).

Figure 5.15 is a classification tree developed from the thermal water data matrix using CHAID growing method with TDS as the dependent variable and K-40 activity as the independent variable. The recursive algorithm that does the plotting picked K-40 activity as the only independent variable because of its near normal distribution (Table 5.11). The tree has only one split (depth of 1) with a root node and 9 terminal nodes. Each of the terminal nodes has one sample each save for nodes 4 and 7 which have 2 and three samples each. The sample in node 1 has K-40 activity equal to or below 73.20 Bq/Kg with a predicted TDS of 2.564 %m/m; only sample W12 fits this description. The sample in node 2 has K-40 activity above 73.20 Bq/Kg but equal to or below 80.599 Bq/Kg with a predicted TDS value of 2.092 %m/m. Only sample W1 fits this description. Node 3 has 1 sample whose K-40 activity is above 80.599 Bq/Kg but equal to or below 85.209 Bq/Kg with predicted TDS of 2.349 %m/m- sample W2. For node 4, K-40 activity should be above 85.209 Bq/Kg but equal to or below 96.14 Bq/Kg with predicted TDS of 3.0635 %m/m. Two samples W5 and W6 fit the description for node 4. Node 5 has K-40 activity above 96.14 Bq/Kg but equal to or below 98.17 Bq/Kg and predicted TDS of 2.16 %m/m; only sample W3 fits this description. Node 6 has K-40 above 98.17Bq/Kg but equal to or below 98.18Bq/Kg with a predicted TDS value of 3.068 %m/m- sample W4. Based on the description for node 7 from the tree in Figure 5.15, three samples- W8, W10 and W11 would fit into the node. Samples W9 and W7 would fit into nodes 8 and 9 respectively. This tree model can be used to predict TDS levels of any other spring in Lake Magadi basin based on its K-40 activity. The algorithm used K-40 activity as the only independent variable to construct the model because of its near normal distribution as opposed to as the other radionuclides and parameters whose distributions were clearly non normal, some almost polar (Temp, TOC, pH). Because of the polar nature of the other parameters, classification trees constructed with any of them as the dependent variable or as the only independent variable had only one split and two terminal nodes - one for each of the polar ends. This can be seen in Figures 5.16(a) to (h) where all the 12 samples are grouped into only two terminal nodes hence poor prediction by models.

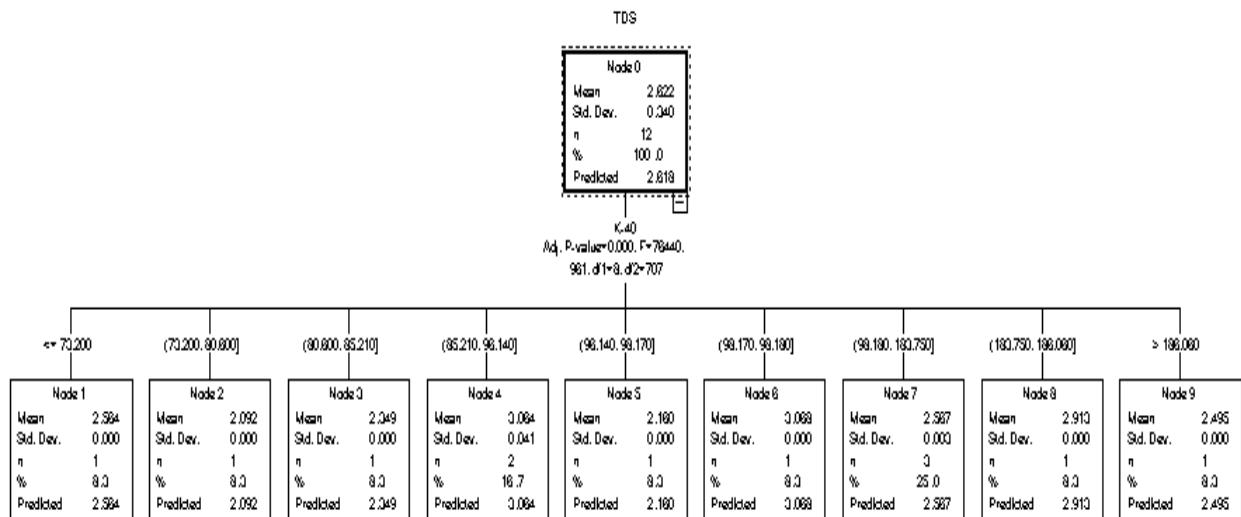
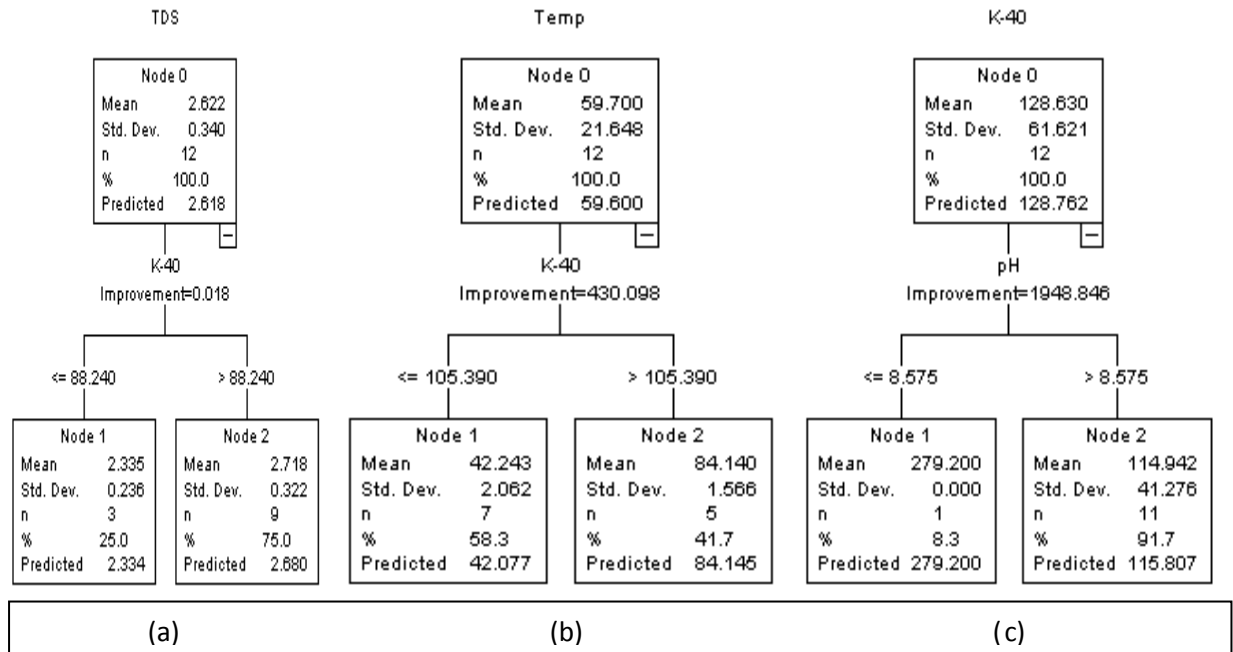


Figure 5.15: CT for predicting spring TDS based on their K-40 activity.



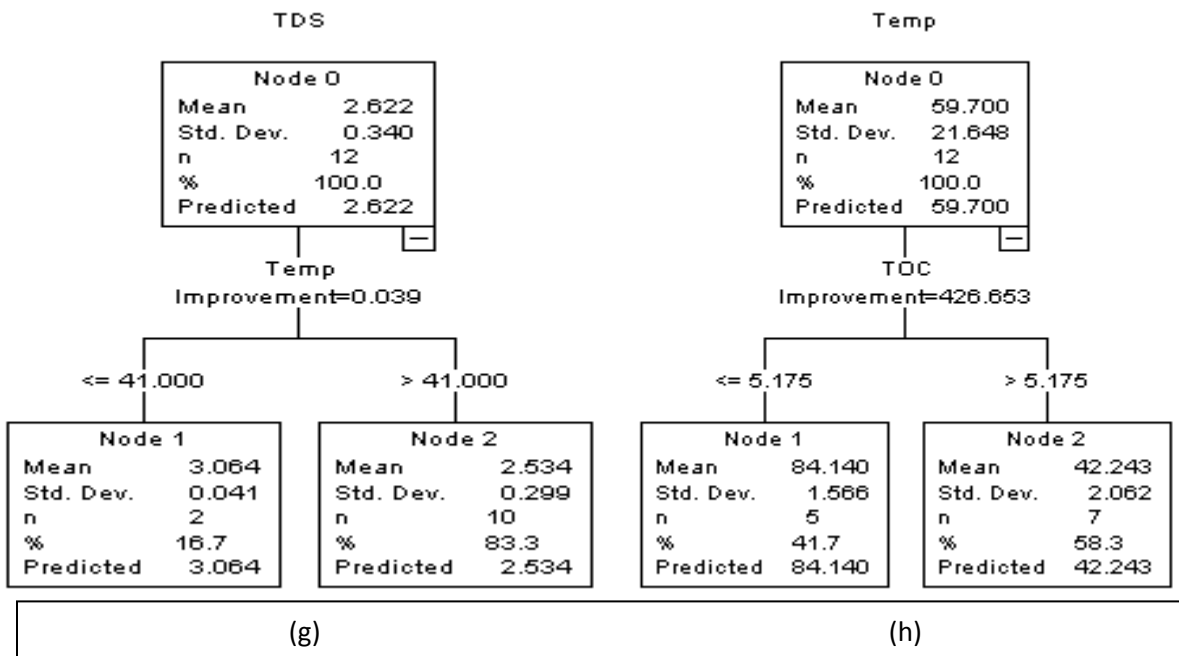
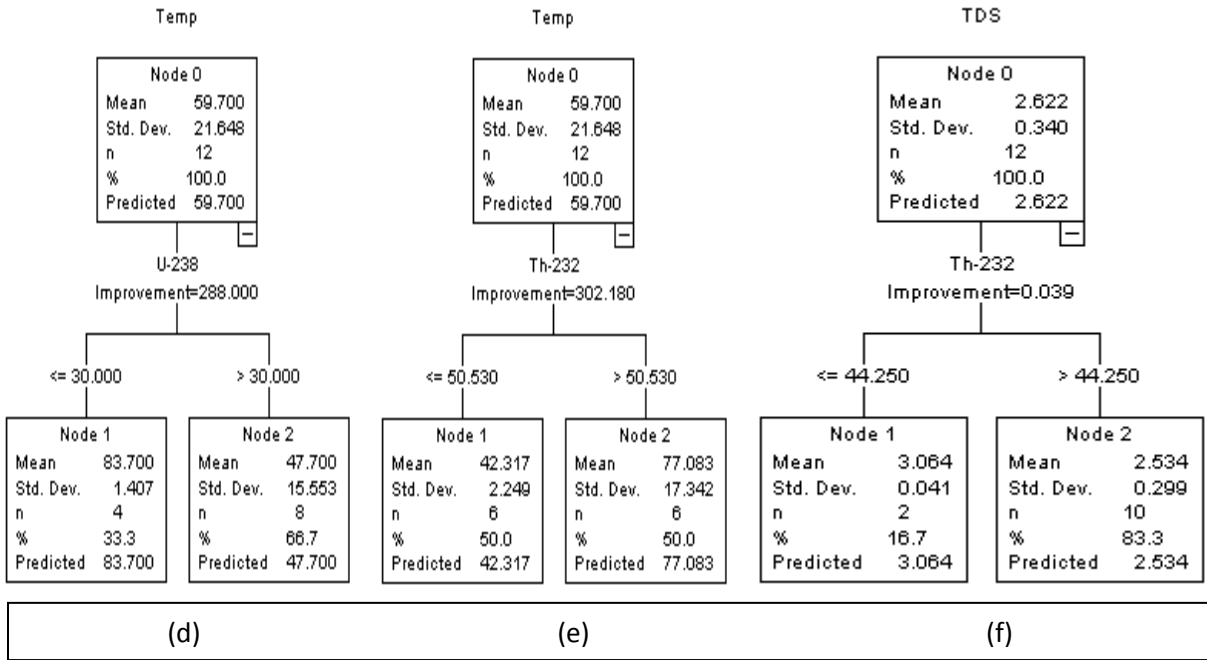
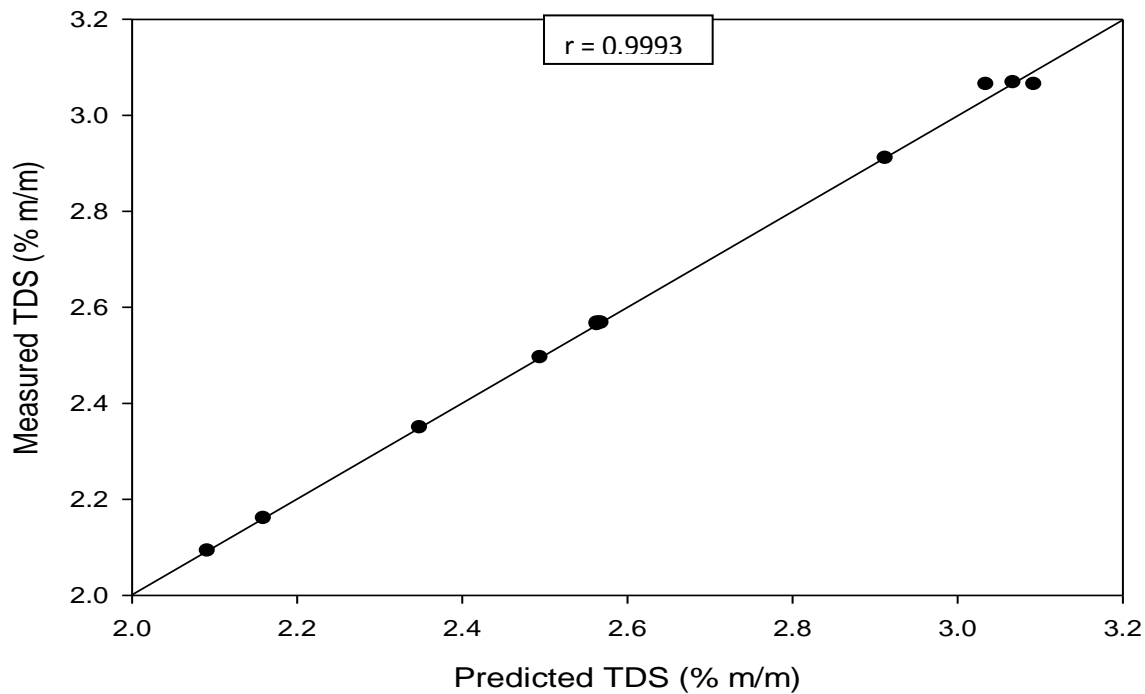


Figure 5.16: CTs for predicting spring water parameters.

Table 5.20 compares spring TDS levels as measured in the laboratory to those predicted using the classification tree in Figure 5.15 based on the stratification technique while Figure 5.17 shows correlation between the measured and predicted values. The high correlation between the two sets of values shows the effectiveness of the model in predicting spring TDS levels based on their K-40 activity concentration.

**Table 5.18:** Comparison between measured and predicted spring TDS values

Spring No.	TDS (% m/m) $\pm 0.034$	
	Measured	Predicted
1	2.092	2.092
2	2.349	2.349
3	2.160	2.160
4	3.068	3.068
5	3.035	3.064
6	3.093	3.064
7	2.495	2.495
8	2.564	2.567
9	2.913	2.910
10	2.569	2.567
11	2.567	2.567
12	2.564	2.564



**Figure 5.17:** Correlation between measured and predicted spring TDS values

## Chapter Six

# CONCLUSION AND RECOMMENDATIONS

Radionuclide analysis and multivariate exploratory characterization of the Magadi basin geothermal field has been done using HPGe based gamma-ray spectrometry and PCA, HCA and CT. Activity concentrations of K-40, U-238 and Th-232 in trachyte rocks, thermal waters, sediments and trona from the Magadi basin have been measured in relation to TDS, pH, s.g. and TOC of thermal waters and CEC of sediment. PCA, HCA and CT have been used to classify, delineate regimes of spring inflows and model their TDS levels based on K-40 activity concentrations.

The mean concentrations of K-40, U-238 and Th-232 radionuclides in the trachyte rocks from Lake Magadi basin in Bq/Kg are  $1613.98 \pm 13.96$ ,  $162.26 \pm 13.53$  and  $120.12 \pm 15.09$  respectively. These range from the lowest levels of 922.71, 69.95 and 83.26 to the highest levels of 1852.30, 260.40 and 184.29 for the three radionuclides respectively. Rocks from the north of the Magadi basin have higher activity concentrations than those from other sections of the basin. K-40 and Th-232 radionuclides are accumulating within the Magadi basin with enrichment coefficients of 1.2 and 1.6 respectively due to enhancement and immobilization of NORMs in shore sediment by the hot springs. The accumulation is however not as significant as would be expected because of low level radioactivity in the spring recharges. Heat improves Th-232 sorption capacity of the shore sediments. The southern springs have higher U-238 activities while the northern ones have higher K-40 and Th-232 activities compared to the rest.

The mean K-40, U-238 and Th-232 activities in sediments and spring waters in Bq/Kg are  $1875.80 \pm 10.75$ ,  $131.21 \pm 9.94$  and  $188.21 \pm 5.58$  and  $127.55 \pm 21.71$ ,  $41.73 \pm 22.3$  &  $55.85 \pm 17.8$  respectively. These values show that the Lake Magadi endorheic basin is a sink for radionuclides from the spring inflows and weathering of surrounding volcanics in addition to both wet and dry atmospheric deposition, making it a quasi HBRA with the radionuclide levels in shore sediment being approximately 5, 4, and 6 times the world average values respectively but lower than the minimum values in typical HBRA. Statistical analysis gives log normal distribution of the radionuclides, indicating an uneven spatial distribution within the basin, probably due to different radionuclide signatures of the spring recharges.

Trona samples have same radionuclide signatures as spring waters. The Magadi Soda Company does not contribute to further radiogenic pollution in Lake Magadi by disposing of settler tailings from its plant back into the lake. Through use of PCA and HCA analyses, three different regimes of spring inflows that contribute to and affect the quality of trona in the lake have been delineated:  $\text{Na}_2\text{CO}_3$  and NaCl rich inflows from the south;  $\text{NaHCO}_3$  rich inflows from the north; and saline fluid inflows from the host bedrock bounding the western edges of the lake. Decision

tree (CT) modeling has been used to create a model for predicting spring TDS levels based on their K-40 activities.

The hottest springs have higher K-40 and Th-232 activities while the cooler ones had higher U-238 activities; K-40 and Th-232 activities in spring waters correlate positively while U-238 activity correlates negatively with temperature. Alkalinity and TDS of the springs correlate negatively with K-40 and Th-232 activities but positively with U-238 activity while their TOC correlates negatively with K-40 activity concentration but positively with U-238 activity concentration. Although the concentrations of spring waters vary considerably from 2.160 % to 3.093 % of dissolved solids, there is a remarkable constancy in their  $^{232}\text{Th}/^{40}\text{K}$  ratio, varying minimally from 0.394 to 0.602.

Multivariate chemometric analysis of the radionuclide levels, gamma spectral finger prints and distributions in relation to thermal water temperatures, pH, TDS, TOC, and sediment CEC reveal marked diversity in the geochemical properties of the source rocks responsible for the spring solutes and more significantly, the presence of an underlying uranium-rich rock source. Analysis of the radionuclide ratios indicates that the geochemical immobilizations of U-238 and Th-232 in groundwater flows are the same in the entire basin.

Because sampling for this study was done during the dry season, it would be important to monitor these spring water parameters at different times in the course of an average year so as to determine any seasonal variations. To confirm the contribution of natrocarbonatite ash from the Oldonyo Lengai volcano towards the trona accumulations at Lake Magadi, TDS of the southern springs should be monitored whenever the volcano erupts. Water balance studies between Lakes Magadi and Natron should also be done to establish any groundwater links between the two lakes. This will confirm or disapprove if indeed Lake Natron provides underground recharge for Lake Magadi.

Spring number 1 (GPS location  $36^{\circ}11.20'E$ ,  $1^{\circ}54.10'S$ ) is the most alkaline at pH 9.82 despite not being the most concentrated. This is not consistent with expectation since TDS correlates positively with alkalinity of the spring waters. In a recent study of the highly alkaline saline Magadi environment and its relevance to understanding the habitability of the planet Mars by Lottie (2012), the same spring recorded the highest pH at 10.01. This should be a point of interest for future geochemical studies around Lake Magadi.

Further tests should be done on the settler tailings from the Magadi Soda Company to ascertain that the company does not introduce any form of chemical pollution by disposing of the same back into the lake. Such tests should include trace heavy metal analysis. The waters of the lake should also be analyzed and compared with the results for spring waters. Such analysis should include radioactivity measurements, TDS, pH and trace heavy metal analysis. It is also

recommended that trace heavy metal analysis be done on the spring waters and sediments to establish if the trace elements could be accumulating in the basin.

Despite having a small bridge across it, the effect of the causeway on the physical-chemical parameters of the lake waters on either side should be investigated. Further analysis of TDS and NORM of the lake waters should also be done in order to geochemically characterize all the water sources of the lake and hence confirm or disapprove suspected underneath inflows.

Chemometrics should be applied to a larger sample set in order to build models that can predict sampling location, spring temperature and other physico-chemical parameters of any sample from its gamma spectral fingerprint.

Such studies should also be done on Lake Natron in Northern Tanzania and the results compared to those for Lake Magadi.

## REFERENCES

Achola, S.O., Patel, J.P., Mustapha, A.O. and Angeyo, H.K.(2012), Natural Radioactivity in the High Background Radiation Area of Lambwe East, Southwestern Kenya, *Radiation Protection Dosimetry* 2: 1-6.

Agora, J.O.(2012), Assessment of Natural Radioactivity Levels and Radiation Risk due to the Different Rock Types in the Kerio Valley Region of Kenya, M.Sc Thesis, Kenyatta University.

Ammar, H.F., Deschamps, P., Chikir, N., Hamelin, B. and Zouari, K.(2011), Uranium isotopes as a tracer of groundwater evolution in Complexe terminal aquifer, Tunisia; Presentation at the International Symposium on Isotopes in Hydrology, Marine Ecosystems, and Climate Studies, Oceanographic Museum of Monaco, France.

Angeyo, H.K., Patel, J.P., Mangala, J.M., and Narayana, D.G.S. (1999), Radioisotope Photon-Excited Energy Dispersive X-Ray Fluorescence Technique for the Analysis of Organic Matrices, *X-ray Spectrometry* 27, 205 – 213.

Arogunjo, A.M. (2007), Terrestrial Gamma Radiation and the Radiological Implication in South Western Nigeria, *Journal of Applied Sciences* 7(11): 1534-1537.

Avrahmov, N., Yechieli, Y., Lazar, B. and Sivan, O.(2011), Characterization of the carbon system in the saline groundwater of the Dead Sea, Presentation at the International Symposium on Isotopes in Hydrology, Marine Ecosystems, and Climate Studies, Oceanographic Museum of Monaco, France.

Baker, B.H. (1987), Outline of the Petrology of the Kenya Rift Alkaline Province: Geological Society, London, Special Publications, 30:293-311.

Baker, B. H. (1958), Geology of the Magadi Area, Geological Survey of Kenya Report No. 42, Govt. Press- Nairobi, Kenya.

Balochi, M.A., Qureshi, A.A., Waheed, A. and Ali, M.(2012), A study of Natural Radioactivity in Khewra Salt Mines, Pakistan, *J. Radiat. Res.*, 53: 411-421.

Becht, R. (2005), Ground Water Links Between Kenya rift Valley Lakes, M.Sc Thesis, International Institute of Aerospace Survey and Earth Sciences, Netherlands.

Bell, K., Dawson, J.B. and Farquhar, R.M.(1973), Strontium Isotope Studies of Alkaline Rocks: The Active Carbonatite Volcano Oldonyo Lengai- Tanzania, *Journal of Geological Society of America*, 84(3): 1019-1030.

Brereton, R.G. (2003), *Chemometrics: Data Analysis for the Laboratory and Chemical Plant*, John Willey & Sons, Bristol.

Bulmer, M.G.(1979), Principles of Statistics, Dover & Co. Inc, NY.

Burcham, W.E. (1988), Elements of Nuclear Physics, Longman, Singapore.

Burger, H., Sheehan, A., and Jones, C. (2006), Introduction to Applied Geophysics, W.W. Norton & Co. Inc, New York.

Clarke, M.C.G., Woodhall, D.G., Allen, D.J. and Darling, W.G. (1990), Geological, Volcanological and Hydrogeological Controls on the Occurrence of Geothermal Activity in the Area Surrounding Lake Naivasha Kenya, British Geological Survey Report to the Ministry of Energy, Kenya.

Debertin, K. and Helmer, R.G.(1998), Gamma and X-ray Spectrometry with Semiconductor Detectors, North Holland, Amsterdam.

Dawson, J.B. and Gale, N.H.(1990), Uranium and thorium in alkali rocks from the active carbonatite volcano Oldoinyo Lengai – Tanzania, Journal of Environmental Geochemistry,30:217-225.

Eugster, H.P. (1986), Lake Magadi, Kenya: a model for rift valley hydrochemistry and sedimentation, J. Geological Society, London, 25: 177-189.

El-bahi, M.S.(2002), Radioactivity levels of salt for natural sediments in the in the northwestern desert and local markets in Egypt, Applied Radiation and Isotopes 58:143-143.

Faber, E., Vengosh,A., Garrielli,I., Marie, A., Bullen,J.D., Mayer,B., Polak,A. and Sharit,U. (2012), The geochemistry of ground water resources in the Jordan valley: The impact of rift valley brines.

Farmaki, G.E., Nikolaos, S.T., Simeonov, V. and Efstathiou, E.C. (2012) A Comparative Chemometric Study for Water Quality Expertise of the Athenian Water Reservoirs, Environ. Monit. Asses, 184:7635-7652.

Franklin, C.E., Johnson, I.A., Crockford, T. and Kamunde, C.(1995), Scaling of oxygen consumption of Lake Magadi tilapia, a fish living at 370C, Journal of Fish Biology, 46:829-834.

Githiri, J.G., Patel, J.P., Barongo, J.O. and Karanja, P.K. (2011), Application of Euler Deconvolution in Determining Depths to Magnetic Structures in Magadi Area, Southern Kenya Rift, Journal of Applied Geophysics, Science and Technology, 13(1):142-157.

Goraieb, K, Lopes, A.S., Sato, C.A., Segatelli, M.G., Silva, V.P., Verzoto, J.C., and Bueno, M.I.M.S. (2006), Characterization of Portland Cements by X-ray Spectrometry allied to Chemometrics, J. Chemometrics, 20: 455-463.

Gordon, R.G. (2008), Practical Gamma Ray Spectroscopy, John Willey and Sons, New York. (25-28)

Hibbert, D.B., Minkkinen, P., Faber, N.M., and Wise, B.M. (2009) IUPAC Project: A glossary of concepts and terms in chemometrics, Anal. Chim. Acta 642, 3-5.

IAEA (1987), Preparation and Certification of IAEA Gamma Spectrometry Reference Materials, IAEA/RL/148, Vienna, Austria.

IAEA (2003), Guidelines for radioelement mapping using gamma-ray spectrometry data, IAEA report, Vienna, Austria.

Ibs-Von, S.M., Blumenstein, S., Wagner, R., Hollnack, D. and Wohlenberg, J.(2001), Seismicity, Seismotectonics and Crustal structure of the southern Kenya Rift-new data from Lake Magadi area, International Journal of Geophysics 146: 439-453.

Jennejohn, D.(2009), Research and Development in Geothermal Exploration, Geothermal Energy Association Bulletin.

Jing, D., Deguang, W., Linfang, H., Shilin, C. and Minjian, Q. (2011), Application of Chemometrics in Quality Evaluation of Medicinal Plants, J. Medicinal Plants Research 5(17): 4001-4008.

Johnson, B.,(2011) Measuring Radionuclides in the Environment- IAEA training course material, Argonne National Library, USA.

Kansaana, C., Darko, E.O., Scharndorf,C., Adukpo, O.K., Faanu, A., Lawluri, H. and Kpeglo, D.O. (2012), Determination of Natural Radioactivity in Saline Waters and Salt from Panbros Salt Industry of Accra, Ghana, Int. J. Science and Technology 2(3): 107-112.

Keith, L.H.(1988), Principles of environmental sampling, American Chemical Society Professional Reference Book, American Chemical Society.

Kessler, T., Hoffman, P., Greve, T., and Ortner, H.M. (2002) Optimization of the identification of chemical compounds by energy dispersive x-ray fluorescence spectrometry and subsequent multivariate analysis, X-ray Spectrom. 31, 383-390.

Kerich, R., Renaut, R. W. and Bonli, T (2010), Trace Element Composition of Cherts from Alkaline Lakes in the East African Rift: A probe of ancient counterparts, J. Sedimentation in continental rifts, 73: 275-294.

Kenneth, R. and Randy, J. (1998), Chemometrics: A practical guide, John Willey and Sons Inc., New York, 56-67.

Kim, G., Kim, T.H. and Church, T.M. (2005), Po-210 in the environment: biogeochemical cycling and Bioavailability, *Earth Planet Letts.* 14: 271-284.

Knoll, G.F. (1997) *Radiation Detection and Measurement* 2<sup>nd</sup> Ed, John Willey & Sons, New York.

Korum, M., Kovacic, K. and Kozar, L.J.(2011), Concentrations of tritium and members of the uranium and thorium series in groundwater in Slovenia and their implication for managing groundwater resources, Presentation at the International Symposium on Isotopes in Hydrology, Marine Ecosystems and Climate Studies; Oceanographic Museum of Monaco, France.

Kurt, V. and Peter, F. (2008), *Introduction to Multivariate Statistical Analysis in Chemometrics*, CRC Press, New York.

Lima, A., Albanese, S.and Cicchella, D.(2005), *Applied Geo-chemistry*, 20, 611-625.

Lottie, E.D.(2012), An astrobiological study of an alkaline-saline hydrothermal environment, relevant to understanding the habitability of Mars, PhD thesis, University College London.

Minervini, J.M. (1998), Radiogenic Isotope Investigation of Sources, Transport, and Deposition of Rare Earth Elements in the Owens Lake Drainage Basin, Eastern California, MSc Thesis, University of Pittsburgh, USA.

Mohanty, A.K., Sengupta, D., Das, S.K., Vijayan, V. and Saha, S.K. (2004), Natural radioactivity in the new discovered high background radiation area on the eastern coast of Orissa, India, *Radiation measurements-International congress series* 1276(38): 153-165.

Muno, F.A. (2002), *Water Balance of the Southern Kenya Rift Valley Lakes*, M.Sc Thesis, International Institute of Aerospace Survey and Earth Sciences, Netherlands.

Mustapha, A.O. (1999), Assessment of Human Exposures to Natural Sources of Radiation in Kenya, *Radiation Protection Dosimetry*, 82:285-292.

Murad, A., Aldahan, A., Hou, X.L., Hussein, S. and Possnert, G.(2011), Natural radioactivity of groundwater from the United Arab Emirates (UAE), Presentation at the International Symposium on Isotopes in Hydrology, Marine Ecosystems, and Climate Studies, Oceanographic Museum of Monaco, France.

Mutie, A.M.(2012), Characterization of microalgae species from selected lakes in Kenya and their potential in bio-fuel production, MSc Thesis, University of Nairobi, Kenya.

Nicholas, T. (1995), *Measurement and Detection of Radiation*, Taylor and Francis, 2<sup>ND</sup> Ed., Washington DC. (381-433).

Nielsen, J.M. and Dahi, E.(2011), Fluoride Contamination and Mineralogical Composition of East African Magadi(Trona), Second International Workshop on Fluorosis Prevention and Defluoridation of Water, Copenhagen, Denmark.

Oliveira, L., Antunes, A.M. and Bueno, M.I. (2010), Direct Chromium Speciation using X-ray Spectrometry and Chemometrics, X-ray Spectrometry, 39: 279-284.

Osenbrueck, K., Bretzler, A., Stadler, S., Ehser, A., Ruprecht, J.S., and Gloaguen, R. (2013), Groundwater flow pattern and water-rock interaction in the Ethiopian Rift Valley, Technical report of the Water & Earth System Science Research Centre, Univ. Tuebingen, Germany.

Otwoma, D., Patel, J.P., Bartilol, S.K. and Mustapha, A.O. (2013), Estimation of Annual Effective Dose and Radiation Hazards Due to Natural Radionuclides in Mount Homa, Southwestern Kenya, Radiation Protection Dosimetry, 2013: 1-8.

Parkinson, J. (1914), The African trough in the neighbourhood of the Soda Lakes, Journal of Geology 154: 33-49.

Patel, J.P. (1991), Environmental radiation survey of the area of high background radioactivity of Mrima hill of Kenya, Discovery and Innovation 3(3): 31-36.

Peters, K., Ramos, B.L. and Zumberge, J. (2011), Circum-Arctic Petroleum Systems defined using Biomarkers, Isotopes, and Chemometrics; Search and Discovery article #30146.

Pizarro, P., Rodriguez, S.T., Notario, N.P. and Gonzalez, J.M.(2008), Usefulness of chemometrics to classify pottery sherds belonging to the south east of USA, Paper presentation at the 2<sup>nd</sup> Ed of the Mediterranean meeting on Multivariate Analysis and Chemometry applied to Environmental and Cultural Heritage, Venstotene Island, Italy.

Phillips, H. (1981), The periodic table of elements, Almelo, Netherlands.

Rajesh, P., Vedhagiri, S.J., Ramasmy, V. and Meenakshisundaram,V.(2013), Measurement of level of natural gamma emitting radionuclides in charnockite rocks of Kalrayan Hills, India, Archives of Applied Science Research, 5 (2):278-286.

Ramasamy,V., Senthil, S. and Meenakshisundaram, V.(2009), Distribution of Natural Radionuclides and Minerals in Beach Sediments from North East Coast of Tamilnadu, India, African Journal of Basic and Applied Sciences, 1(1-2):15-20.

Randolph, P.S. (1996), Experimental Gamma-Ray Spectroscopy and Investigations on Environmental Radioactivity, Spectrum Techniques Publishers, Tennessee, USA.

Riaroh, D and Okoth, W (1994), The Geothermal Fields of the Kenya Rift, Tectonophysics 236: 117-130.

Richard, K. (1998), *Chemometric Techniques for Quantitative Analysis*, Narcel Dekker, INC Network.

Science Daily US (2008), Iodized table salt may be low in Iodine: Health concerns, Annual report.

Stevens, J.A.(1932), Lake Magadi and its alkaline springs, Unpublished report of the Magadi Soda Company Ltd., Kenya.

Surdam, R.C. and Eugster, H.P. (1976), Mineral Reactions in the Sedimentary Deposits of Lake Magadi Region, Kenya, *Journal of Geological Society of America*, 87(12): 1739-1752.

Tagma,T., Warner, N., Bouchaou, L., Ettayfi, N. and Vengosh, A. (2012), Radium, Uranium and trace metals contamination in Al Bahira aquifer of Youssofia area, Morocco, *Environmental Monitoring Assessment*, 148(3):227-236.

Tahir, S.N. and Alaaamer, A.S. (2008), Determination of natural radioactivity in salt and radiation doses due to its ingestion, *Journal of Radiation and Isotopes* 28: 233-236.

UNESCO (2008), Great Rift Valley Eco-system, United Nations Educational, Scientific and Cultural Organization World heritage centre report.

UNSCEAR (2000), Sources of Ionizing Radiation, United Nations Scientific Committee on the Effects of Atomic Radiation, report to the general assembly.

UNSCEAR (1998), Sources of Ionizing Radiation, United Nations Scientific Committee on the Effects of Atomic Radiation report to the general assembly.

Voncina, E., Voncina, D.B., Mirkovic, N. and Norvic, M. (2007), Chemometric Characterization of the Quality of Ground Waters from Different Wells in Slovenia, *Acta Chim. Slov.* 54:119-125.

Warner, N., Tagma, T., Vinson, D., Bouchaou, L., Ettayfi, N. and Vengosh, A.(2011), Evaluation of Sr, B, and Ra isotopes from Geothermal Source Water from Central and Southern Morocco, *Proceedings from the International Symposium on Isotopes in Hydrology, Marine Ecosystems, and Climate Studies*; Oceanographic Museum of Monaco, France.

Yanda, P.Z. and Madulu, M.F.(2005), Water Resource Management and Biodiversity Conservation in the Eastern Rift Valley Lakes, Northern Tanzania, *Physics and Chemistry of the Earth*, 30: 717-725.

Yadav, D.N. and Sarin, M.M. (2009), Ra-Po-Pb isotope systematic in waters of Sāmbhar salt Lake, Rajasthan (India): geochemical characterization and particulate reactivity.

## APPENDIX

### A. Comparison of T<sub>0</sub> and TDS values with previous measurements on the same springs

Spring No.	T <sub>0</sub> (°C) ± 0.1		TDS (%m/m) ± 0.034	
	Present study	Stevens(1932)	Present study	Stevens(1932)
1	43.30	45.50	2.092	2.090
2	41.80	35.50	2.349	2.320
3	44.60	38.50	2.260	2.160
4	44.20	44.20	3.068	3.120
5	40.20	40.00	3.035	3.010
6	39.00	39.00	3.093	3.102
7	85.90	85.00	2.495	2.480
8	85.00	85.00	2.564	2.560
9	84.70	81.00	2.913	2.850
10	83.10	81.50	2.569	2.760
11	82.00	81.60	2.567	2.740
12	42.60	44.20	2.564	2.412

### B. pH measurements

pH values of thermal water samples were determined in the laboratory using a HANNA pH-211 Microprocessor pH meter with a temperature compensation probe. The measurements were done with the thermal water temperatures between 22.80 °C and 23.20 °C. The pH meter was first calibrated using a standard alkaline buffer solution.

### C. TDS and s.g. measurements

TDS levels of the thermal waters were determined gravimetrically after evaporation of known masses of the waters on glass evaporating dishes. It was assumed that there were no organic solutes in the waters. s.g. values were determined from measurements of volume and mass.

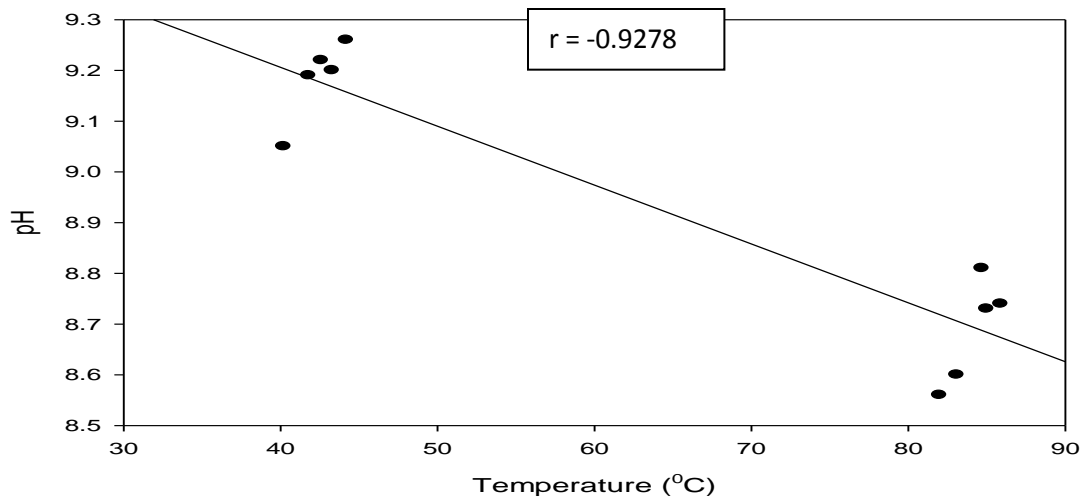
#### D. CEC measurements

The ASTM D7503 standard test method for CEC measurements was used. The pulverized samples from gamma-ray spectrometry were used for the test. The samples were thoroughly homogenized before measurements were done. The samples were washed in high quality de-ionized water through a 75 microns sieve to remove any excess salts. 100g of the washed samples were treated with an index ion solution containing these ions so as to force those existing in the samples into solution. The total concentrations of the soluble cations in the solution were then measured titrimetrically by treating the samples with ammonium acetate solution.

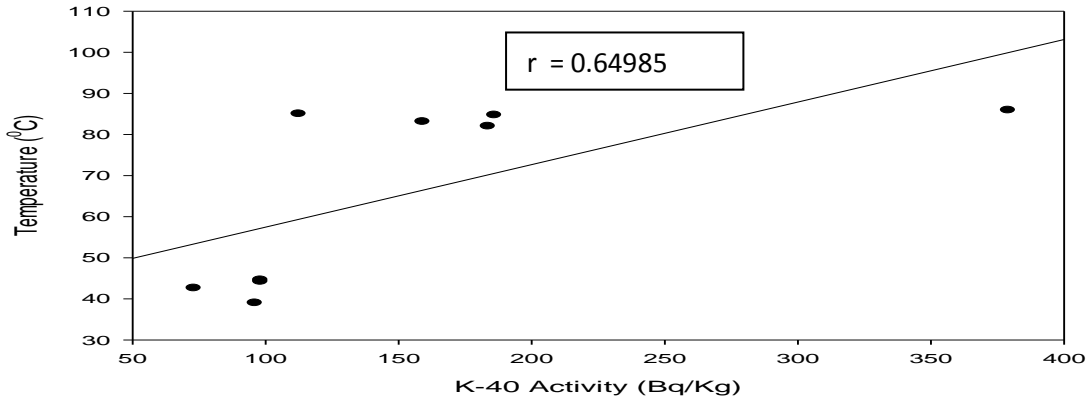
#### E. TOC measurements

Thermal water samples were thoroughly shaken to homogenize them before measurements. Small measured quantities were then mixed with high quality de-ionized water. These were then preserved with concentrated sulphuric acid to a pH of 2 and refrigerated at 4<sup>0</sup>c before digestion. The samples were digested in acidified potassium chromate (IV) solution in order to oxidize organic carbon compounds into CO<sub>2</sub> and H<sub>2</sub>O. The COD levels were then determined by redox titration using ferrous ammonium sulphate (FAS) as the titrant and ferroin (1,10 phenanthroline ferrous sulphate) as the indicator.

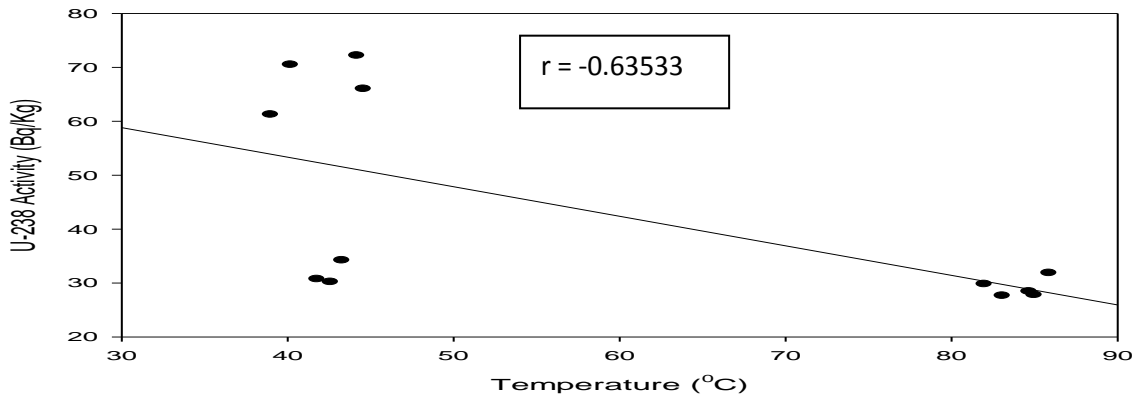
#### F. Correlation between spring pH and temperature



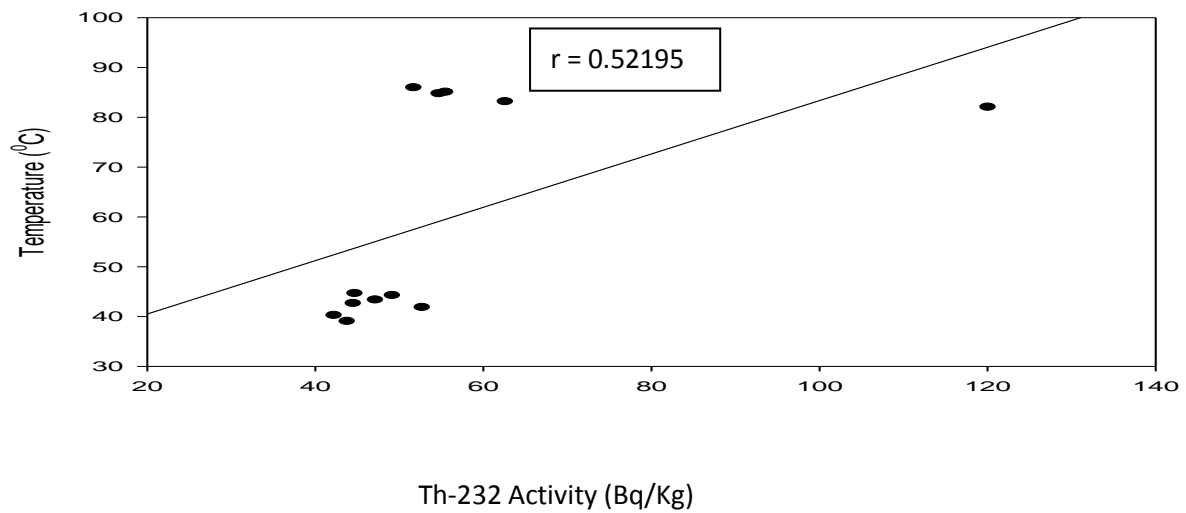
**G. Correlation between spring temperature and K-40 activity**



**H. Correlation between spring U-238 activity and temperature**



**I. Correlation between spring temperature and Th-232 activity**



**J: Limits of kurtosis for normal distribution (Bulmer, 1979)**

Size of sample	5%	1%
0 – 5	-1.058 - 1.058	-1.342 - 1.342
6 – 10	-0.950 - 0.950	-1.397 - 1.397
11 – 15	-0.862 - 0.862	-1.275 - 1.275
16 – 20	-0.777 - 0.777	-1.152 - 1.152
21 – 25	-0.771 - 0.771	-1.061 - 1.061

**K: Limits of skewness factor for normal distribution (Bulmer, 1979)**

Size of sample	5%	1%
0 – 200	-0.49 – 0.57	- 0.63 – 0.98
201 – 400	-0.36 – 0.41	-0.48 – 0.67
401 – 600	-0.30 – 0.34	-0.40 – 0.54
601 – 800	-0.26 – 0.29	-0.35 – 0.46
801 – 1000	-0.24 – 0.26	-0.32 – 0.41